UNIVERSITY OF CALIFORNIA SAN DIEGO

Evolving Stress-Tolerant Microbial Strains using the Multilayered Instrument for Continuous Adaptive Laboratory Evolution (MICALE)

A thesis submitted in partial satisfaction of the requirements
for the degree Master of Science

in

Marine Biology

by

Maile Heyer

Committee in charge:

Professor Jeff Bowman, Chair
Professor Douglas Bartlett
Professor Andrew Barton

2022

The thesis of Maile Heyer is approved, and it is acceptable in quality and form for publication on microfilm and electronically.

University of California San Diego
2022

DEDICATION

In recognition of the members of the Bowman Lab for their contributions to this degree ranging from laboratory work to critical feedback to emotional support.

TABLE OF CONTENTS

LIST OF ABBREVIATIONS

MICALE	Multilayered Instrument for Continuous Adaptive Laboratory Evolution, the name given to the chemostat-like apparatus developed during this thesis.
ALE	Adaptive Laboratory Evolution, an experimental method that employs strictly controlled conditions to produce microbial strains with a desired phenotype.
TLM	Top Layer Media, the less-dense media that is permissive for wild type growth, constituting the upper area of the MICALE and being continuously replenished.
BLM	Bottom Layer Media, denser media with an added stressor that sits below the TLM and remains static.
PL	Permissive Layer, used to represent the upper-most sampling valve with access to media that is majority TLM and constantly flowing.
IL	Interface region, used to represent the sampling valve below the PL where the TLM and BLM meet, creating a gradient of mixed media.
SL	Stress Layer, used to represent the sampling valve at the middle region of MICALE that is presumably majority BLM.
BL	Base region, used to represent the bottom-most sampling valve.
OD_{600}	Optical Density measurement of a sample, taken at a wavelength of 600 nm. OD_{600} is used as an indication of the cell count, or amount of cellular biomass, present in a sample.
MIC	Minimum Inhibitory Concentration, represents the lowest concentration of a substance that inhibits growth.
WGS	Whole Genome Sequencing.
EPS	Extracellular polysaccharides.

LIST OF FIGURES

LIST OF TABLES

LIST OF GRAPHS

ABSTRACT OF THE THESIS

Evolving Stress-Tolerant Microbial Strains using the
Multilayered Instrument for Continuous Adaptive Laboratory Evolution (MICALE)

by

Maile Heyer

Master of Science in Marine Biology

University of California San Diego, 2022

Professor Jeff Bowman, Chair

We developed the Multilayered Instrument for Continuous Adaptive Laboratory Evolution (MICALE), a novel apparatus for Adaptive Laboratory Evolution (ALE) of microbial strains with increased stress resistance. MICALE has two distinct media types separated by density. The less-dense top layer media (TLM) is permissive for growth of the wild type. A constant flow of media and removal of waste maintains a continuous culture in the upper region only. The denser bottom layer media (BLM) has an added stressor and remains static, allowing for batch-culture growth of an evolved strain. As they arise, mutants with stress-resistant phenotypes can colonize the lower regions. We tested MICALE's ability to produce evolved

strains by subjecting *Escherichia coli* MG1655 to high concentrations of sodium chloride (NaCl,) magnesium chloride ($MgCl_2$,) or the antibiotic ciprofloxacin in the BLM. Measurements during experiments show that MICALE functions as intended; density stratification is maintained, and the media flow controls the population size in the upper layer. We tested for stress-tolerant phenotypes by measuring the optical density (OD_{600}) of MICALE samples alongside the ancestor in increasing amounts of stressor. From the resulting OD_{600} curves, we extracted values representing stress-resistance using a novel analysis developed for atypical growth curves. We then performed whole genome resequencing followed by *breseq* to identify mutations linked to observed phenotypes. Contamination, however, prevents us from determining whether MICALE is effective at producing strains with increased stress tolerance. Our work provides a foundational methodology and outlines improvements for future ALE experiments to successfully evolve stress tolerant strains using MICALE.

INTRODUCTION

Adaptive Laboratory Evolution (ALE) is an experimental method that uses a specific set of conditions to "hijack" Darwinian-style evolution in order to produce microbial strains with a desired phenotype[1]. The experimental conditions determine the fitness levels of phenotypes present in the population, increasing the relative fitness of the desired phenotype. As a result, natural selection chooses mutants with the desired phenotype, directing the evolutionary trajectory of the microbial population. Sequencing of ALE-evolved strains reveals the genetic mutations responsible for these observed phenotypes. These genetic changes are often the result of a complex network of changes that go beyond our current understanding of gene expression and cellular machinery[2,3]. Therefore, ALE, is a powerful tool for strain development because the selective pressure drives cells to optimize their cellular machinery, without *a priori* knowledge on the matter[4,5]. The self-optimized strain can then be further manipulated through genome engineering. During ALE, the laboratory environment is precisely controlled, allowing the experimental conditions to be linked to the observed phenotypes for replicable evidence on how factors influence evolutionary outcomes[6]. Furthermore, samples from multiple timepoints during the experiment can be stored indefinitely and revived for a genetic and phenotypic record of the experiment. These records can show the evolutionary trajectory that took place to achieve the final strain, expanding our understanding on the molecular basis of evolutionary adaptation and population dynamics[6,7].

One of the most common uses of ALE is to study microbial stress responses to growth-limiting conditions and the adaptations that provide increased tolerance[2]. In both natural and unnatural environments, microorganisms are exposed to stressors that impact their ability to function, limit their growth, and affect the broader microbial community and ecosystem[1,8,9].

Understanding microbial stress, stress tolerance, and evolution towards stress tolerance is a central point to many of the questions surrounding microbial systems such as industrial biotechnology, clinical infections and medicines, soil health, sanitization, astrobiology, antibiotic resistance, and much more[10]. For example, high soil salinity caused by drought[11,12], exposure to ethanol during industrial bioproduction[1,13], and acidic conditions in the human intestinal tract[14,15] are stressors that have driven genetic adaptations for increased tolerance in microbial populations, whether naturally or during experiments.

Despite the use of ALE to study microbial stress responses, there are critical challenges involved with its execution: the wild type must be able to survive the initial conditions, the selective pressure must sort out strains with increased stress tolerance, and stress tolerance must be coupled with increased fitness for natural selection to act on the favored phenotype, all the while maintaining a controlled environment. If these challenges are successfully addressed, the ALE experiment will produce microbial strains that have specifically evolved in response to the experimental conditions.

The first challenge for laboratory evolution towards stress tolerance is that the experiment must expose wild type cells to stress, potentially harming the cells past what is needed for successful evolution. For this paper, we define a stressor as an external molecule, such as an antibiotic, or a physical property, such as high temperature or pressure, that causes an environment to be near or surpass the limit of an organism's physiological tolerance and impairs its ability to function[16]. While stress may not always be fatal to microorganisms, it can cause irreversible damage, prevent growth and reproduction, and trigger a wide range of regulatory changes that alter gene expression and even alter the genome's structure itself such as by inducing mutagenesis[10,17–19]. Some of these changes may fulfill the goals of ALE to produce

strains with better fitness against a stressor but too much damage can result in a failed evolution experiment.

Contrary to the first challenge, the second challenge requires that there is enough external stress to select for mutants with stress tolerance and against other phenotypes. If the stress level is too weak, there will not be enough selective pressure on cells to maintain energy-costly stress adaptations, or the low levels of selection may not select for the mutations with the highest tolerance to stress[19]. Therefore, an effective ALE experiment must apply the appropriate amount of evolutionary pressure (stress) to sort out mutants with the desired phenotype (stress tolerance)[3].

Achieving a balance between sufficient stress to select for adapted strains and not too much stress is difficult because of inadequate understanding for how microbes respond to stress. Consequently, it remains unclear how to measure stress on microbial systems in the first place[10]. Our inability to measure microbial stress limits common ALE experimental methods since the level of stress is increased artificially. Common ALE experiments are performed with batch cultures or a continuous culture device, known as a chemostat. During batch culture experiments, cell populations are transferred at fixed intervals from flask to flask with increasing amounts of selective pressure[2]. Chemostats, on the other hand, operate in a single bioreactor, maintaining a continuous culture of cells steady-state growth by continuously supplying media and removing waste. The fresh supply of media lacks one key nutrient so that cells are starved and grow at a reduced rate[20]. The selective pressure is increased overtime by changing the components of the inflowing media. Both methods increase the level of stress and selection by a predetermined amount at a predetermined time, imposing a time constraint on evolution, without an

understanding of how the cells have responded or if they will be able to respond. These methods, therefore, have a limited ability to achieve a balance between too little and too much stress.

The third challenge addresses the fundament of Darwinian evolution that ALE is based on; during ALE, the favorable phenotype must correspond with increased fitness because natural selection will choose mutants based on their fitness in the environment. Typically, increased fitness of bacterial cells is determined by their ability to survive and replicate at a faster rate in trying conditions[3,21] but other components of fitness besides maximum growth rate exist as well[22]. For ALE experiments that seek to increase tolerance to a stressor, the favorable phenotype, stress tolerance, is directly linked to increase fitness because these strains survive better. The difficulty, however, is controlling the conditions such that adapting stress-tolerance has more advantages than the energetic cost of these adaptations and is more fit than other phenotypes, such as those that allow evasion of the stress altogether. If all cells are exposed to a stressful agent, then adapting tolerance is favorable. However, it is difficult to determine the optimal amount of stress to expose cells to, as discussed prior.

To overcome these challenges, we believe that the most effective way to evolve cells with increased stress tolerance is to employ a spatially increasing gradient of stress. A spatial increase of stress allows cells to evolve at their own pace, removing any time constraints on evolution. The wild type can survive in low-stress regions while stress-tolerant mutants are sorted out simply by their existence in high-stress regions, addressing the first two challenges of ALE[19]. For the third challenge to ALE, the relative fitness of stress-tolerant phenotypes is increased because mutants are provided with unused space and nutrients [23]. Mutations for stress-tolerance, therefore, will be naturally selected for fixation in the population. Microbial populations can be further pushed to evolve to the stressor by increasing the nutrient

concentration in high-stress regions, making colonization of the stressful regions the better evolutionary strategy. Lastly, an added benefit of using a structured gradient is that the heterogeneous environment supports diversity in the population, facilitating adaptation.

A spatial-increase in stress facilitates adaptation by providing intermediate steps and accelerates the rate of evolution by maintaining the diversity present in the population. ALE experiments with the MEGA-plate and microfluidic gradient chamber, by Baym *et al*.[24] and Zhang *et al.*[23] respectively, used a spatial increase in antibiotic to produce cells with high antibiotic resistance. By providing intermediate steps with moderate amounts of selective pressure, both experiments produced strains with high levels of microbial resistance. In Zhang *et al.*[23], when microorganisms were exposed to a high level of antibiotics without intermediate steps, they were not able to adapt. The gradual increase in stress, therefore, allowed cells to reach a higher level of antibiotic resistance. Additionally, the heterogeneous environment, as opposed to a homogeneous one, increased the rate of adaptation. The connected microenvironments provide ecological opportunity for populations to diversify and potentially evolve new mutants with the ability to cope with higher levels of stress[16,25]. The microcosm experiment by Rainey and Travisano[25] showed that a structured, heterogeneous environment increased the diversity in a population by allowing bacteria to occupy different niches, reducing competition. Homogeneous environments, like those in chemostats and shaken batch cultures, on the other hand, have reduced genetic diversity in which populations may get stuck with a "quick fix" mutation[19]. Furthermore, studying evolution within a heterogeneous environment has better applications to evolution outside of the laboratory. For example, pathogenic bacteria colonize on heterogeneous surfaces that allow for higher diversity, potentially increasing the rate of antibiotic-resistant phenotypes compared to *in vitro* studies with homogeneous cultures[17].

Despite the evidence presented in favor of evolution studies in a heterogeneous environment, ALE experiments are still dominated by use of batch cultures and chemostats and there are few examples of ALE with a heterogeneous set up[2]. Furthermore, the available methods, such as the MEGA-plate and microfluidic gradient chamber, are currently limited to studying antibiotic resistance with model organisms, excluding other organisms with great potential for biotechnological use. For example, marine microorganisms with stress tolerance adaptations, such as desiccation resistance and high salinity tolerance.

We have developed a novel approach to ALE using a multi-layer bioreactor (Figures 1 and 3), called the Multilayered Instrument for Continuous Adaptive Laboratory Evolution (MICALE). In our approach, the bioreactor has two distinct media types separated by density. The less-dense top layer media (TLM) operates as a traditional chemostat and is permissive for steady-state growth of the wild type. The denser bottom layer media (BLM) has an added stressor, such as salt or magnesium chloride, but does not have in-flowing or out-flowing media, allowing for batch-culture-style growth of an evolved strain. The media types mix at their interface, creating a spatial gradient from mostly TLM to mostly BLM, thereby forming an increasing gradient in the concentration of a stressor and nutrients. Cells with stress tolerant phenotypes can colonize the lower regions of media at their own pace.

The MICALE apparatus provides a permissive area for wild type survival while and offers unrestricted access to stressful regions for adapted strains, without imposing time constraints on evolution. We hypothesized that the nutrient difference between the TLM and BLM along with the controlled growth in the upper region would amount to sufficient resource limitation couple stress tolerance with increased fitness. We set out to establish and support the use of MICALE as a viable method for ALE to produce microbial strains with increased

tolerance to environmental stress. In doing so, we aim to answer two main questions: (1) Does MICALE function as intended, and (2) does it produce cell strains with increased tolerance to the stressor?

With high concentrations of sodium chloride (NaCl,) magnesium chloride ($MgCl_2$,) and the antibiotic ciprofloxacin in the BLM, we grew *Escherichia coli* MG1655 (*E. coli*) in MICALE for two to four weeks. The model bacteria *E. coli* was selected for this experiment for easier validation of the methods before attempting to grow more challenging microorganisms with MICALE. Each selected stressor exposed the bacteria populations to a different type of hostility intended to drive the course of genetic adaptation. High salinity adds osmotic and ionic stress to cells and may reduce the solubility of metabolites[26]. Chaotropic stress, caused by solutes such as $MgCl_2$, disrupts intermolecular forces thereby destabilizing, denaturing, and inhibiting important molecules in a cell such as proteins, enzymes, and membranes[27,28]. Ciprofloxacin, a quinolone antibiotic, targets enzymes essential for bacterial DNA replication and is commonly used to treat infections caused by *E. coli* and other Gram-negative bacteria[29]. It is necessary to note that some do not consider the toxic effect of antibiotics to be a type of cellular stress; antibiotics have specific target sites and modes of action, compared to stressors like magnesium chloride that act on multiple cellular mechanisms[10]. However, it has been shown experimentally that ciprofloxacin and other antibiotics trigger stress-induced mutagenesis, a bacterial response to stress characterized by a transient mutator state[18,30,31]. Therefore, stressing *E. coli* ciprofloxacin, in addition to NaCl and $MgCl_2$, allows us to study the differing evolutionary responses to three unique types of stress.

During each run, we tested samples to monitor conditions within MICALE and preserved cell samples. The saved samples and ancestor strain were subjected to a series of growth tests to

observe different growth phenotypes that could indicate increased tolerance to the stressor. After the phenotypic assessment, we performed whole-genome resequencing analysis to identify genetic changes that may be linked with the observed phenotypes.

The aim of this study was to refine the methods involved with MICALE and to provide an accessible and customizable avenue for microbial strain development with ALE. MICALE is designed to address the limitations of ALE by maintaining a continuous culture of wild type cells while facilitating adaptation to a stressor using a gradient, all within a liquid-media environment. In doing so, MICALE expands the range of stressor types and microorganism species that can be studied using ALE. If successful, MICALE would be a valuable tool to observe evolution dynamics in real-time and produce new microbial strains.

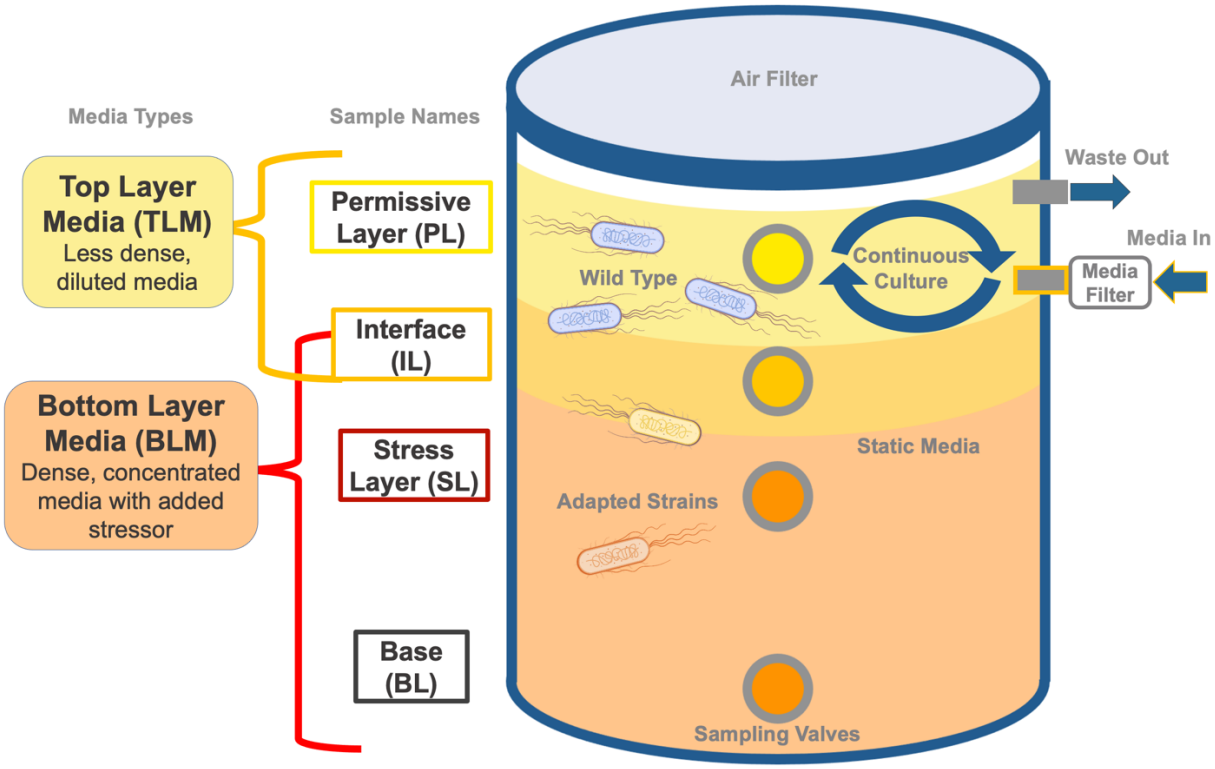

Figure 1: Multilayered Instrument for Continuous Adaptive Laboratory Evolution (MICALE)
The two media types, the permissive TLM and stressful BLM, are vertically stacked by density. Sampling valves access four different regions of the density gradient that we have named the permissive layer (PL), interface (IL), stress layer (SL), and base (BL). In the upper region consisting primarily of TLM, fresh media is constantly brought in while waste is removed, forcing cells into steady-state growth. The lower layer remains static, allowing unrestricted growth for cells adapted to the stressor. The starting concentration of stressor in the BLM was 100 ppt of sodium chloride (NaCl), 300 mM/L magnesium chloride ($MgCl_2$), and 120 µg/mL ciprofloxacin (2000 xMIC). Some images used to construct this diagram are sourced from BioRender.com.

METHODS

MICALE Media Types and Stressor Concentration

Figure 1 illustrates the system within MICALE created using two layers of different media, separated by density. The top layer media (TLM) was made of LB broth diluted to 50% and constituted the top 250 mL of media in MICALE. The lower 900 mL of the bioreactor contained bottom layer media (BLM) made of fully concentrated LB broth, 100 g/L of sucrose, and a high concentration of a stressful compound. The sucrose in the BLM increased the density of the media so that it sat below the TLM. There was no physical barrier or separation between the TLM and BLM, just density stratification. In the upper region only, pumps brought in fresh TLM and removed waste at an equal rate. The BLM remained static.

Samples were taken from MICALE using valves placed evenly down the apparatus. These valves divided the media into four sections, each with a distinct microenvironment created by the layering of the TLM and BLM: the permissive layer (PL) in which media is constantly flowing and is majority TLM, the interface (IL) that sits at the now-blurred boundary between the two media types, and the stress layer (SL) followed by the base (BL) that contain majority BLM and remain static (Figures 1 and 2).

The starting concentration of stressor in the BLM was at the Minimum Inhibitory Concentration (MIC) or higher. This ensured that any observed growth in the lower layer of MICALE was due to adaptation rather than a preestablished tolerance of the ancestor strain. In total, three compounds were tested in the BLM during separate runs at concentrations determined to be above the ancestor's tolerance: 100 g/L of sodium chloride (NaCl), 300 mM/L magnesium chloride ($MgCl_2$), and 120 µg/mL ciprofloxacin (2,000 xMIC).

Determination of the Minimum Inhibitory Concentration

For the high salinity MICALE run, the starting concentration of NaCl in the BLM was determined with a growth test in increasing concentrations of NaCl. A liquid culture of the ancestor strain was diluted 1:100 into media with 5, 60, 80, 100, and 120 ppt NaCl on a 96-well microplate and the optical density (OD_{600}) measured every fifteen minutes for 48 hours. OD_{600} activity was observed at 80ppt NaCl but not at 100 ppt.

For the chaotropic stress MICALE run, the starting concentration of $MgCl_2$ was determined based on previous lab work done by a collaborator, Luke Fisher, in the Bartlett Lab at UCSD, unpublished work. This previous work determined that *E. coli* MG1655 can grow well at 150 mM $MgCl_2$ but cannot grow at 300 mM $MgCl_2$.

For the antibiotic ciprofloxacin, the MIC was determined by closely following the protocol outlined by Wiegand *et al.* (2008)[32]. A brief description of the steps are as follows. The OD_{600} of a fresh broth culture of the ancestor strain was measured to be 0.370 absorbance units. This starting absorbance is lower than the McFarland standard of 0.5 absorbance equating to roughly $1x10^8$ cfu/mL. To check that this starting concentration of cells was sufficient, agar plates were streaked with 100 µL of a 1:1000 dilution of the cell culture and incubated during the MIC analysis. This agar plate had growth of well over 50 colonies ($5x10^5$ cfu/mL), a sufficient starting cell count for the analysis, so the MIC determination was not repeated.

The culture with 0.370 absorbance was diluted 1:100 in sterile LB broth. Several dilutions of LB broth and ciprofloxacin were pipetted in triplicate onto a 96-well plate, following the protocol. Diluted cell culture was then added to the wells. In total, each experimental well had 0.2mL of liquid with ciprofloxacin concentrations of 0.01, 0.01, 0.03, 0.05, 0.06, 0.07, 1.0, 1.2, and 1.5 µg/mL. Additional triplicate wells were added for a sterile control (LB broth and

ciprofloxacin) and a growth control (LB broth and cell culture.) All samples were pipetted in the center-most wells of the plate to reduce measurement interference from evaporation. The initial OD_{600} of the plate was measured then the plate was incubated at 37ºC with the lid overnight. After incubation, the final OD_{600} was measured. The final absorbance results showed growth activity at 0.05 µg/mL ciprofloxacin, but not higher, so the MIC was determined to be 0.06 µg/mL ciprofloxacin. Taking into consideration the MEGA-plate experiment[24] that evolved *E. coli* with resistance to ciprofloxacin at 20,000 xMIC, the starting concentration of ciprofloxacin in the BLM was 2,000 xMIC ciprofloxacin (120 µg/mL).

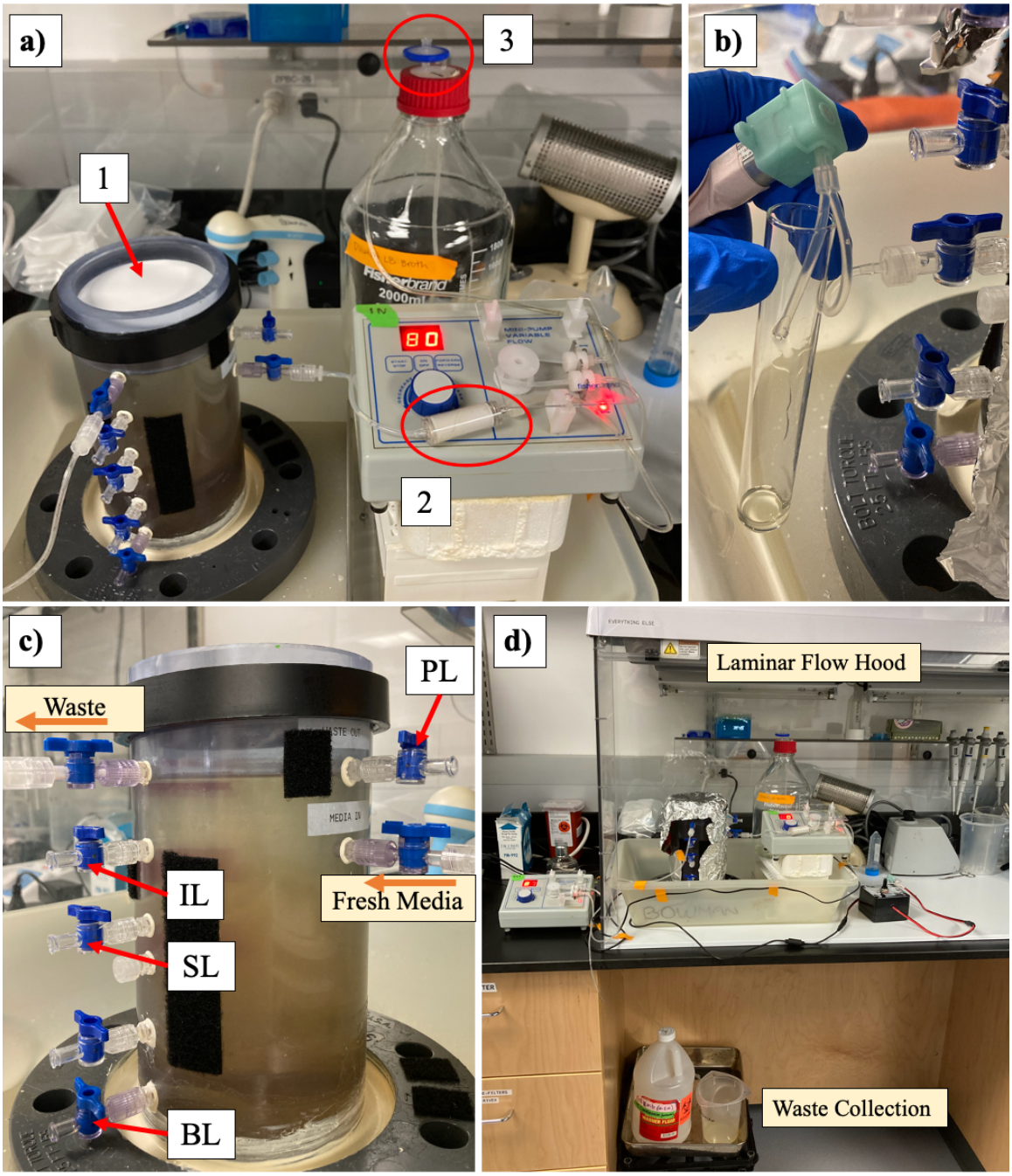

Figure 2: Photos of the MICALE system
a) Media bottle and pump connected to the apparatus. Numbers highlight the three types of filters used in the system: **a.1)** 0.2-micron membrane filter acting as the lid of the apparatus for sterile airflow. **a.2)** 0.2-micron sterivex filter through which media passes before entering the apparatus. **a.3)** 0.2-micron millex filter for sterile airflow into the media bottle. **b)** The small peristaltic pump sampling from a valve. **c)** A close-up of the valves along the MICALE housing: red arrows point to valves with their respective labels and orange arrows show the direction of flow. The valve second from the bottom was not used. Note that the PL valve and Waste valve are switched, compared to Figure 1, due to incorrect drilling height of the valves. The density separation between the TLM and BLM media types is visibly shown: the media at the top is a clear yellow until the IL valve where the media becomes a darker yellow. **d)** The experimental set-up. MICALE, the media pump and stock bottle, and sampling pump remain in a UV-sterilized laminar flow hood. Waste is removed by a pump on the outside of the hood and collected in a bottle underneath.

MICALE Set Up and Inoculation

Figure 2 illustrates the laboratory set up of MICALE. Each MICALE experiment was assembled and kept in a laminar flow hood with frequent UV light sterilization (Figure 2d). The structure of MICALE was a hollow tube of thick plastic with a base for stability and valves spaced from top to bottom (Figure 2c). The apparatus was cleaned by rinsing with Milli-Q water and ethanol then sterilized with UV light as it cannot be autoclaved. A membrane filter sealed the top of the apparatus, allowing sterile airflow (Figure 2a, arrow #1).

MICALE was filled by pumping media through the lowest valve, starving with 250 mL of TLM followed by 900 mL of BLM. By pumping media in from the bottom, the TLM remained stacked on top of the denser BLM.

Pumps flowing both in and out of the system were turned on for equilibration before adding cell cultures. A peristaltic pump connected to the top-most valve removed waste media and collected it in a bottle outside of the sterile hood (Figures 2c and 2d). A pump within the sterile hood pumped fresh media into MICALE through a valve located just above the sampling valve that represented the interface (IL). This pump drew fresh media from an autoclaved 2-liter bottle that remained in the sterile hood and pumped the media through a 0.2-micron sterivex filter before it entered MICALE (Figure 2a, arrow #2). When the media ran low, freshly autoclaved media was poured into the stock bottle after the hood was UV sterilized. A 0.2-micron filter on the lid of the stock media bottle allowed sterile airflow (Figure 2a, arrow #3).

Once the MICALE set up was complete and sterilized with UV light, it was wrapped with aluminum foil to prevent any damage to the cells with UV light. *E. coli* was inoculated to the top of the apparatus using a syringe with 1 mL of the fresh ancestor culture. The time of inoculation represented t=0.

Sampling from MICALE

During the first 48 hours of a run, samples were taken at intervals of one to three hours during the daytime to track cell growth up to steady state. Afterwards, samples were taken at minimum once every two days. Due to slower growth in the antibiotic run, the sampling frequency was reduced to only twice a day for the first couple days, followed by sampling once a day at most. Sampling was performed using a small peristaltic pump to slowly remove 2 mL of media from each valve to avoid disturbing the density stratification (Figure 2b). The small pump was flushed with ethanol after each sample and kept in the sterile hood. At least once a week, an additional 0.5 mL of media was collected and archived as a frozen glycerol stock.

With each sample, the OD_{600}, salinity or density, and pH was measured. For OD_{600}, 0.2 mL of sample was pipetted in triplicate onto a 96-well plate along with sterile TLM and BLM as controls for a single-time measurement of turbidity. During the high salinity run, the salinity was measured with a refractometer instead of density. These measurements were taken only with the PL and IL samples because the salinity of the lower layers was out of range for the refractometer. For the chaotropic and antibiotic stress runs, density was calculated by measuring 0.1 mL of sample in triplicate. The pH was measured only during the antibiotic run, using a pH probe.

The flow rate was calculated by removing and measuring the amount of media waste in the collection bottle and dividing by the amount of time that had passed since the previous media collection. Time points when the flow was purposefully stopped (to replace a filter, for example) were excluded from the flow rate calculation to prevent the added time from underestimating the flow rate. When the filter clogged and the flow stopped on its own, the media waste was measured and an estimated flow rate was calculated based on the previous collection. After calculating the estimated flow rate, the rest of the time was recorded as having a flow rate of zero

mL per hour. For example, the flow had stopped sometime in the last 24 hours since the last waste collection. The last flow rate calculation was 30 mL/hr and there was now 10 mL of waste in the collection bottle. Since the flow rate could be no faster than the previous 30 mL/hr, the flow was estimated to have continued for at least 3 hours before completely stopping. Thus, the recorded flow rates were 30 mL/hr for three hours and 0 mL/hr for the remaining 21 hours.

Bacterial Strain and Culture Conditions

The ancestor culture used in each experiment was from a frozen glycerol stock of *Escherichia coli* K-12 strain MG1655[33], sampled from the Bartlett Lab at UCSD. Before each experiment, a sample of the frozen ancestor culture was spread onto agar plates with Luria Broth (LB) medium (Lennox) and incubated at 37°C. A single colony was transferred from the plate into 10 mL of liquid LB medium and incubated at 37°C overnight, or until turbid. 1 mL of this liquid culture was inoculated into the top layer of MICALE, marking the start of the run.

Samples obtained from MICALE runs were cultured before further analysis, an overall schema of which is described in Figure 3. During runs, samples directly from MICALE were frozen at -80ºC with a 1:1 ratio of glycerol. Frozen samples chosen for analysis were streaked onto LB/agar plates and a colony was transferred into 5-10 mL of LB broth medium to grow a dense culture. The culture media would often have some level of the stressor, based on the conditions within the MICALE gradient, such as the type and amount of stressor, and which layer the sample came from (Figure 3b). When transferring colonies to broth, the concentration of stressor in the broth matched that in the agar media. Culturing in media with stressor was to maintain evolutionary pressure to prevent evolved cells from back-mutating. Samples from the lower, high-stress region were cultured in media that contained a moderate amount of stressor

that was low enough to allow growth but high enough to prevent back-mutation (Figure 3b). Since the optimal concentration of stressor to achieve growth but prevent back-mutation was not known, samples were grown in multiple concentrations. High salinity stress samples were cultured in media with 0, 40, and 60 ppt NaCl, chaotropic stress samples were grown in 0, 200, and 250 mM $MgCl_2$, and the antibiotic stress samples were grown in 0, 0.6, and 15 μg/mL ciprofloxacin. Samples were also cultured in blank LB media to observe the colony morphologies of the full bacterial community present in the sample instead of just those selected by one media type. Examples of the colony diversity observed in different concentrations of stressor can be seen in Figures 8 and 10.

From the isolated broth cultures in various media types, samples were selected for growth in the adaptation analysis, described after this section (Figure 4.) The cultures in which media type were chosen for the adaptation analysis based on the culture's ability to produce a turbid culture, what region of MICALE the sample came from, and curiosity. For example, the SL and BL samples used in the adaptation analysis were from cultures of the respective samples in media with the highest level of stressor possible, since the SL and BL samples come from the high-stress BLM region. The PL and IL samples chosen for analysis were generally from the cultures with blank LB media. Sometimes, the PL and IL samples cultured in media with a stressor were used in the analysis to see if adaptation to the stressor could occur in the permissive media. For samples with interesting colony morphologies, such as a PL sample from the chaotropic run (Figure 8b) and IL sample from the antibiotic run (Figure 10b), two colonies of different morphology were used in the analysis to understand how the colony phenotype may correspond with stress tolerance.

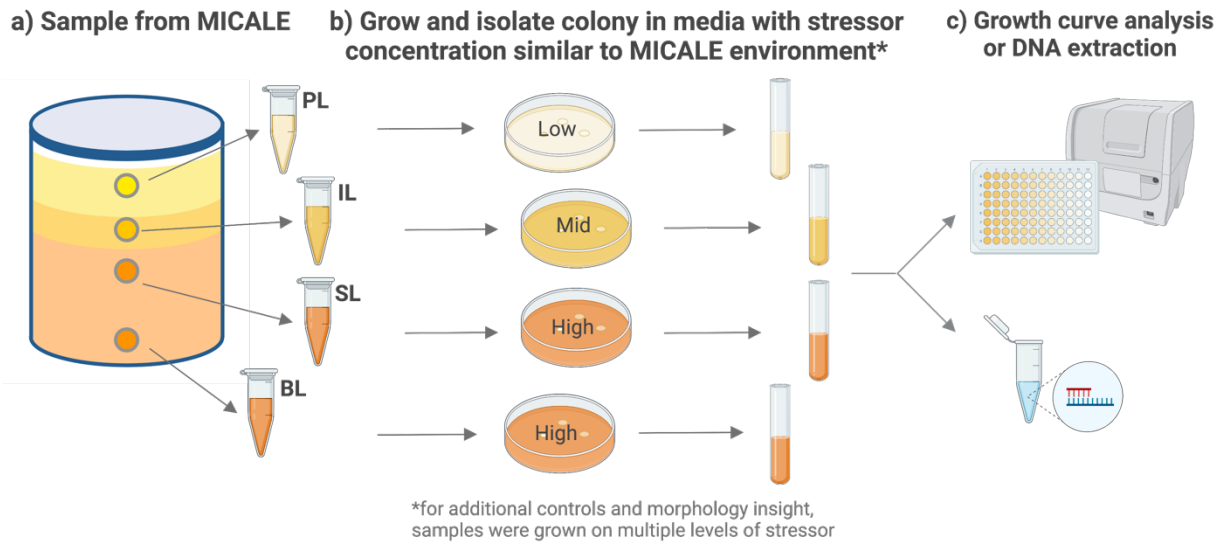

Figure 3: General MICALE Procedure
The overall MICALE procedure from experimental runs to the start of further analyses. **a)** samples are taken from the four valves, used for measurements, and frozen with glycerol. **b)** samples of interest are spread onto agar plates (directly from MICALE or from frozen stock) with a concentration of the stressor that corresponds to the region of MICALE the sample came from. Isolated colonies are then transferred into broth with the same concentration of stressor. **c)** isolated cultures are used for a growth curve analysis (the adaptation analysis, described in Figure 4) or used for DNA extraction, followed by WGS. This image was created with help from BioRender.com.

Revealing Stress-Tolerant Phenotypes with the Adaptation Analysis

Illustrated in Figure 4, the adaptation analysis is our test to qualitatively compare the ability to grow in the presence of the stressor between the ancestor and MICALE-grown samples. Turbid broth cultures from isolated colonies were diluted 1:100 in sterile broth with increasing amounts of stressor. These dilutions were vortexed before pipetting 0.2 mL in triplicate onto a 96-well plate (Figure 4b). The microplate reader then measured OD_{600} every 15 minutes over the span of four days while incubating the plate at 37°C with the plate lid on. The measurements resulted in triplicate OD_{600} curves that represent the growth of each sample well on the 96-well plate (Figure 4c). The high salinity and chaotropic stress adaptation analyses were completed once whereas the antibiotic analysis was repeated for two total trials. Growth metrics were extrapolated from the growth curves (described below) for numerical comparisons between

samples (Figure 4d) and to fit a logistic dose-response curve of each sample's response in a stressor (Figure 4e).

The samples chosen from the high salinity run were frozen stocks of the PL, SL, and BL samples that had been taken at the end of the run (two weeks) and one SL sample from the first 25 hours (Table 2). The samples used in the adaptation analysis had been in media with a NaCl concentration of 60 ppt, and the ancestor was cultured on blank LB media. The samples were diluted into LB media with 5, 45, 60, 75, and 90 ppt NaCl then plated on the 96-well plate. Normal LB media with no additional salt added had an NaCl concentration of 5 ppt.

For the chaotropic stress run, samples from both two weeks and four weeks into the run were selected for analysis (Table 4). The samples, including the ancestor, were cultured in media with 0, 200, and 250 mM $MgCl_2$ (Figure 8). The IL samples were not plated on 200 mM $MgCl_2$ plates due to limited resources. The ancestor was grown on plates with the same $MgCl_2$ concentration as the samples to see if the culturing process was causing genetic change significant enough to affect the growth phenotypes observed during the adaptation analysis. Cultures were diluted into media with 0, 200, 250 and 300 mM $MgCl_2$ then pipetted onto the 96-well-plate to start the four-day analysis.

The samples chosen for the antibiotic-stress adaptation analysis were from the end of the antibiotic stress MICALE run, sampled on the 14^{th} day (Table 6). Samples were cultured grown in media with no antibiotic, 0.6 µg/mL ciprofloxacin (10 xMIC,) and 15 µg/mL ciprofloxacin (250 xMIC) were transferred into 5mL of LB broth with the same amount of antibiotic (Figure 10). The only exception is the BL sample was grown in 0.6 µg/mL ciprofloxacin then transferred to LB broth with 15 µg/mL ciprofloxacin. Once turbid, the broth cultures were diluted into media with no antibiotic, 0.6 µg/mL, 6 µg/mL, and 60 µg/mL ciprofloxacin then pipetted onto a 96-

well plate and placed in the microplate reader to start the analysis. A portion of the broth cultures used for the analysis were frozen in glycerol. For a repeat trial of the adaptation analysis, these frozen stocks were revived in broth media matching the level of antibiotic they were originally cultured in.

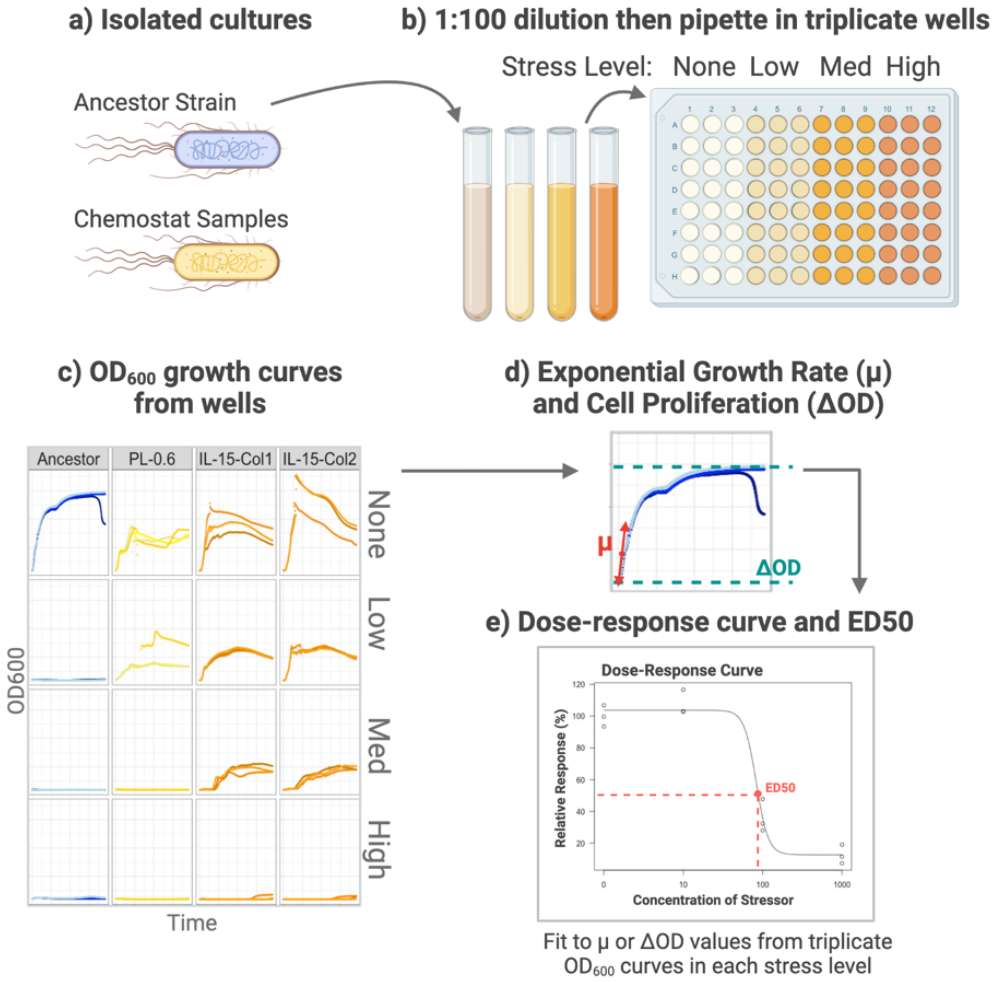

Figure 4: Adaptation Analysis Overview
a) MICALE samples and the ancestor are isolated and cultured in broth as described in Figure 3. **b)** Cultures are individually diluted 1:100 in sterile media with no stressor and low, medium, and high concentrations of stressor. These dilutions were pipetted into triplicate wells onto a 96-well plate. OD_{600} measurements were taken for each well over the span of four days, producing individual growth curves, seen in **c).** Each facet of the graph shows the three curves obtained from the triplicate wells of a sample and media treatment. **d)** For each OD_{600} curve, the maximum rate of growth over a span of 75 minutes is designated the exponential growth rate, μ, and the subtracted difference between the maximum and minimum OD_{600} measurements, ΔOD, is designated the cell proliferation. These values are presented as relative percentages of each sample's response in media with no stressor. **e)** For each sample, a logistic curve was fit to the triplicate relative exponential growth rate or relative cell proliferation values across all media types. This curve represents a sample's relative response to increasing doses of a stressor, known as a dose-response curve. The value for ED50 is the effective dose of the stressor at which a 50% decrease in the maximal response (100%) is observed. This image was created with help from BioRender.com.

Exponential Growth Rate and Relative Cell Proliferation

To statistically compare growth between samples, two parameters were extracted from the OD_{600} curves resulting from the adaptation analysis: relative exponential growth rate and relative cell proliferation (Figure 4d). To find the exponential growth rate, μ, growth curves are normally fit to a standard sigmoidal function, such as the Gompertz model. However, these OD_{600} curves were too irregular to be well fit with a standard function, as seen in Figure 5a. Instead, Daniel Padfield's instructions[34] were followed to fit a rolling regression onto natural log transformed OD_{600} curves that produced linear regression lines between six measurements at a time (75 total minutes), shifting by 1 measurement, over the curve (Figure 5b).

The exponential growth rate was determined to be the maximum slope of any of the regression lines, denoted by μ_{stress} for growth curves in media with stressor and μ_{blank} for that in blank LB media [1]. Any slope maxima that appeared to be due from anomalies in the data, such as a quick jump in OD_{600} after biofilm formation, were filtered out. This ensured that the maximum slope occurred during the time that visually represented exponential growth (near the start of the curve). The triplicate μ_{blank} calculations were averaged to obtain the values representing that sample's growth in media without stress, $\bar{\mu}_{\text{control}}$ [2]. The percent relative exponential growth rate was obtained by dividing each μ by the $\bar{\mu}_{\text{control}}$, then multiplying by 100 [3]. Finally, the three relative exponential growth rate values for each sample and media type were averaged [4].

[1] $$\mu_{\text{stress or blank}} = \text{max slope of } f(\text{time}, \ln(\text{OD}_{600}))$$

[2] $$\bar{\mu}_{\text{control}} = \frac{\mu_{\text{blank 1}} + \mu_{\text{blank 2}} + \mu_{\text{blank 3}}}{3}$$

[3] $$\%\ \text{Relative Exponential Growth Rate} = 100\ \text{x}\ \frac{\mu_{\text{stress or blank}}}{\bar{\mu}_{\text{control}}}$$

[4] $$\text{Average \% Relative Exponential Growth Rate} = 100\ \text{x}\ \left[\left(\frac{\mu_{\text{stress 1}} + \mu_{\text{stress 2}} + \mu_{\text{stress3}}}{\bar{\mu}_{\text{control}}}\right)\right]$$

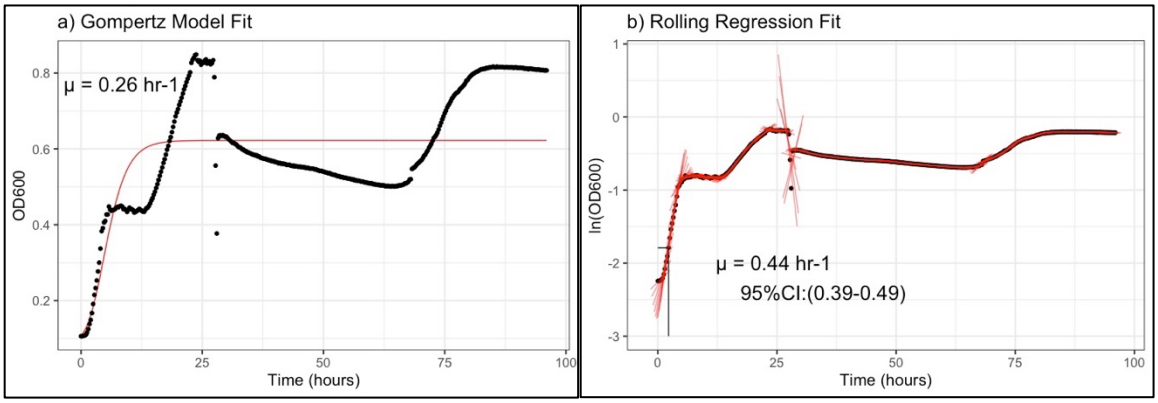

Figure 5: Comparing Different Models for Extracting the Exponential Growth Rate
Figure 5 compares the Gompertz model fit versus a rolling regression fit onto the OD_{600} data from the PL-0.6 sample (Table 6) growing in blank LB media during trial one of two for the antibiotic adaptation analysis. Black dots represent the OD_{600} data and red lines represent the model's fit. **a)** The exponential growth rate, μ, calculated by the Gompertz model is 0.26 hr^{-1}. The Gompertz model was a poor fit for the wide range of OD_{600} curves obtained. **b)** The exponential growth rate from the maximum slope obtained by the rolling regression is 0.44 hr^{-1}. Black lines represent where the maximum slope occurs.

Relative cell proliferation was calculated for each OD_{600} curve (three curves per media type per sample) first by finding ΔOD_{stress}, the subtracted difference for each curve grown in media with the stressor and that grown in blank media, ΔOD_{blank} [5]. Any OD_{600} curves that showed an abnormal jump and fall in optical density, caused by variables such as biofilm formation, were filtered out so that ΔOD was calculated using OD_{600} values that more accurately represented the actual cell count. Each sample's three ΔOD_{blank} calculations were averaged to obtain the $\overline{\Delta OD}_{control}$ [6]. The percent relative cell proliferation was calculated by dividing the ΔOD by $\overline{\Delta OD}_{control}$ and multiplying by 100 [7]. Lastly, the three relative cell proliferation values for each sample and media type were averaged [8].

[5] $$\Delta OD_{\text{stress or blank}} = OD_{max} - OD_{min}$$

[6] $$\overline{\Delta OD}_{control} = \frac{\Delta OD_{blank\,1} + \Delta OD_{blank\,2} + \Delta OD_{blank\,3}}{3}$$

[7] $$\%\ \text{Relative Cell Proliferation} = 100\ \text{x}\ \frac{\Delta OD_{\text{stress or blank}}}{\overline{\Delta OD}_{control}}$$

[8] $$\text{Average \% Relative Cell Proliferation} = 100\ \text{x}\ \left[\left(\frac{\Delta OD_{stress\,1} + \Delta OD_{stress\,2} + \Delta OD_{stress3}}{\overline{\Delta OD}_{control}}\right)\right]$$

Dose-Response Curves and Effective Dosage (ED) Calculations

Using the exponential growth rate and relative cell proliferation values derived from the OD_{600} growth curves, dose-response curves were fit to understand how sensitive each sample strain was to an increase in stressor concentration (Figures 4e and 6). The dose-response curves were generated using the drc R package[35,36], modeled with the four-parameter logistic function given by:

$$[9] \qquad f\big(x,(b,c,d,e)\big) = c + \frac{d-c}{1+\exp\{b(\log(x)-\log(e))\}}$$

The parameters *d* and *c* represent the upper limit and lower limit of the logistic curve, respectively. The parameter *e,* also referred to as ED50, is the dosage that occurs half-way between *d* and *c* and can be calculated with Equation [10] and [11]. The logistic function is symmetrical around *e.* The fourth parameter, *b,* is the relative slope around *e*, also known as the Hill coefficient. More information on the parameters is described in Seefeldt *et al.*[37].

ED*y* is the effective dosage quantity at which the maximal response, *d,* is decreased by *y%,* yielding a response that is (100-*y%*) of *d* [10]. Since the model is symmetrical around *e,* the amount that *d* is decreased by, *y* percent, is a proportion of the total distance between *d* and *c.* Note that the distance between *d* and *c* is not the distance between *d* and 0.

$$[10] \qquad \mathrm{ED}y = e\left(\frac{y}{100-y}\right)^{\frac{1}{b}}$$

$$[11] \qquad \mathrm{ED}50 = e(1)^{\frac{1}{b}}$$

The ED50 dosage for each sample serves as a metric for sensitivity to the stressor that can be compared between samples. However, when this model was applied to the data, the logistic fit sometimes resulted in a negative lower limit, *c* (Figure 6a). This produced an over-estimated

value for ED50 since the 50% decrease was measured by the distance between *d* and *c* and not between the observed maximum and minimum response values of the data.

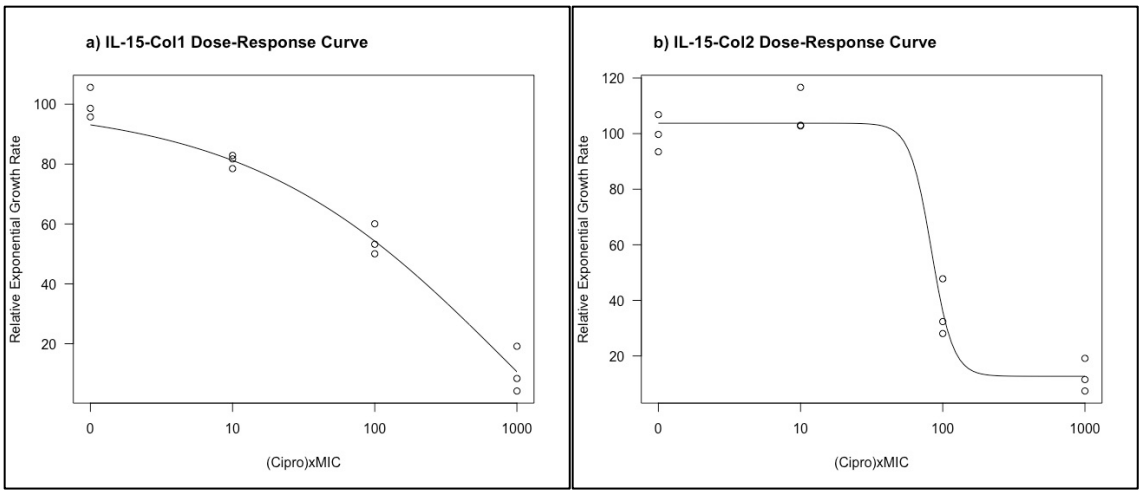

Figure 6: Dose-Response Curves for Relative Exponential Growth Rate
Dose-response curves fit to the relative exponential growth rate over an increasing concentration of ciprofloxacin in units of minimum inhibitory concentration (MIC) for **a)** IL-15-Col1 sample and **b)** IL-15-Col2 sample grown during trial 1 of the antibiotic adaptation analysis (Table 6). The lower limit of the logarithmic fit, *c*, for **a)** is -75.5, producing the convex-curve shape instead of the expected biological growth curve seen in **b)** in which the lower limit is 12.7. For **a)** the unadjusted ED50 value is a ciprofloxacin concentration of 926.79 xMIC which is considerably high and not what is observed in the data. The $ED50_{adjusted}$ value is 130.13 xMIC, which more closely aligns with a 50% decrease from the maximum growth rate. For **b)** the unadjusted ED50 value is 103.73 xMIC and the $ED50_{adjusted}$ is 87.29 xMIC.

To account for the over-estimated ED50 values, new $ED50_{adjusted}$ values were calculated using the *y* percentage that represented a decrease of *d* that is half the value of *d* [12, 13]. The resulting ED*y* was plugged into the drc package that calculated the concentration of media at which the response was decreased by *d*/2. This adjustment was made across all dose-response models so that all reported ED50 values (Tables 3, 7, and 5) represent a 50% decrease in the maximum response. See the caption in Figure 6 for an example of the raw and adjusted ED50 values.

$$[12] \quad y = 100 \times \frac{\frac{d}{2}}{(d-c)}$$

$$[13] \quad \mathrm{ED50}_{\mathrm{adjusted}} = EDy = e\left(\frac{100\times\frac{\frac{d}{2}}{(d-c)}}{100-\left(100\times\frac{\frac{d}{2}}{(d-c)}\right)}\right)^{1/b}$$

The ED50 was calculated for both the relative exponential growth rate and cell proliferation dose-response curves for each sample. Some samples could not be fit with a dose-response curve because they grew poorly or not at all in the stressor, thereby providing insufficient depth of data points for the logistic function to be fit. This problem occurred especially for the antibiotic samples that could not grow in ciprofloxacin, such as the ancestor (Figure 11). Samples that could not be fit to a model were excluded from ED50 analysis.

To obtain ED50 values for the ancestor strain in ciprofloxacin, the dose-response curves were fit to the relative exponential growth rate and cell proliferation values obtained from the MIC growth test in which the ancestor was grown in smaller increments of ciprofloxacin thereby providing enough resolution to fit a logistic function. It is recognized that the MICALE samples were grown on a much larger, low-resolution scale of ciprofloxacin, resulting in ED50 values that are much less precise. However, the samples clearly grew in the presence of ciprofloxacin, unlike the ancestor. Thus, for the purpose of this paper, the ED50 values were seen as an accurate representation of the observed difference in antibiotic resistance between MICALE samples and the ancestor.

Statistical Analysis

Differences between the density of the sample layers and control media types were assessed using a pairwise Welch two-sample t-test in RStudio with unpaired data, unequal variance, non-pooled standard deviations, and no p-value adjustment options[38,39]. Statistical analyses were not performed with any ED50 values. The ED50 sample size was too small to allow for a calculation of significance. Future MICALE runs with more replicates should perform a t-test to calculate the significance of the ED50 values.

DNA Extraction and Sequencing

Two rounds of DNA extraction were performed with different protocols. The first round extracted DNA from the high salinity and chaotropic stress experiments and the second round extracted from the antibiotic experimental samples. For the high salinity and chaotropic stress experiments, frozen samples and ancestors of interest were spread onto LB/agar plates with a concentration of stressor matching their origin: blank LB/agar, 60 ppt NaCl LB/agar, or 200 mM $MgCl_2$. The frozen high salinity samples had come directly from MICALE. The frozen chaotropic stress samples were from broth cultures of the isolated colonies that were grown up for use in the adaptation analysis. Colonies from the agar plate cultures were inoculated into broth with the same concentration of stressor. Once turbid, 2 mL of broth culture was centrifuged, and the resulting pellet transferred into a new tube with sterile Milli-Q water. DNA extraction was performed using the Zymo *Quick*-DNA Fungal/Bacterial Miniprep Kit. Afterwards, the DNA concentration was measured with a Qubit. Samples with DNA concentrations less than 2 μg/uL were extracted again.

For the antibiotic experiment, frozen samples and ancestors of interest were transferred directly into sterile broth with a concentration of ciprofloxacin of 0, 0.6, or 15 μg/mL. It was not necessary to isolate a colony prior to the broth culture because these frozen stocks had come from the isolated cultures grown up for the adaptation analysis, rather than samples straight from MICALE. After incubating for two days at 37°C, 1.5 mL of the culture was transferred into a 2 mL Eppendorf tube and centrifuged. The resulting pellet was extracted into an effluent sample using the MagMAX Microbiome Ultra Nucleic Acid Isolation Kit, followed by DNA extraction with the KingFisher Flex system, and DNA concentration readings with a Qubit.

Extractions were sent to the UCSD Microbiome Core, who performed library preparation utilizing protocols and primers published on the Earth Microbiome Project website[40,41]. The UCSD Microbiome Core utilizes an Illumina NovaSeq 6000 belonging to the UC San Diego IGM Genomics Center that was purchased with funding from a National Institutes of Health SIG grant (#S10 OD026929).

Identification of Genetically Evolved Strains

Whole-genome resequencing analysis was performed using the *breseq* pipeline[42] to identify mutations present in MICALE-grown samples that were distinct from the ancestor. Illumina forward and reverse reads were quality filtered to remove reads with a quality score less than 30 using the sequence preprocessor fastp[43] and checked the results with FastQC[44]. The filtered reads were mapped in *breseq* to the *E. coli* K-12 MG1655 reference genome accessed from the National Center for Biotechnology Information (accession no. GCA_000005845.2)[33]. Out of the 24 samples sequenced from the high salinity and chaotropic stress runs, six samples had a mapped percentage less than 98%. All antibiotic samples had mapped percentages of less than 5%. Low mapped percentages indicated the sample identity was not *E. coli* MG1655. To identify the samples, the first and last ten lines of the fastq files were manually changed to fasta format then inputted the fasta sequences into a GenBank BLAST search[45]. Each search match was a bacterial genus different from *E. coli,* indicating that these samples were contaminated. For the non-contaminated MICALE-derived sequences, mutations identified by *breseq* were compared to the mutation results for the ancestor strain used to inoculate each run. Mutations overlapping with the ancestor were removed to reveal only mutations distinct from the ancestor.

RESULTS

Spatial Gradient of Stress in MICALE

Density or salinity measurements during each MICALE run show that a difference in density between the upper and lower regions was maintained throughout the run. In the high salinity run, the measured salinity of samples from the PL and IL valves remained constant and separated (Graph 1a). The refractometer salinity of samples from the IL layer, where top-layer media (TLM) meets bottom-layer media (BLM), stayed above 29 ppt NaCl for the run duration with an average salinity of 31 ppt NaCl. The PL samples, where media is majority TLM, stayed below 16 ppt NaCl with an average salinity of 14 ppt NaCl. A two-sample t-test compared the salinity of the two layers returns a p-value of 2.2e-16, confirming that the salinity of the two sampling valves is significantly different, despite the PL and IL valves being relatively close to each other (Table 1a).

For the chaotropic stress and antibiotic runs, the density of each layer fluctuated but overall remained separated and distinct (Graphs 1c and 1d). During the chaotropic stress run, the density of the IL, SL, and BL decreased slightly overtime while the PL density stayed relatively constant (Graph 1c). There were noted fluctuations in the density measurements in the first 100 hours that appear to be somewhat similar across the four layers. Despite these fluctuations in density, the PL and SL sample measurements from the chaotropic stress run never crossed; the SL is always denser than the PL for the entire month-long run.

For the chaotropic stress run, the average density of the PL, IL, SL, and BL layers was 0.9821, 1.0006, 1.0235, 1.0363 g/mL, respectively. The measured density of sterile and separated TLM and BLM controls was 0. 9923 and 1.0551 g/mL, respectively. We performed a pairwise independent t-test comparison of all the densities, the full results of which can be

viewed in Table 1b. Our t-test showed the PL and IL density measurements are statistically different the BLM control, the SL layer, and BL layer measurements with p-values less than 0.05. On the other hand, the PL and IL measurements are not distinct from the TLM control measurements with p-values greater than 0.05. Similarly, the BL densities are statistically indifferent from the BLM control but different from the TLM control. We expected this since media from the bottom of MICALE should be the densest and most static. The SL sample densities, on the other hand, are statistically different from both the TLM and BLM controls, as well as different from the other sampling layers. Despite there being no physical barrier between the TLM and BLM, the PL and IL sampling layers stayed indistinct from the TLM and remained statistically different from the denser media in the SL, BL, and BLM samples. Like in the high salinity run, the densities of adjacent sampling valves are statistically different: the PL and IL densities differ with a p-value of 5.4e-08 and IL and SL densities with a p-value of 2.7e-10.

Similar to the chaotropic stress run, the density measurements from the antibiotic run fluctuated but remained distinct between layers (Graph 1d and Table 1c). Sterile TLM and BLM media, before being added to MICALE, had respective densities of 0.9890 and 1.041 g/mL. The average density of the PL, IL, SL, and BL samples was 0.9921, 1.001, 1.025, and 1.029 g/mL, respectively. When compared for statistical difference, the PL densities are similar to the TLM control, and the SL and BL densities are similar to the BLM control and to each other (Table 1c). The IL sample densities are statistically different from both the TLM and BLM controls and each of the three other samples, like the SL densities from the chaotropic stress run.

Graph 1: Salinity and Density Measurements of MICALE Layers
a) Refractometer salinity measurements of PL (yellow) and IL (orange) samples during the high salinity stress run that lasted two weeks. Dashed line represents the average salinity. **b)** Regions of MICALE that sample names refer to. Density measurements of each of the four layers during **c)** the month-long run chaotropic stress run and **e)** the two-week long antibiotic run. For visual clarity, the SL and BL measurements are separated from the PL and IL measurements. Dashed lines represent the density measurements for the control media, TLM (light pink) and BLM (dark pink). Boxplots show the median and range of the density measurements.

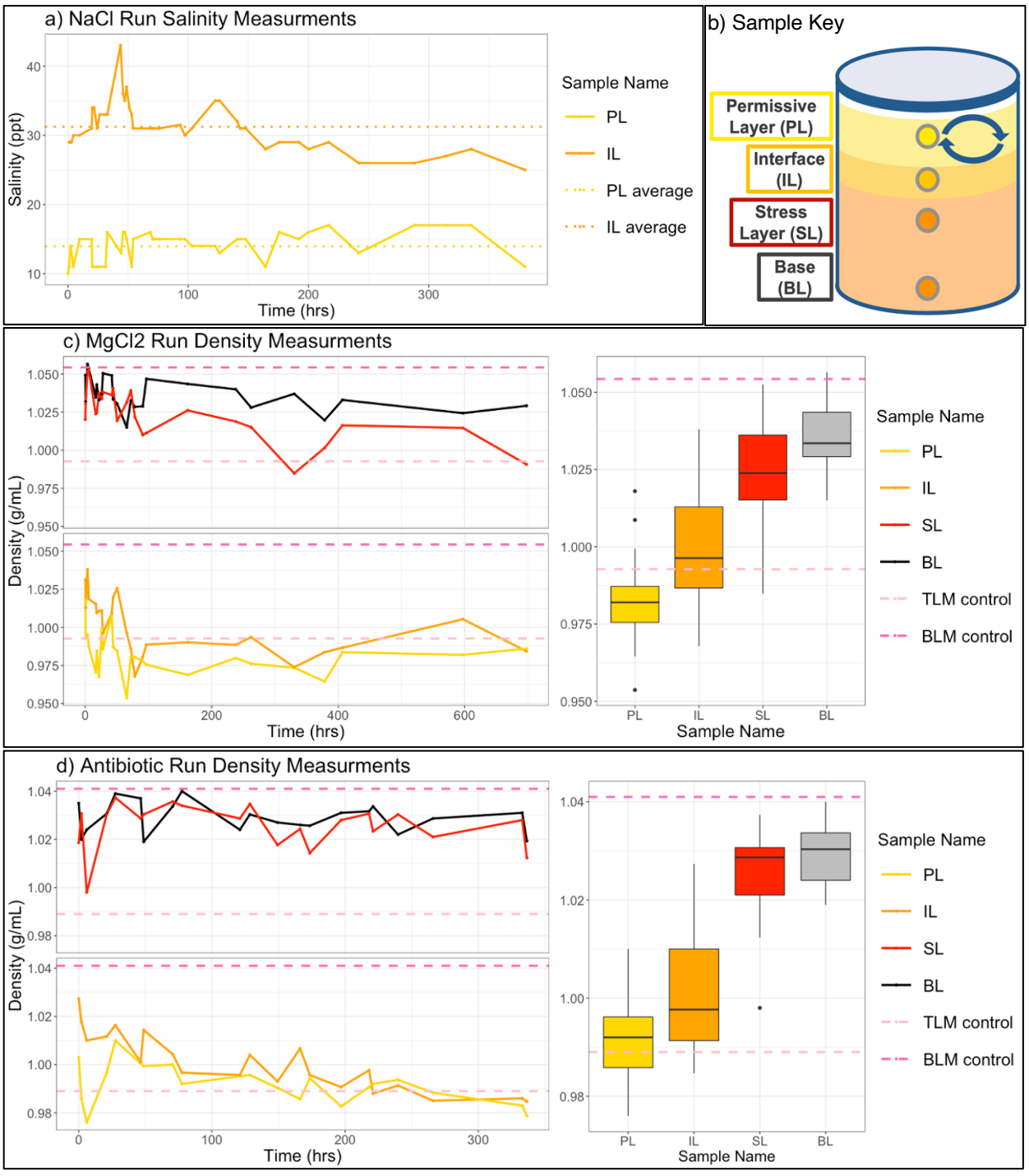

Table 1: Assessment of Differences of the Salinity or Density between Sample Layers
P-value results from independent t-test comparisons between the four sample layers, PL, IL, SL, and BL, and the control medias, TLM and BLM, for **a)** salinity measurements from the high salinity run, **b)** density measurements for the chaotropic stress run, and **c)** density measurements for the antibiotic stress run. For **a),** comparisons are only made between the PL and IL samples.

a) NaCl Salinity T test

	PL
IL	2.2e-16

b) $MgCl_2$ Density t test

	TLM	BLM	PL	IL	SL
BLM	0.00045	-	-	-	-
PL	0.28787	0.00030	-	-	-
IL	0.37448	0.00121	5.4e-08	-	-
SL	0.01203	0.01531	< 2e-16	2.7e-10	-
BL	0.00269	0.08984	< 2e-16	< 2e-16	5.7e-05

c) Antibiotic Density t test

	TLM	BLM	PL	IL	SL
BLM	0.02250	-	-	-	-
PL	0.49279	0.03213	-	-	-
IL	0.04237	0.04749	0.00276	-	-
SL	0.00069	0.22868	< 2e-16	6.2e-11	-
BL	0.00071	0.32574	< 2e-16	1.1e-14	0.24006

Cell Growth, OD_{600} measurements, Flow rate, and pH

OD_{600}, flow rate, and pH measurements with observed cell growth characteristics provided information on the dynamics of *E. coli* growth in the MICALE apparatus. For the high salinity stress run, the measured OD_{600} of the three sampled layers, the PL, IL, and SL, all increased within the first 25 hours (Graph 2a). Afterwards, the OD_{600} of the IL and SL samples stayed relatively stable, compared to the PL that spiked and dipped regularly. The media flow during the high salinity run fluctuated regularly, mostly caused from mechanical pump issues (Graph 3a). When compared with the measured flow rate, the OD_{600} of the PL spiked at times when the flow rate dropped off and stabilized when the flow rate was constant. The OD_{600} of the other samples did not show a similar trend with flow rate. Lastly, it is notable that cultures of the

high salinity stress MICALE samples took a long time to grow. Even when incubated at 37ºC, agar plates of the samples took over four days to grow small colonies.

For the chaotropic stress run, the OD_{600} of the PL, IL, SL, and BL layers increased within the first 25 hours then began to stabilize (Graph 2c). The OD_{600} for the PL and BL sample layers frequently spiked, as seen in the PL OD_{600} at 500 hours, for example. These spikes occurred when goopy aggregates, suspected to be extracellular polysaccharides (EPS) were collected in the sample vials thereby altering the turbidity of the liquid sample and producing a high OD_{600} measurements (Figure A1). Majority of these cell aggregates were seen near the top of MICALE, attached to the walls and collecting at the bottom of MICALE. Consequently, the PL and BL OD_{600} measurements were affected the most, causing the spikes seen in Graph 2b. These spikes in the data make it difficult to draw comparisons between OD_{600} and the flow rate.

The OD_{600} measurements during the antibiotic run were much lower than the other runs (Graphs 2d and 2e). The IL, SL, and BL layer OD_{600} rose to just over 0.08 absorbance in the last 200 hours, compared to the high salinity and chaotropic stress runs that reached well over 0.1 absorbance in the first 48 hours. Meanwhile, cells grew in high densities in the in-valve and tubing that fresh media flowed through, clogging the filter; cells were escaping from the ciprofloxacin inside MICALE, following the flow of antibiotic-free media. Like the high salinity run, the antibiotic PL OD_{600} peaked during times when the flow rate dipped, for example at around 125 hours there is a large spike in PL OD_{600} when the flow rate had all but stopped due to mechanical issues (Graph 3c). OD_{600} measurements for all antibiotic sample layers rose in the last 200 hours then appear to drop by the final sample. This drop is also seen in the final density measurements. It is important to note that the day prior to the final sample, when the OD_{600} measurements appear to rise, it was observed that the filter had clogged sometime in the previous

48 hours and there was no media flow. The filter was fixed to allow media to flow for another 24 hours before the final sample was taken. The return of the flow rate is presumably what decreased the cell density (OD_{600} measurements) by the time of the final sample.

Noting that waste from the salinity and chaotropic stress runs smelled fermented, we measured pH during the antibiotic run because we suspected that cells may be undergoing anerobic fermentation. The starting pH measurements for the antibiotic stress samples were 6.93, 6.93, 6.90, and 6.95 for the PL, IL, SL, and BL samples, respectively (Graph 4). The pH measurements for the lower two valves stayed between 6.7 and 7 at the start of the run. However, starting at around 125 hours, the pH in the IL started to decrease, followed by the other layers at around 200 hours. The PL layer decreased somewhat but continued to fluctuate between 6.1 and 6.7. The IL, SL, and BL layers, on the other hand, decreased sharply. The IL sample region had the lowest pH measurement of 5.45 at 266 hours. The final pH measurements at the end of the run for the PL, IL, SL, and BL samples were 6.6, 5.74, 5.67, and 6.28, respectively.

Graph 2: OD_{600} Measurements by Sample Layer
OD_{600} measurements of each sample layer for the duration of the **a)** high salinity, **c)** chaotropic, and **d,e)** antibiotic stress MICALE runs. Dashed lines represent the average OD_{600} measurements for the TLM (light pink) and BLM (dark pink) controls. **d)** All four samples from the antibiotic run. **e)** Antibiotic samples without PL samples for visual clarity. **b)** The region of MICALE that samples come from.

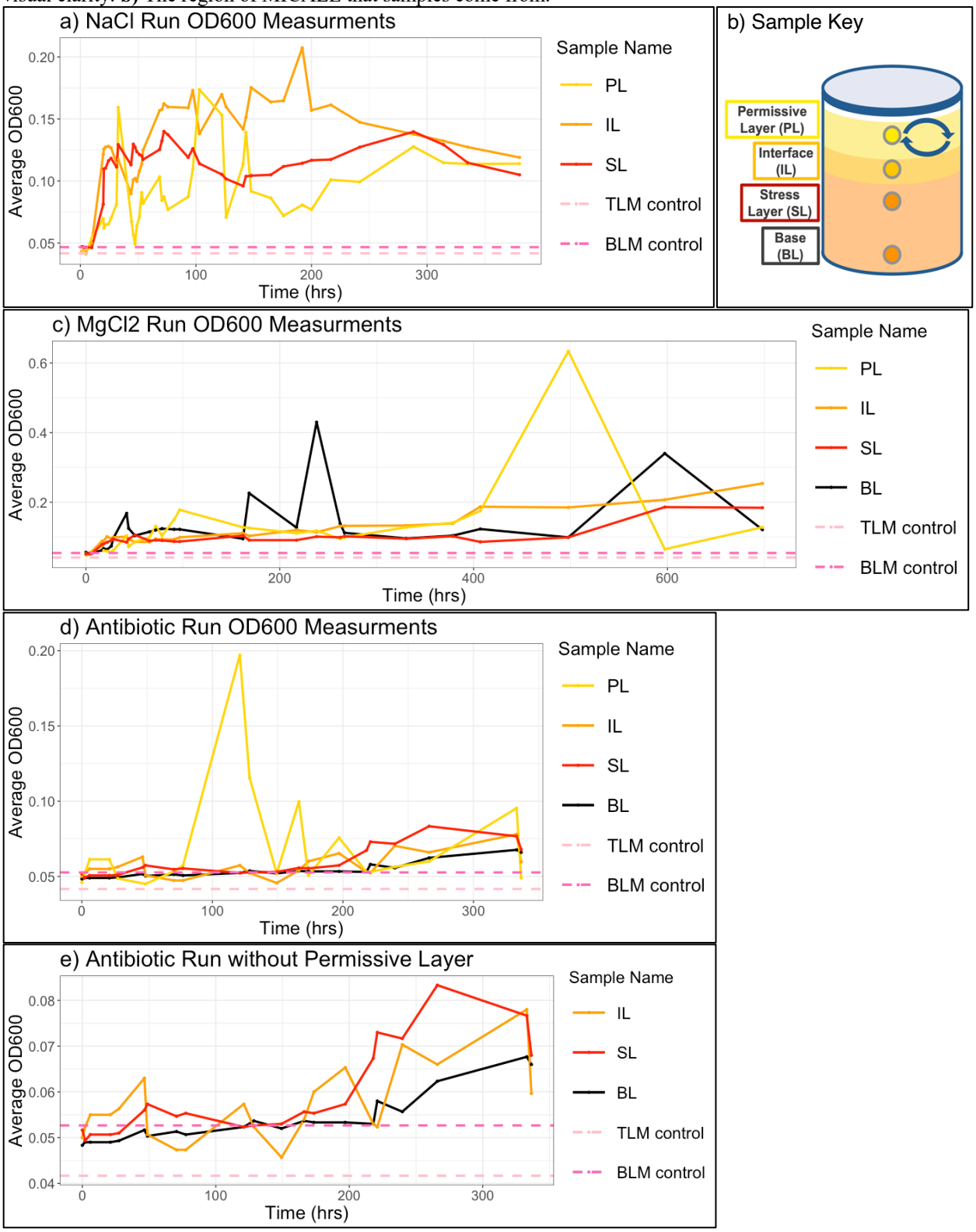

Graph 3: Media Flow Rate with Permissive Layer OD_{600}
Shown in purple dashed lines, the estimated flow rate (mL/hr) of media during runs, calculated by measuring the waste in the collection bottle divided by the time since the last measurement. The yellow line shows the OD_{600} measurements of the PL layer for the high salinity **a),** chaotropic **b),** and antibiotic **c)** stress runs for a comparison between the biomass in the upper region of MICALE with the flow of media that also occurred in the upper region.

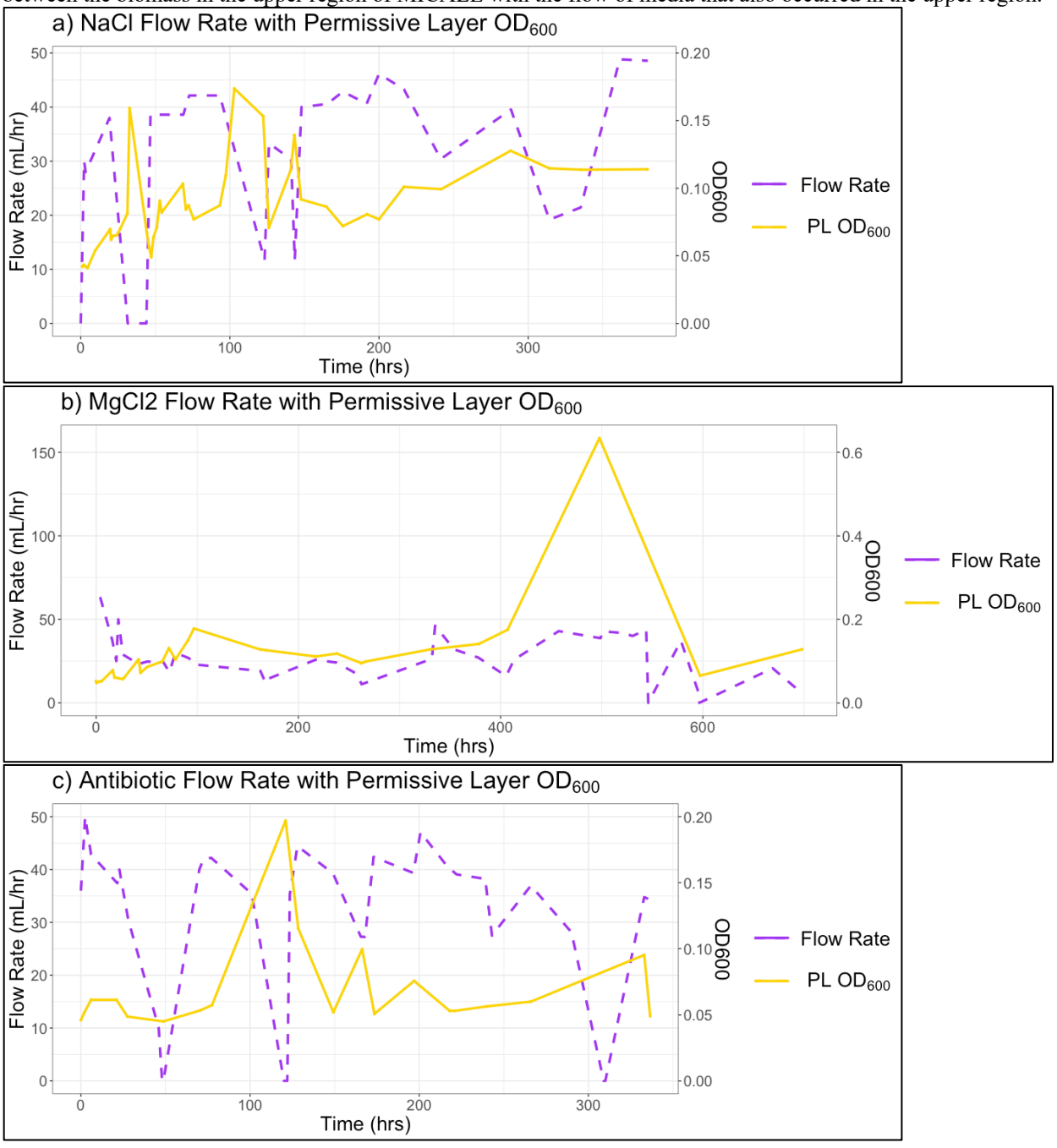

Graph 4: Antibiotic Run pH Measurements
The measured pH of each sample layer, the PL, IL, SL, and BL, during the antibiotic stress run that lasted two weeks. The initial pH measurements were 6.93, 6.93, 6.90, and 6.95 and the final were 6.60, 5.74, 5.67, and 6.28 for the PL, IL, SL, and BL, respectively.

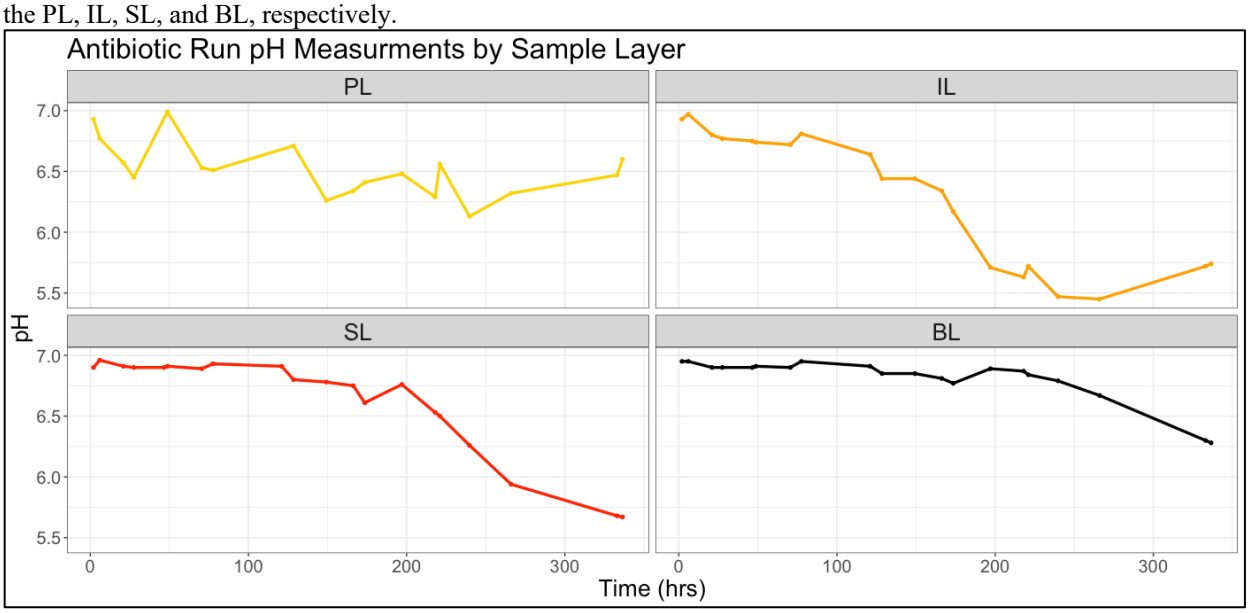

High Salinity Adaptation Analysis

During the high salinity adaptation analysis, isolated MICALE samples grew in a higher concentration of NaCl than the ancestor (Figure 7). The samples grown in the adaptation analysis were three samples from the end of the run, PL, SL_{final}, and BL, one sample from the first 25 hours, SL_{early}, and the Ancestor (Table 2). Over four days these samples were grown in triplicate in media with salinity concentrations of 5, 45, 60, 75, and 90 ppt NaCl (Figure 7a). The three samples taken at the end of the MICALE run showed growth in every level of salinity with all average cell proliferation values over 5% (Figure 7c). For each sample the cell proliferation, denoting the amount of biomass, decreased with increasing salinity, except for the PL and SL_{final} that increased their average cell proliferation values from 75 to 90 ppt NaCl. The Ancestor and SL_{early} sample reached average cell proliferation values less than 5% in 90 ppt NaCl and 75 and 90 ppt NaCl, respectively, denoting no growth.

There was remarkable variation in the shape of the OD_{600} curves between samples, especially in higher salinities (Figure 7a). Between samples, the time at which exponential growth occurred, the rate of exponential growth, and total amount of cellular biomass differed, forming unique growth curve shapes. For all samples, the average exponential growth rate decreased in similar fashion from 5 to 60 ppt NaCl, except for the PL sample that did not decrease in 60 ppt NaCl (Figure 7b). Starting at 75 ppt NaCl, however, we observed greater variation in average exponential growth rate as the samples decreased or increased their growth rate different amounts: from 60 to 75 ppt NaCl, the PL, SL_{early}, and Ancestor decreased their exponential growth rate by 35.0, 28.9, and 22.9 percent, respectively, whereas the SL_{final} decreased by only 7.8 percent and the BL increased by 7.7 percent. The resulting relative growth rate for the PL, SL_{early}, Ancestor, SL_{final}, and BL was 18.3, 3.1, 15.5, 19.7, and 40.2 percent. Some samples decreased their exponential growth rate with increasing salinity whereas others maintained or even increased their exponential growth rate.

In 75 ppt NaCl, the SL_{final} and PL produced curves with varying steepness but overall had longer and lower slopes and very similar exponential growth rates (Figure 7a). The Ancestor and BL sample, on the other hand, had more defined areas of exponential growth and a leveled-off stationary phase. Starting just before 50 hours, the OD_{600} measurements for one Ancestor measurement in 75 ppt NaCl looked fuzzy, indicating instrumental noise likely from an external factor like evaporation. These measurements were filtered out before statistical analysis. In 90 ppt NaCl, the curves for the PL, SL_{final}, and BL samples were shorter, showing signs of growth much later in time. The SL_{final} and BL samples in 90ppt showed a lot of variation within the triplicate wells. Abnormal, small spikes in the data, such as that seen at around 30 and 90 hours

for the BL and SL_{final}, respectively, could not be ruled out as instrument noise and were included in further analysis.

The BL sample's average exponential growth rate increased from 60 to 75 and to 90 ppt NaCl with relative values of 32.5, 40.2, and 42.8 percent, respectively (Figure 7b). On the other hand, the relative cell proliferation of the BL sample decreased as salinity increased (Figure 7c); in higher salinities, the BL sample reached higher maximum growth rates but lower overall biomass. The PL and SL_{final} sample reached their lowest maximum growth rate in 75ppt with percent responses of 18.3%, and 19.7%. In 90 ppt NaCl, both samples increased their exponential growth rates to 25.9% and 27.0%. The ancestor's response was more typical, producing its lowest exponential growth rate and cell proliferation values in the highest concentration of salinity.

The ED50 values from the NaCl adaption analysis, listed in Table 3, showed nearly an inverse relationship between the ranking of sample's ED50s for exponential growth rate and cell proliferation (Figures 7d and 7e). The Ancestor had the highest ED50 calculated from the exponential growth rate, with a 50% decrease in the max growth rate occurring at a salinity of 53.5 ppt NaCl (Figure 7d). On the other hand, the Ancestor had the lowest cell proliferation ED50 value of 40.3 ppt NaCl, excluding the PL sample which had a very low value (Figure 7e). Opposite of the Ancestor, the BL sample had the lowest growth rate ED50 value of 46.0 ppt NaCl and highest cell proliferation ED50 of 52.7 ppt NaCl, excluding the SL_{early} and PL anomalies. The SL_{final} sample had similar ED50 concentrations of 48.8 and 48.3 for growth rate and cell proliferation, respectively. The SL_{early} strain had the lowest growth rate ED50, matching the fact that it was the only sample unable to grow in 75 ppt NaCl. The PL sample had a very low cell proliferation growth rate ED50 of 33.0, compared to its growth rate ED50 of 50.9. These

ED50 values matched the trends extracted from the PL curves: from 60 to 75 ppt NaCl, the PL sample's average cell proliferation decreased whereas the average exponential growth rate stayed nearly the same.

Chaotropic Stress Adaptation Analysis

Figure 9 shows the results of the chaotropic stress adaptation analysis in which the samples were grown for four days in 0, 200, 250, and 300 mM $MgCl_2$. The samples selected for the $MgCl_2$ adaptation analysis can be found in Table 4. No samples showed signs of growth in 300 mM $MgCl_2$, the starting concentration of magnesium chloride in the BLM of MICALE. Most of the samples did not grow in 250 mM $MgCl_2$ either. Only the Anc-000 and PL-000-Col1 showed signs of growth in 250 mM $MgCl_2$; The PL-000-Col1 had one well that showed a rise then fall of OD_{600} in the last 60 hours of the run. The Anc-000 triplicate wells in 250 mM $MgCl_2$ had an early bump and fall in OD_{600} in the first 24 hours then slowly rose over time (Figure 9a, third row). While the bump may be due to growth, the slow rise following the bump could be because of evaporation. Anc-000 was plated on the edge of the 96-well plate, the wells that are the most affected by evaporation (Figure A2). If there was cell growth at the start, evaporation would increase the cell density in the wells without requiring any cell growth. Other measurements that were likely affected by evaporation were the Anc-000 and SL-200-W4 curves in blank media (Figure 9a, top row). Both samples have wells with large abnormal peaks near the end of the run and both wells were plated on corners of the 96-well plate. The corner wells were observed to be the most affected by evaporation, causing the large OD_{600} peaks (Figure A2). The other samples in blank LB also appear to be affected by evaporation, just not as much as the corner wells; small rises in OD_{600} can be observed in the measurements of other samples in blank

LB, such as for IL-000-W4 and SL-200-W4. All samples had one well on the outer row of the plate. Since all samples in blank LB appeared to be somewhat effect from evaporation, we filtered out the last 20 hours of measurements for all samples in blank LB.

When plated on agar, both the Ancestor and PL samples grew at least one colony on plates with 250 mM $MgCl_2$ (Figure 8a). It was therefore not surprising that these samples showed growth in 250 mM $MgCl_2$ during the adaptation analysis (Figure 9a, third row). However, these two samples had multiple isolates in the adaptation analysis (Anc-000, Anc-200, PL-000-Col1, PL-000-Col2, and PL-200) that were unable to grow in 250 mM $MgCl_2$. It was unexpected that the only two isolates that grew in 250 mM $MgCl_2$ were samples cultured in media without magnesium chloride.

PL-000-Col1 was a large, spreader colony and PL-000-Col2 was a smooth, round colony (Figure 8b). PL-000-Col2 could not grow in any media with $MgCl_2$ whereas PL-000-Col1 was one of the best performing isolates. The OD_{600} curves in blank LB for PL-000-Col1 and PL-000-Col2 are shaped different than the other curves (Figure 9a); most samples had smooth, "L" shaped curves while the PL samples had boxy, jagged measurements. WGS results identified these two PL samples as contaminated with *Pseudomonas* (Table 4). PL-000-Col1 had the lowest OD_{600} measurements in blank LB. In 200 mM $MgCl_2$, most samples had "S" shaped curves whereas PL-000-Col1 had curves that were more vertical. This could have affected the downstream exponential growth rate and cell proliferation calculations by inflating the relative response of the sample in magnesium chloride (Figures 9b and 9c); in 200 mM $MgCl_2$, PL-000-Col1 reached an average cell proliferation value of 130% the cell proliferation value in blank LB.

When averaged between triplicates, the OD_{600} of the PL-000-Col1, PL-200, and SL-W4 reached a higher average in 200 mM $MgCl_2$ than in blank LB media. The highest OD_{600} reached

was one triplicate well for the PL-000-Col1 sample with a maximum OD_{600} of 1.479 whereas the SL-W2 had the highest average OD_{600} of 1.399. Both maximums were obtained in media with 200 mM $MgCl_2$. Unsurprisingly, the SL-W2 sample had the highest relative cell proliferation in 200 mM $MgCl_2$ of 140.8% (Figure 9c). The PL-000-Col2 was the only sample that had a relative cell proliferation less than 5% in 200 mM $MgCl_2$, considered as no growth. For the other samples in 200 mM $MgCl_2$, the cell proliferation values were 74.0, 94,0, 130.3, 129.3, 86.5, and 102.2 percent for Anc-000, Anc-200, PL-000-Col1, PL-200, IL-000, and SL-W4, respectively. The values for the average exponential growth rate in 200 mM $MgCl_2$ were 41.7, 32.0, 54.0, 26.5, 33.5, 22.2, and 42.3 percent for the Anc-000, Anc-200, PL-000-Col1, PL-200, IL-000, SL-W2, and SL-W4, respectively (Figure 9b).

Substantial growth only occurred in blank media and 200 mM $MgCl_2$ thereby producing dose-response curves and ED50 values that are very similar, depending on only the growth obtained in 200 mM $MgCl_2$ to determine the outcome of the logistic fit (Figures 9d and 9e). The exception being the PL-000-Col2 sample that could not grow in magnesium chloride, producing much lower ED50 values. The ED50 values represent the concentration of $MgCl_2$ at which the exponential growth rate or cell proliferation response in media without $MgCl_2$ is decreased by 50%, determined by a logarithmic fit of the data (Table 5). Excluding PL-000-Col2, all exponential growth rate ED50 values fell between the Anc-000 value of 183.2 and that for PL-000-Col1 of 203.0, the highest value. The Anc-200 growth rate ED50 of 189.0 is slightly higher than that from the Anc-000 of 183.2, a similar trend seen for the cell proliferation where the Anc-200 is close but slightly higher than the Anc-000 with ED50 values of 215.8 and 214.1, respectively. For relative cell proliferation ED50 values, there is slightly more variation with samples ranging between 214.1 from the Anc-000 and IL-000-W4 and 240.2 for PL-000-Col1.

PL-000-Col1 also has the highest ED50 for relative cell proliferation with a $MgCl_2$ concentration of 240.2. The relative cell proliferation ED50 values for the PL-200-W4, SL-200-W2, and SL-200-W4 are close behind with ED50 values of 234.7, 235.2, and 234.9, respectively. The IL-000 sample has an ED50 cell proliferation value that is farther from the other samples and closer to the ancestor samples with a value of 214.1 Lastly, like its growth rate ED50, the PL-000-Col2 sample had a very low ED50 value of 128.1.

Antibiotic Stress Adaptation Analysis

The two adaptation analyses for the antibiotic samples, described in Table 6, have similar trends across trials (Figure 11). In both trials, the observed growth response in ciprofloxacin increases from top to bottom in MICALE; the ancestor had no resistance to ciprofloxacin, the upper regions of MICALE, mainly PL, had mild resistance, and the samples from lower in MICALE, IL, SL, and BL, had the highest amount of resistance. In both trials, the IL-15-Col1, IL-15-Col2, SL-15, and BL-15 samples had OD_{600} curves in ciprofloxacin up to 100 xMIC. These same samples also each had at least one well with a small OD_{600} measurement in 1000 xMIC, starting at about 60 hours. The ancestor, on the other hand, did not show signs of growth in any media with ciprofloxacin in both trials. Lastly, the PL-00, PL-0.6, and IL-00 samples had mixed responses between the two trials but overall could not grow in 100 or 1,000 xMIC.

All samples had similar-looking colony morphologies, regardless of the amount of ciprofloxacin in the agar media (Figure 10a). The exception is the IL sample which grew colonies with diverse morphology (Figure 10b). This diversity, however, was only seen on agar with 250 xMIC ciprofloxacin and not on the plates with lower amounts of ciprofloxacin.

During growth in the adaptation analysis, many of the samples formed visible clumps, possibly from biofilm or EPS production. This caused quick jumps in the OD_{600} measurements that did not correspond with an increase in the cell count. Before further analysis, OD_{600} measurements, therefore, were filtered out starting at the time of the first jump.

A similar pattern of increasing resistance from top to bottom in MICALE is observed in the average cell proliferation values (Figures 12c and 12d). In trial 1, the Ancestor, PL-00, PL-0.6, IL-00, IL-15-Col1, IL-15-Col2, and BL-15 samples reached a cell proliferation value less than 5% at 10, 10, 100, 100, 1000, 1000, and 1000 xMIC, respectively (Figure 12c). Therefore, these samples were considered to have no growth at those concentrations. The SL-15 sample in trial 1 grew in all concentrations, obtaining cell proliferation values over 5%. In 1000 xMIC, the IL-00 had an average cell proliferation of 5.3% which could indicate growth. However, the average cell proliferation in 100 xMIC was only 0.6% so the observed increase in cell proliferation in the higher antibiotic concentration is likely due to factors other than cell growth, such as evaporation.

While most of the lower-layer samples had cell proliferation values less than 5% in 1000 xMIC in trial 1, these samples were able to reach average cell proliferation values above 5% in trial 2 (Figure 12d). The IL-15-Col1, SL-15, and BL-15 from trial 2, therefore, are considered to have growth in all levels of ciprofloxacin tested. The other samples in trial 2, for the Anc, PL-00, PL-0.6, IL-00, and IL-15-Col2, reached average cell proliferation values lower than 5% in 10, 100, 100, 100, and 1000 xMIC, respectively.

The highest overall exponential growth rate reached in trial 1 was 107.5% by IL-15-Col2 in 10 xMIC (Figure 12a). Despite this increase in growth rate, the cell proliferation value in 10 xMIC for IL-15-Col2 was only 61.5% (Figure 12c). IL-15-Col2 also had the fastest

exponential growth rate in trial 2, reaching a growth rate in 10 xMIC that is 101.6% the rate reached in blank LB (Figure 12b). The cell proliferation value, however, was only 90.9% of the cell proliferation response seen in blank LB (Figure 12d). In media with 100 and 1000 xMIC ciprofloxacin, however, the IL-15-Col2 does not hold its spot as the sample with the highest growth rate. Instead, in 100 xMIC, IL-15-Col1 and BL-15 had the highest relative growth rate of 54.4% in trial 1 and 66.6% in trial 2, respectively.

In trial 2, the four lower-region samples that showed growth in high levels of antibiotics, IL-15-Col1, IL-15-Col2, SL-15, and BL-15, all had very similar growth rates in blank media and 10 xMIC ciprofloxacin (Figure 12b). In 10 xMIC, their growth rates were 90.5, 101.6, 90.6, and 97.2 percent of that in media without antibiotic, respectively. With exponential growth rates each above 90% their growth rate in blank media, these four samples are barely affected by ciprofloxacin at 10 xMIC. Their cell proliferation values in 10 xMIC were also very similar to that in blank LB (Figure 12d).

The dose-response curves and ED50 values from the antibiotic analysis OD_{600} curves were greatly affected by a sample's response in 10 xMIC and 100 xMIC. The dose-response curves were fit over a wide range of ciprofloxacin concentrations, 0 to 1000 xMIC. Therefore, there are some drastically different calculations for ED50 for samples that performed slightly different in trial 1 versus trial 2 (Figure 13 and Table 7). For example, the BL-15 sample performed much better in trial 2, especially in 100 xMIC, resulting in and ED50 value of 172 xMIC for the growth rate and 112 xMIC for cell proliferation. In trial 1, however, the ED50 values for BL-15 were 20 for growth rate and 21 for cell proliferation. There are also differences in ED50 values between the growth rate and cell proliferation for one sample in the same trial. For example, in trial 2 the IL-15-Col1 sample had a growth rate ED50 value of 95 and a cell

proliferation ED50 value of 186 (Table 7). This major difference is due to the sample's large decline in growth rate from 10 to 100 xMIC (Figure 12a) compared to a smaller decrease in cell proliferation (Figure 12b).

Just like the adaptation analysis growth curves, the ED50 values show clear grouping of the lower four samples, IL-15-Col1, IL-15-Col2, SL-15, and BL-15, with higher resistance to ciprofloxacin (Figure 13). The MICALE samples that could not grow past 10 xMIC, PL-00, PL-0.6, and IL-00, group lower than the four samples listed prior but still have large ED50 values than the Ancestor that showed no growth in any media with antibiotic.

Since the Ancestor could not grow in any ciprofloxacin, the data could not be properly fit to a logarithmic dose-response curve. Instead, we used the growth data from the MIC test to fit dose-response curves and obtain ED50 values. We wanted multiple ED50 values for the Ancestor to perform downstream statistical significance tests. The triplicate wells for the MIC test were split into three groups to fit three dose-response curves for three ED50 values. During the MIC test, the Ancestor was grown on a very fine scale of ciprofloxacin, resulting in ED50 values less than 0.3 xMIC, or 0.018 μg/mL ciprofloxacin. These ED50 values make sense because they are less than our observed MIC value of 0.06 μg/mL and the literature's value of 0.05 μg/mL.

Figure 7: High Salinity Adaptation Analysis
a) High salinity stress adaptation analysis OD_{600} Curves. Columns from left to right are the samples Ancestor (Anc,) SL_{early}, PL, IL, SL_{final}, and BL (Table 2). Rows are separated by the concentration of NaCl in the growth medium: 5, 45, 60, 75, and 90 ppt NaCl from top to bottom. Samples are colored based on their origin: Ancestor (blue), PL (yellow), SL (red), and BL (black). Individual lines represent one well of three triplicate wells inoculated for each sample in each media type for a total of 96-wells. Values extrapolated from the OD_{600} curves are shown as dots and solid lines of the **b)** Average Exponential Growth Rate and **c)** Average Cell Proliferation values of a sample. Triplicate wells are averaged and expressed as a percentage of the response in media without any added NaCl (5 ppt NaCl). Vertical dotted lines show the concentration of NaCl at which the ED50 for each sample was calculated. Log-transformed ED50 values were calculated by fitting a logarithmic dose-response curve to the **d)** exponential growth rate and **e)** cell proliferation values. ED50 values are shown numerically in Table 3.

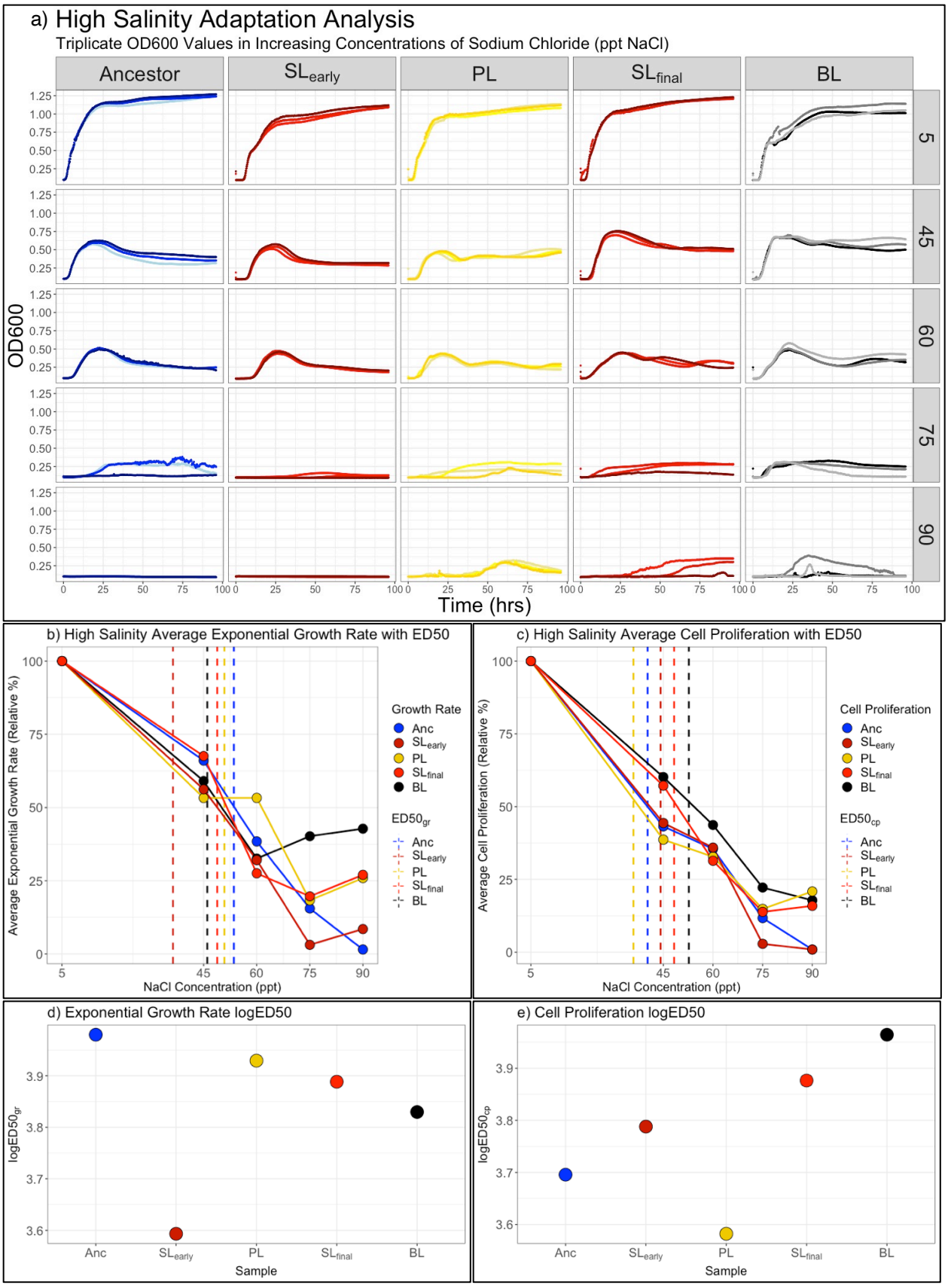
a) High Salinity Adaptation Analysis
Triplicate OD600 Values in Increasing Concentrations of Sodium Chloride (ppt NaCl)
Ancestor
SLearly
PL
SLfinal
BL
5
45
60
75
90
OD600
Time (hrs)
b) High Salinity Average Exponential Growth Rate with ED50
Average Exponential Growth Rate (Relative %)
NaCl Concentration (ppt)
Growth Rate
Anc
SLearly
PL
SLfinal
BL
ED50gr
c) High Salinity Average Cell Proliferation with ED50
Average Cell Proliferation (Relative %)
Cell Proliferation
ED50cp
d) Exponential Growth Rate logED50
logED50gr
Sample
e) Cell Proliferation logED50
logED50cp

Table 2: Summary of High Salinity Stress Samples
Descriptions of the samples from the high salinity run used in further analysis. White rows highlight samples used in the adaptation analysis (Figure 7). Grey rows are samples that were only sequenced. Before the adaptation analysis and DNA extraction, colonies were selected from the samples grown on media with different concentrations of NaCl, indicated by the "NaCl in Culture Media (ppt)". The column for *breseq* results describes if the sample was fully mapped to the *E. coli* reference genome or contaminated. For fully mapped samples, the number of distinct mutations, if at all, is listed. A description of the mutations can be seen in Table 8. Samples that did not map to the reference genome have the highest-matching BLAST result listed as the likely identity of the sample.

Name in Analysis	Sample Origin	Time of Sample (days)	NaCl in Culture Media (ppt)	*Breseq* Results
Anc	Ancestor	-	5	Fully mapped
SL_{early}	Stress Layer	1	60	Partially contaminated: E. coli and *Bacillus*
PL	Permissive Layer	14	60	Contaminated: *Bacillus*
SL_{final}	Stress Layer	14	60	Contaminated: *Bacillus*
BL	Base	14	60	Fully mapped: no distinct mutations
PL-05	Permissive Layer	14	5	Fully mapped: no distinct mutations
IL-05	Interface	14	5	Fully mapped: three mutations
IL-60	Interface	14	60	Contaminated: *Bacillus*

Table 3: NaCl ED50 Values (ppt NaCl)
The exponential growth rate and cell proliferation ED50 values for each sample, calculated from the OD_{600} curves from the adaptation analysis. The ED50 value represents the concentration of NaCl at which a response is 50% of the observed response in LB media (5 ppt NaCl).

Sample Name	Relative Growth Rate ED50	Relative Cell Proliferation ED50
Ancestor	53.5	40.3
SL_{early}	36.4	44.2
PL	50.9	36.0
SL_{final}	48.8	48.3
BL	46.0	52.7

a)

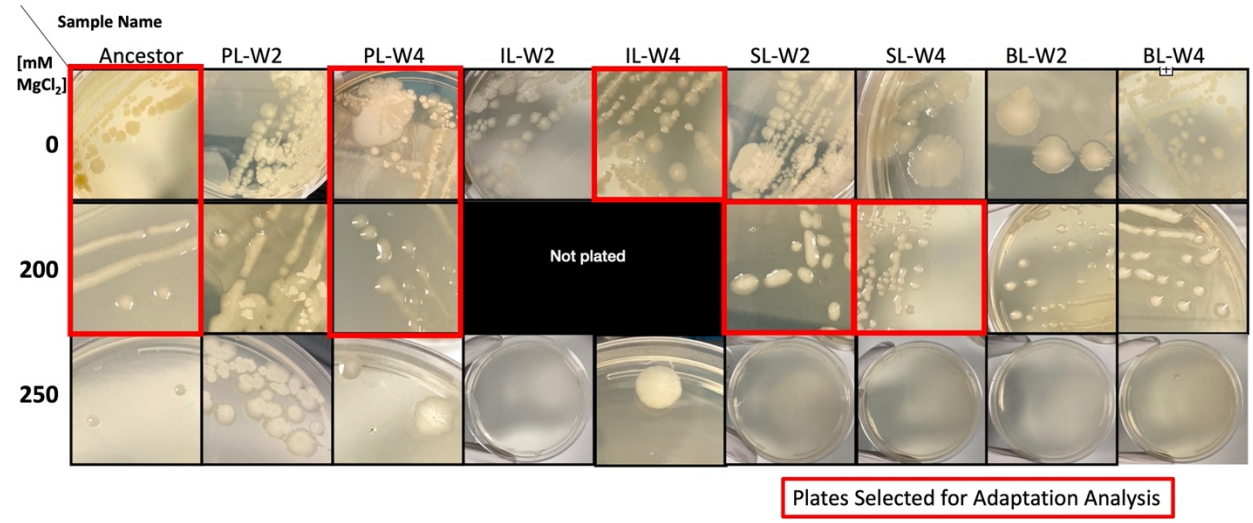

b)

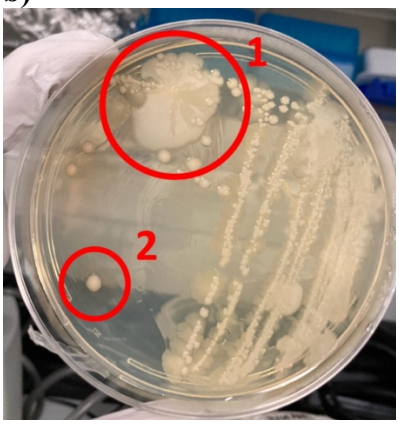

Figure 8: Colony Morphologies of Chaotropic Stress Samples
a) Photos of agar plates streaked with samples from the chaotropic stress run. The origin of the sample is listed at the top: permissive layer (PL), interface (IL), stress layer (SL), base (BL), and the ancestor strain. The number following the sample origin represents at which week during the run the sample was collected (Table 4). Each sample was plated on LB/agar with 0, 200, and 250mM $MgCl_2$, except for those indicated. Many samples did not grow in 250mM $MgCl_2$. Red boxes highlight samples selected for the adaptation analysis (Figure 9a). **b)** a close-up of PL-W4 plate on 0 mM $MgCl_2$ agar, highlighting the colonies selected for analysis. Colony 1 has spread out very far in an unsymmetrical pattern whereas colony 2 remained smooth and round.

Figure 9: Chaotropic Stress Adaptation Analysis
a) Chaotropic stress adaptation analysis OD_{600} Curves. Columns from left to right are the samples Anc-000, Anc-200, PL-000-Col1, PL-000-Col2, PL-200-W4, IL-000-W4, SL-200-W2, and SL-200-W4 (Table 4). Rows are separated by the concentration of $MgCl_2$ in the growth medium: 0, 200, 250, and 300 mM $MgCl_2$ from top to bottom. Samples are colored based on their origin: Ancestor (blue), PL (yellow), IL (orange), and SL (red). Individual lines represent one well of three triplicate wells inoculated for each sample in each media type for a total of 96-wells. Values extrapolated from the OD_{600} curves are shown as dots and solid lines of the **b)** Average Exponential Growth Rate and **c)** Average Cell Proliferation values of a sample. Triplicate wells are averaged and expressed as a percentage of the response in media without any $MgCl_2$. Vertical dotted lines show the concentration of $MgCl_2$ at which the ED50 for each sample was calculated. Log-transformed ED50 values were calculated by fitting a logarithmic dose-response curve to the **d)** exponential growth rate and **e)** cell proliferation values. ED50 values are shown numerically in Table 5.

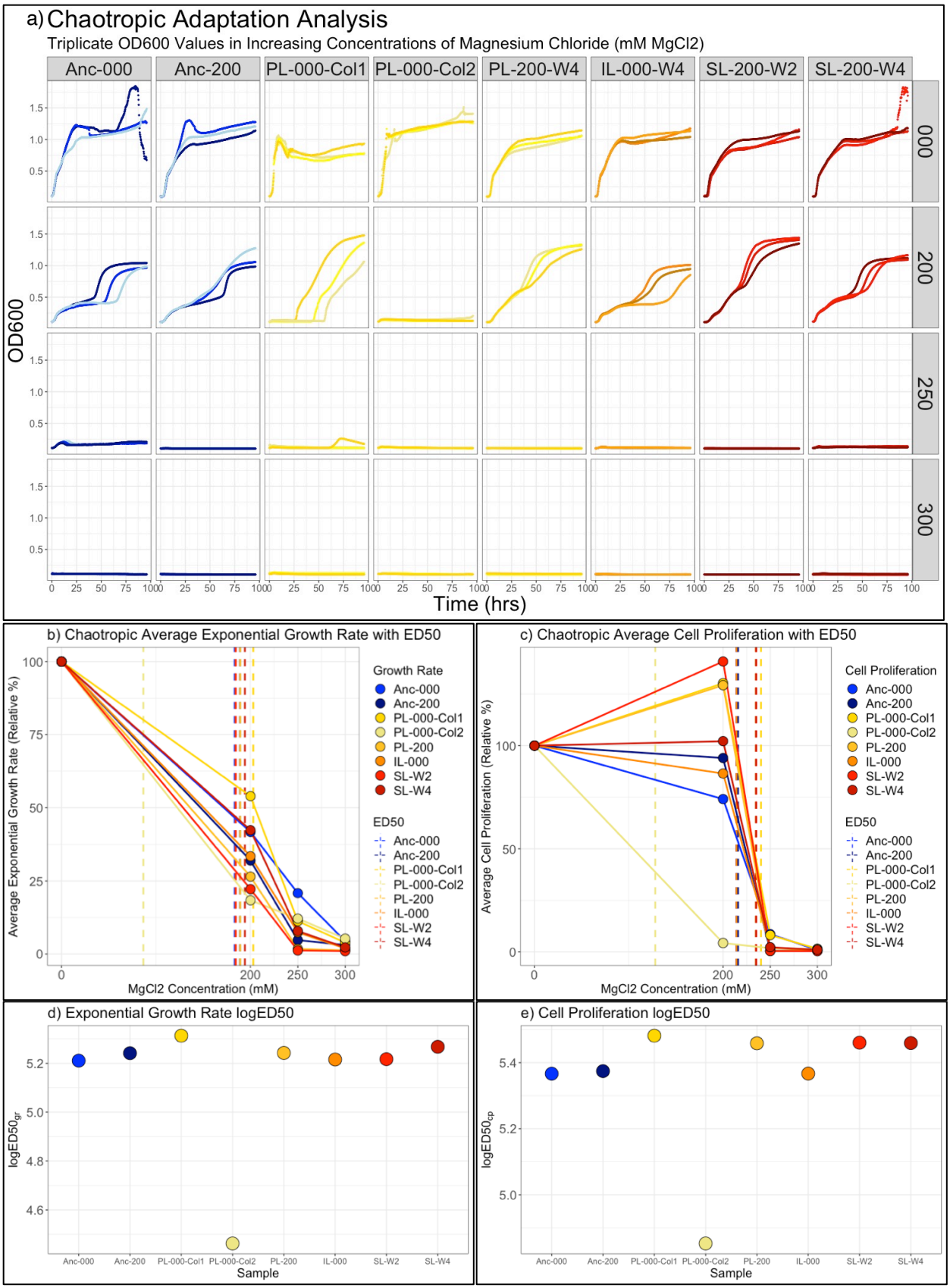
a) Chaotropic Adaptation Analysis
Triplicate OD600 Values in Increasing Concentrations of Magnesium Chloride (mM MgCl2)
Anc-000
Anc-200
PL-000-Col1
PL-000-Col2
PL-200-W4
IL-000-W4
SL-200-W2
SL-200-W4
000
200
250
300
OD600
Time (hrs)
b) Chaotropic Average Exponential Growth Rate with ED50
Average Exponential Growth Rate (Relative %)
MgCl2 Concentration (mM)
Growth Rate
Anc-000
Anc-200
PL-000-Col1
PL-000-Col2
PL-200
IL-000
SL-W2
SL-W4
ED50
c) Chaotropic Average Cell Proliferation with ED50
Average Cell Proliferation (Relative %)
MgCl2 Concentration (mM)
Cell Proliferation
d) Exponential Growth Rate logED50
logED50gr
Sample
e) Cell Proliferation logED50
logED50cp
Sample

Table 4: Summary of Chaotropic Stress Samples
Descriptions of the samples from the chaotropic run used in further analysis. White rows highlight samples used in the adaptation analysis (Figure 9a). Grey rows are samples that were just sequenced. The name of the sample indicates where the sample came from (Ancestor, PL, IL, SL, or BL,) the concentration of $MgCl_2$ that the sample was cultured in before analysis (000 or 200 mM,) and the time that the sample was taken (two weeks or four weeks.) Samples PL-000-Col1 and PL-000-Col2 indicate separate colonies with different morphologies from the same culture plate (Figure 8b). The column for *breseq* results describes if the sample was fully mapped to the *E. coli* reference genome or contaminated. For fully mapped samples, the number of distinct mutations, if at all, is listed. A description of the mutations can be seen in Table 8. Samples that did not map to the reference genome have the highest-matching BLAST result listed as the likely identity of the sample.

Name in Analysis	Sample Origin	Time of Sample (weeks)	$MgCl_2$ in Culture Media (mM)	*Breseq* results
Anc-000	Ancestor	-	0	Fully mapped
Anc-200	Ancestor	-	200	Fully mapped
PL-000-Col1	Permissive Layer, colony 1	4	0	Contaminated: *Pseudomonas*
PL-000-Col2	Permissive Layer, colony 2	4	0	Contaminated: *Pseudomonas*
PL-200-W4	Permissive Layer	4	200	Fully mapped: no distinct mutations
IL-000-W4	Interface	4	0	Fully mapped: no distinct mutations
SL-200-W2	Stress Layer	2	200	Fully mapped: one mutation, missing 2 mutations
SL-200-W4	Stress Layer	4	200	Fully Mapped: one mutation
PL-000-W2	Permissive Layer	2	0	Fully mapped: no distinct mutations
PL-200-W2	Permissive Layer	2	200	Fully mapped: no distinct mutations
IL-000-W2	Interface	2	0	Fully mapped: no distinct mutations, missing 1 mutation
BL-000-W2	Base	2	0	Fully mapped: no distinct mutations
BL-200-W4	Base	4	200	Fully mapped: three mutations

Table 5: $MgCl_2$ ED50 Values (mM $MgCl_2$)
The relative exponential growth rate and relative cell proliferation ED50 values for each sample, calculated from the OD_{600} curves from the adaptation analysis. The ED50 value represents the concentration of $MgCl_2$ at which a response is 50% of the observed response in media without $MgCl_2$.

Sample Name	Relative Growth Rate ED50	Relative Cell Proliferation ED50
Anc-000	183.2	214.1
Anc-200	189.0	215.8
PL-000-Col1	203.0	240.2
PL-000-Col2	86.7	128.1
PL-200-W4	189.1	234.7
IL-000-W4	184.1	214.1
SL-200-W2	184.4	235.2
SL-200-W4	194.0	234.9

a)

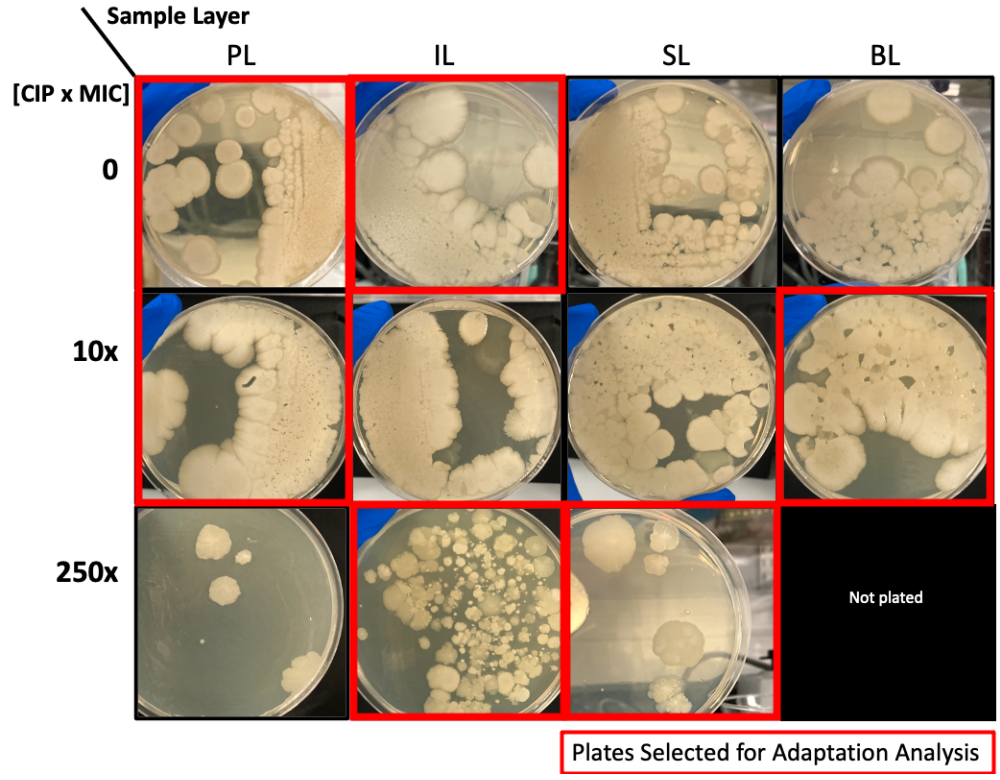

b)

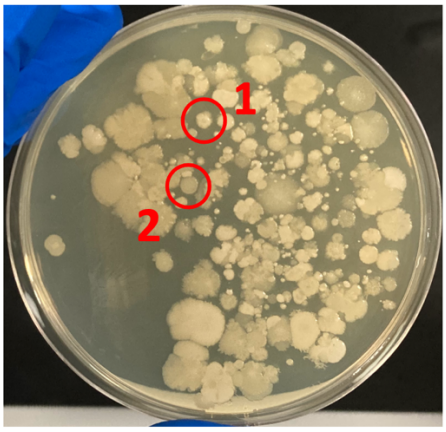

Figure 10: Colony Morphologies of Antibiotic Stress Samples
a) photos of agar plates streaked with MICALE-grown samples from the end of the two-week antibiotic run. The origin of the sample is listed at the top: permissive layer (PL), interface (IL), stress layer (SL), and base (BL). Each sample was plated on LB/agar with 0, 10, and 250 x MIC ciprofloxacin, except for the BL sample. Red boxes highlight samples selected for the adaptation analysis (Figure 11). Colonies were inoculated into broth with the same amount of ciprofloxacin, except for a colony from the BL 10 xMIC sample that was transferred into broth with 250 xMIC. **b)** a close up of the IL sample plated on 250 xMIC. Circles highlight the two colonies with different morphologies that were used in analysis (IL-15-Col1 and IL-15-Col2). Colony 1 was opaque-white with undulate edges and a dot in the center. Colony two was less opaque, round, and had more uniformity.

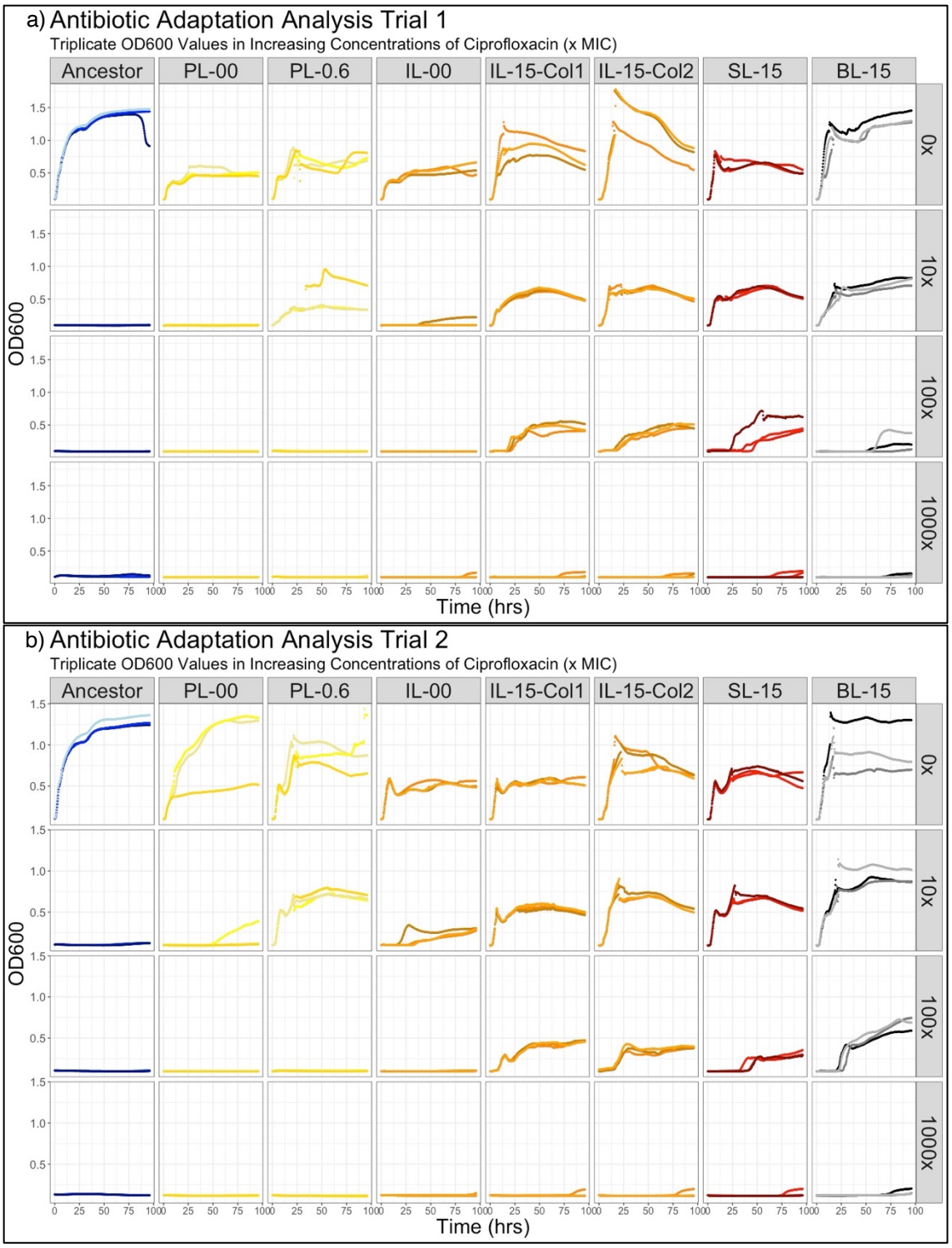

Figure 11: Antibiotic Stress Adaptation Analysis OD_{600} Curves
OD_{600} curves from antibiotic MICALE samples. Measurements taken every 15 minutes over the period of four days for **a) Trial 1** and **b) Trial 2**. Columns from left to right are the samples Ancestor (Anc), PL-00, PL-0.6, IL-LB, IL-15-Col1, IL-15-Col2, SL-15, and BL-15 (Table 6). Rows are separated by the concentration of ciprofloxacin in the growth medium as a factor of the MIC (0.06 µg/mL): 0, 10, 100, 1000 x MIC from top to bottom. Samples are colored based on their origin: Ancestor (blue), PL (yellow), IL (orange), SL (red), and BL (black). Individual lines represent one well of three triplicate wells inoculated for each sample in each media type for a total of 96-wells.

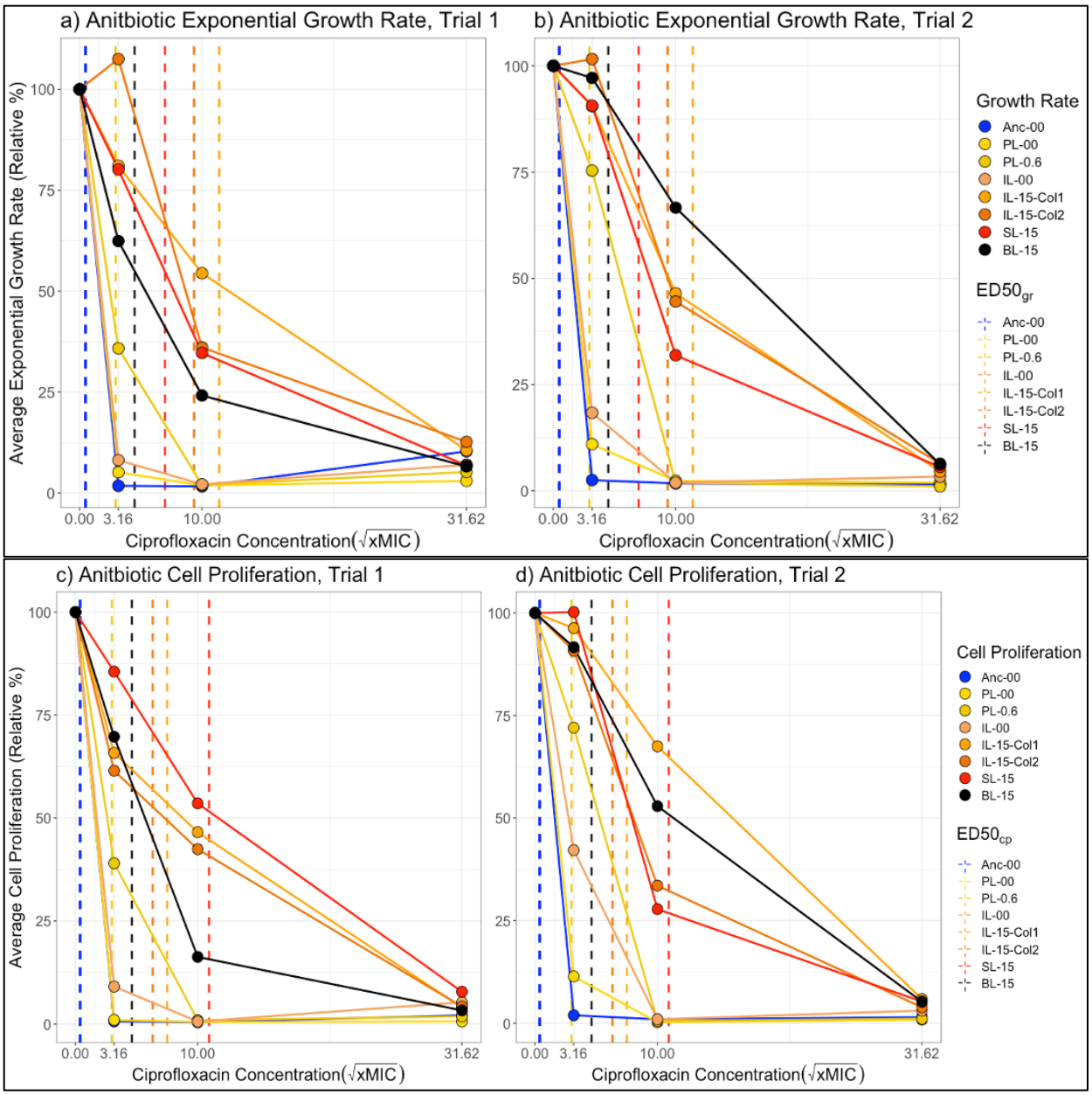

Figure 12: Average Exponential Growth Rate and Cell Proliferation in Ciprofloxacin
Dots and solid lines represent the exponential growth rate or cell proliferation values of a sample, extrapolated from the antibiotic stress adaptation analysis OD_{600} curves in Figure 11. Triplicate wells are averaged and expressed as a percentage of the response in media without any ciprofloxacin. Ciprofloxacin concentration is expressed as the square root of the MIC (0, 10, 100, 1,000 x 0.06 µg/mL). Vertical dotted lines show the concentration of ciprofloxacin at which the ED50 for each sample was calculated (Figure 13). Exponential Growth Rates for **a)** Trial 1 and **b)** Trial 2. Cell Proliferation for **c)** Trial 1 and **d)** Trial 2.

Table 6: Summary of Antibiotic Stress Samples
Descriptions of the samples from the antibiotic stress run used in further analysis. White rows highlight sample used in the adaptation analysis (Figure 11). Grey rows are samples that were sequenced but not used in the adaptation analysis. The name of the sample indicates where the sample came from (Ancestor, PL, IL, SL, or BL) and the concentration of ciprofloxacin that the sample was cultured in before analysis (0, 10, or 250 x MIC) seen in Figure 10. The BL-15 sample was grown on agar with 10 xMIC then transferred to broth with 250 xMIC. All samples were taken from MICALE at the end of the run, after two weeks. Samples named with a "C" for Community are broth cultures grown directly from the original MICALE sample, without prior isolation of a colony. Samples IL-15-Col1 and IL-15-Col2 Col2 indicate separate colonies with different morphologies from the same culture plate (Figure 10b). The *breseq* results column describes if the sample was fully mapped to the *E. coli* reference genome or contaminated. No samples mapped to the reference genome. Instead, the genus of the highest BLAST match is listed as the likely identity of the sequenced contaminant.

Name in Analysis	Sample Origin	Time of Sample (weeks)	Cipro. in Culture Media (ug/mL)	Cipro. Concentration as xMIC(0.06ug/mL)	*Breseq* results
Anc-00	Ancestor	-	0.0	0x	Fully mapped
PL-00	Permissive Layer	2	0.0	0x	Contaminated: *Bacillus*
PL-0.6	Permissive Layer	2	0.6	10x	Contaminated: *Bacillus*
IL-LB	Interface	2	0.0	0x	Contaminated: *Bacillus*
IL-15-Col1	Interface	2	15.0	250x	Contaminated: *Bacillus*
IL-15-Col2	Interface	2	15.0	250x	Contaminated: *Bacillus*
SL-15	Stress Layer	2	15.0	250x	Contaminated: *Bacillus*
BL-15	Base	2	0.6 then 15.0	10 then 250x	Contaminated: *Bacillus*
PL-15	Permissive Layer	2	15.0	250x	Contaminated: *Bacillus*
SL-00	Stress Layer	2	0.0	0x	Contaminated: *Bacillus*
BL-00	Base	2	0.0	0x	Contaminated: *Bacillus*
PL-C	Permissive Layer Community	2	0.0	0x	Contaminated: *Bacillus*
IL-C	Interface Community	2	0.0	0x	Contaminated: *Bacillus*
SL-C	Stress Layer Community	2	0.0	0x	Contaminated: *Bacillus*
BL-C	Base Community	2	0.0	0x	Contaminated: *Paenibacillus*

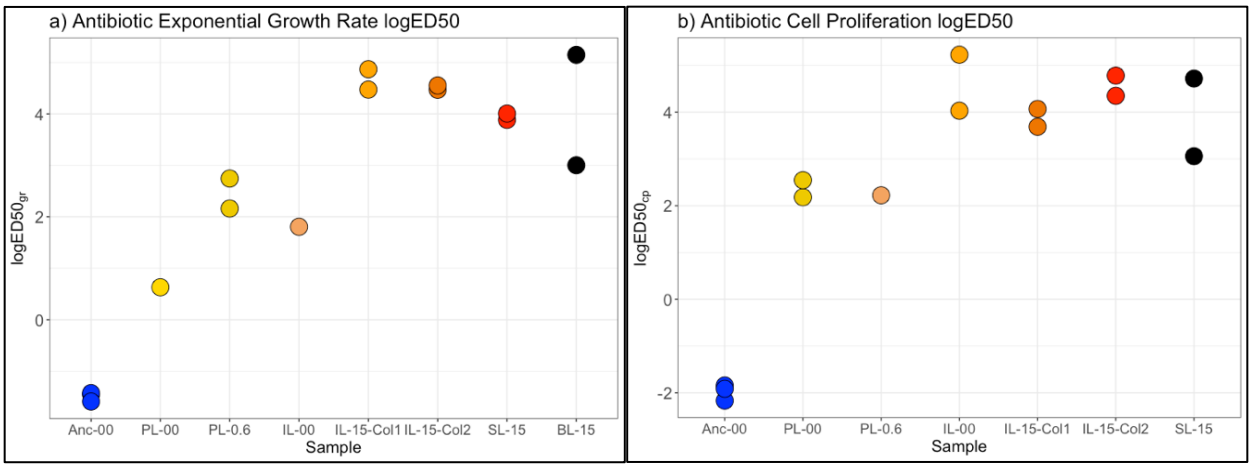

Figure 13: Antibiotic Adaptation Analysis logED50 Values
Log-transformed ED50 values for each sample, calculated by fitting a logarithmic dose-response curve to the exponential growth rate or cell proliferation calculations from each well's OD_{600} curve (Figure 11). The ED50 values for the ancestor (blue) were calculated using data from a test for the MIC rather than the adaptation analysis OD_{600} data. **a)** Exponential Growth Rate ED50 values for both trials. PL-00 and IL-LB samples have one ED50 value because only their Trial 2 data could be fit to a curve. **b)** Cell Proliferation ED50 values for both trials. A dose-response curve could only be fit to Trial 2 for the IL-00 sample. No curves could be fit to the PL-00 sample for cell proliferation.

Table 7: Antibiotic ED50 Values (x $MIC_{ciprofloxacin}$)
The ED50 values derived from both Trial 1 and Trial 2 of the antibiotic adaptation analysis (Figure 11), expressed graphically in Figure 13. Dose-response curves were fit to the exponential growth rate and cell proliferation values calculated from OD_{600} curves for each sample. The ED50 value represents the concentration of ciprofloxacin, expressed as a factor of the MIC (0.06 µg/mL) at which a sample's response in media without antibiotic is decreased by 50%. Sample names are described in Table 6. The ED50 values for the ancestor were calculated using growth rates and cell proliferation values from OD_{600} curves obtained during a test for the ancestor strain's MIC in ciprofloxacin. Dose-response curves were fit to each triplicate well grown during the MIC test to extract three ED50 values.

	Trial 1		Trial 2	
Sample Name	**Relative Growth Rate ED50**	**Relative Cell Proliferation ED50**	**Relative Growth Rate ED50**	**Relative Cell Proliferation ED50**
Anc	n/a	n/a	n/a	n/a
PL-00	a/a	n/a	1.8786	n/a
PL-0.6	8.6809	8.8578	15.5588	12.766
IL-00	n/a	n/a	6.0863	9.2362
IL-15-Col1	130.13	56.293	87.5896	186.32
IL-15-Col2	87.285	39.972	94.896	58.445
SL-15	48.657	119.389	54.9901	77.44
BL-15	20.132	21.3079	172.053	111.977
	MIC Relative Growth Rate ED50	**MIC Relative Cell Proliferation ED50**		
Ancestor, MIC	0.23391 0.240085 0.203954	0.114513 0.1583325 0.147608		

Whole Genome Resequencing

Whole-genome resequencing and analysis with *breseq* performed on samples isolated from high salinity and chaotropic stress MICALE runs revealed samples with mutations distinct from the ancestor and reference genome (Table 8). During analysis with *breseq,* both the ancestor and sample sequences were mapped to a reference genome for the *E. coli* strain[33]. Genetic differences between the samples and reference genome were not counted if the ancestor sample had that same mutation.

Out of the seven samples sequenced from the high salinity run, only one showed distinct mutations. Of the six samples that did not have distinct mutations, four were unable to map, or only partially mapped, to the reference genome. A BLAST search on the NCBI database[46] for a partial segment of these sequences identified the samples to be contaminated with strains of *Bacillus* (Table 2). The three remaining sequences from the PL-05, IL-05, and BL samples had high mapped percentages to the reference genome but only the IL sample had distinct mutations. Only the BL sample was used in the adaptation analysis, but the isolated culture used for sequencing does not come from the same colony that was isolated for the adaptation analysis.

The high salinity IL-05 sample sequence returned three mutations. The first is a single-nucleotide polymorphism (SNP) from G to A in the coding region of the *rlmL* gene. However, the change from the TCG codon to TCA results in the same amino acid, serine. The second mutation is a 1,199 base pair deletion. This deletion removed the Insertion Sequence (IS) mobile element, IS*5,* along with *insH21,* the gene within. The *E. coli* genome on EcoCyc[47] shows *insH21* sitting just over 500 base pairs ahead of the oppAp promoter for the oppABCDF operon. The final mutation in the IL-05 sample is an A to T SNP in an intergenic region, located at position 1,988,051 between the *azuC* and *yecR* genes. Gene locations provided by EcoCyc shows

that this SNP is fifty base pairs upstream of the promoter for the *azuC* gene, located within a CRP-cyclic-AMP transcriptional dual regulator known to inhibit translation of the *azuC* gene.

Out of the eleven samples sequenced from the chaotropic stress run, three samples are predicted by *breseq* to have distinct mutations and two samples returned low mapped percentages (Table 4). PL-000-Col1 and PL-000-Col2 were the only two samples with low mapped percentages. A BLAST search suggests the sequences are from strains of *Pseudomonas.* The three chaotropic-stress samples with distinct mutations are the SL-200-W2, SL-200-W4, and BL-200-W4. These two SL samples are the same as those used for the Adaptation Analysis.

The SL-200-W2 sample had one mutation: the mobile element IS*186* was inserted in reverse into the *crr* gene. This insertion occurred after the 484th nucleotide of the gene's 510 nucleotides, duplicating six of the target nucleotides so that they flanked the ends of the mobile element. In addition to changing the amino acids for the codons following the 484th nucleotide, the mobile insertion adds an early stop codon, shortening the total amino acid sequence by four. It is unclear how much this mutation effects the functional capability of Enzyme IIA^{Glc}, the product of *crr.* In addition to this one mutation, it is notable that SL-200-W2 was missing two mutations that the ancestor had. All other samples, high salinity and chaotropic stress, shared every mutation that their ancestor strain had.

The only mutation in the SL-200-W4 sample sequence was a single SNP, changing C to A in the *sspA* gene at position 3,376,949, about 167 nucleotides before the end of the 639 base-pair-long gene. This SNP replaces an aspartic amino acid with tyrosine in the chain for the stringent starvation protein A, encoded for by *sspA.* Aspartic acid is electrically charged and polar, compared to tyrosine, and aromatic that is neutrally charged and polar site.

Lastly, the BL-200-W4 sample taken at the end of the chaotropic stress run has three predicted mutations. At position 345,083, the mobile element IS*1* was inserted in the reverse position, consequently duplicating nine targeted base pairs to flank its sides. The insertion occurred in an intergenic region 92 base pairs upstream of *yahL* and 313 base pairs downstream of *yahM.* The promoters for *yahM* sit between the insertion and the gene. The proteins associated with *yahL* and *yahM* are uncharacterized. The second mutation is a C to A SNP at position 2,052,866, an intergenic just downstream of the *yeeJ* and just under 800 base pairs upstream of *shiA.* ShiA has been shown to be involved in transport of shikimate, an intermediate compound in biosynthesis of aromatic amino acids[48,49]. The final mutation for BL-200-W4 is a A to G SNP at position 2,754,655 in the gene *ratA.* The SNP changes the amino acid valine to alanine in the ribosome association toxin, RatA. Both amino acids are neutral and nonpolar.

All antibiotic sample sequences, except for the ancestor strains, were unable to map in *breseq*. When a segment of each sequence was plugged into BLAST, the search results for majority of the contaminants returned with more than 98% chance of a strain of *Bacillus.*

Table 8: MICALE-Sample Mutations Distinct from Ancestor Strain

Mutations found in MICALE-grown samples that are distinct from the ancestor strain, revealed from whole genome resequencing analysis. All of the samples listed had mapped more than 99% of their genome to the *E. coli* K-12 MG1655 reference genome. Only one sample from the high salinity run, IL-05, returned distinct mutations. This sample was not grown in the high salinity adaptation analysis. The chaotropic stress run had three samples with distinct mutations, SL-200-W2, SL-200-W4, and BL-200-W4. The BL-200-W4 sample had not been included in the adaptation analysis.

Stressor	Sample	Percent Mapped	Position	Mutation	Annotation	Gene	Description
NaCl	IL-05	99.6	1,008,626	G→A	S261S (TCG→TCA)	*rlmL* →	fused 23S rRNA m(2)G2445 methyltransferase and 23S rRNA m(7)G2069 methyltransferase
			1,299,499	Δ1,199 bp		*insH21*	insH21
			1,988,051	A→T	intergenic (-92/-171)	*azuC* ←/ → *yecR*	uncharacterized protein AzuC/lipoprotein YecR
$MgCl_2$	SL-200-W2	99.6	2,536,312	Δ1bp :: IS*186*(-) +6 bp :: Δ1 bp	coding (479-484/510nt)	*crr* →	Enzyme IIA(Glc)
$MgCl_2$	SL-200-W4	99.7	3,376,949	C→A	D158Y (GAT→TAT)	*sspA* ←	stringent starvation protein A
$MgCl_2$	BL-200-W4	99.6	345,083	IS*1* (–) +9 bp	intergenic (+92/-313)	*yahL* →/ → *yahM*	uncharacterized protein YahL/uncharacterized protein YahM
			2,754,655	A→G	V37A (GTT→GCT)	*ratA* ←	ribosome association toxin RatA
			2,052,866	C→A	intergenic (+852/-777)	*yeeJ* → / → *shiA*	inverse autotransporter adhesin/shikimate:H(+) symporter

DISCUSSION

We built the MICALE apparatus to perform continuous, long-term evolution in a liquid environment, that also fulfills the challenging requirements for ALE stress-tolerance experiments: the experimental conditions must allow for wild type survival while still selecting for stress-tolerant mutants and the desired phenotype must be coupled with increased fitness. We performed three runs with *E. coli* in MICALE in hopes of increasing the cells' tolerance to high levels of sodium chloride, magnesium chloride, and ciprofloxacin. During runs, we took measurements of density, OD_{600}, flow rate, and pH to investigate how the instrument functions and the dynamics of cellular growth in MICALE. We will begin the discussion with our interpretations of these experimental run measurements. We will then use our interpretations to postulate the ways in which MICALE does and does not satisfy the requirements for ALE. In doing so, we intend to answer the following question: does MICALE function as intended?

Following experimental runs, we performed phenotypic and genotypic analyses to see how MICALE-grown strains compared to the ancestor. The adaptation analysis looked at the growth phenotypes in increasing amounts of stress of isolated experimental strains and the ancestor. Using the growth curves from the adaptation analysis, we extracted exponential growth rate and cell proliferation values to calculate the 50% Effective Dosage (ED50) for a quantitative comparison of growth between strains. For the genotypic analysis, we performed genome resequencing with *breseq* to see what genetic changes might have occurred and if the changes relate to the observed phenotypes. We will discuss the results of these two analyses to put forth the evidence in support for and against the presence of stress-adapted strains. This portion of the discussion will answer the following question: did MICALE produce strains with increased tolerance to the intended stressor?

Measurements of the salinity and density confirm that a difference in density is maintained throughout the run, forming a structured environment with a permissive region and a stressful region. Furthermore, we observed significant differences in density between adjacent regions of media, illustrating a stepwise increase in the concentration of stressor that facilitates adaptation and increases diversity. In order to create two separate liquid environments within one apparatus, we increased the density of the bottom layer media (BLM) using sucrose and adding a high concentration of a stressful compound. The top layer media (TLM) is diluted LB broth with no added compounds, making it less dense than the BLM and permissive for growth of the wild type. However, we were concerned that the rate of diffusion between the two media types would be increased by the kinetic input from the flow rate. It was therefore necessary that we measure the density during runs to verify our experimental design. With the exception of salinity, the exact concentration of the stressor cannot be determined during runs. Instead, we interpret the density measurements relative to sterile TLM and BLM and assume that a higher density corresponds with a higher concentration of stressor.

Salinity measurements represented both the density of the media and the concentration of the stressor, NaCl, in the media. The salinity measurements of the PL and IL stayed separate, with the PL remaining lower in salinity than the IL (Graph 1a). Despite the sampling valves being adjacent, an independent t-test supports that the media have significantly different compositions (Table 1a). There are no direct measurements of the salinity in the SL or BL regions because their salinities were out of the refractometer's range. Thus, we can assume that the SL and BL layers had a higher salinity than the IL layer. These salinity measurements demonstrate how our use of two media environments, separated by density, produces a gradient of increasing stress. A gradient of stress provides intermediate steps for cells to adapt increased

tolerance, rather than a large jump, and supports diversity, altogether aiding in adaptation[16,23,25,50].

A similar increasing gradient in stress is seen in the chaotropic and antibiotic stress runs. For both runs, the average density of the sample regions increases sequentially downwards into MICALE (Graphs 1d and 1f). The density of the uppermost sampling region, PL, is statistically the same as the density of the TLM control for both runs (Tables 1b and 1c). This confirms that the upper region is made up of majority permissive media for wild type growth. Similarly, the density in the BL region for both runs is statistically similar to the BLM and dissimilar to the TLM. This is despite the fact that the SL and BL regions do decrease in density during the month-long run (Graph 1c). Since the concentration of stressor in the BLM was above the MIC for the ancestor strain, these results show how the lower region of MICALE remains stressful to wild type strains, adding adequate selective pressure.

The measurements from the chaotropic and antibiotic stress runs also show us how the TLM and BLM mix overtime, creating the interface region. Both the chaotropic and antibiotic runs had one sample layer, the SL and IL layer, respectively, that was statistically different from both the TLM and BLM control media, as well as the other three sampling layers. It is likely, therefore, that these regions were the levels at which the TLM and BLM mixed, perhaps 50/50. This region of change from TLM to BLM was deeper during the chaotropic run, resulting in the SL region that was distinct from both the TLM and BLM and the IL region that was statistically similar to the TLM (Table 1b). During the antibiotic run, the region of permissive media was smaller, with the transition to the BLM occurring higher up; the IL media was statistically dissimilar to both the TLM and BLM while the SL was statistically similar to the BLM (Table 1c). A potential explanation for why the permissive area was larger during the chaotropic run

could be because the overall flow rate was slower than that during the antibiotic run (Graphs 3b and 3c). The difference in the size of the permission region between the two runs may have changed the growth dynamics within. There is no clear evidence, however, how flow rate and the size of the permission region could impact the evolutionary end-result but should be taken into account in future MICALE runs. For example, it might be beneficial to have a larger permissive region in another antibiotic run to reduce the level of antibiotic that cells in the permissive region are initially exposed to.

Fluctuations in density are likely explained by the flow rate. For all three runs, density fluctuates the most at the beginning of the run. We cannot provide concrete explanations for these fluctuations but speculate that it was due in part to the set-up of MICALE and initial flow rate: set-up can disturb the media, causing some mixing and, in each run, the starting flow rate decreased the flow rate sharply within the first 50 hours. During runs, we observed that the density of the IL and SL regions changed during periods of stalling flow rate. For example, after 500 hours of the chaotropic stress run, multiple flow failures occurred in the next 200 hours (Graph 3b). During this time, the IL region density slowly increased, until 600 hours when the flow rate was fixed, and the IL density decreased till it was similar to the PL density (Graph 1c). Though a faster rate of flow may increase the removal of BLM from MICALE, the flow rate also helps maintain the density stratification; the flow adds fresh, low density TLM and removes used media that may have increased in density from mixing with the lower media. If left alone without input of fresh media, diffusion would increase exponentially as the two layers become more and more like each other.

An essential principle to MICALE is that it maintains an area of media permissive for wild type growth with access to areas with higher concentrations of the stressor. These regions of higher stress must increase to a level in which only adapted strains can survive. Between these permissive and inhospitable zones, there must be intermediate levels of stress to facilitate adaptation. Our salinity measurements show that the upper region is low in salinity, permissive for wild type growth. Furthermore, the PL density measurements from the other runs show that the PL remained statistically similar to the TLM, media that is used to culture cells. The BL region density measurements show that the BL region is the same as the BLM. BLM media contains a concentration of stressor that is above the wild type strain's MIC; only adapted strains can grow well in these conditions. Lastly, the four individual sampling regions are statistically different in density (except for the BL and SL regions during the antibiotic run) showing how the density, and therefore the concentration of the stressor, increases from top to bottom in MICALE, providing intermediate steps for adaptation to occur.

The free mobility between media types for cells allowed by MICALE's design, facilitates colonization of new areas with higher selective pressure but also prevents distinction between cells that are alive and adapted, alive but not adapted, or dead. We intended to track the cell growth in each layer using optical density measurements but soon realized that, at most, optical density is a representation of the amount of biomass present. Un-adapted cells may not be able to grow in the stressful layer, but they can still float down from above and contribute to a rise in the OD_{600} measurements.

We first suspected that cell matter from the upper region was significantly affecting our measurements of the lower regions during the high salinity run. Fluorescent microscopy of

samples from the lower layers showed cells that appeared to be alive and dividing. We had hoped this was an indication of lower-layer colonization by adapted cells. However, when these samples were planted on agar with a high concentration of salinity, though still a lower concentration than the initial starting salinity in the BLM, no cultures grew. Thus, cells found in the BLM were not adapted to higher stress. During the chaotropic stress run, goopy cell matter aggregates caused interference in OD_{600} measurements for the PL and BL samples (Figure A1). Looking at the apparatus, the majority of these aggregates could be seen stuck on the walls near the air interface at the top of MICALE. These observations lead us to believe that cells in the upper layer were forming aggregates that eventually fell downwards and collected in the BL layer. Upon taking apart MICALE after the chaotropic run, media in the bottom layer was colored milky white from such a high concentration of these aggregates.

These observations all support that the presence of cell matter in the lower layers does not mean the cells are stress-adapted strains that have colonized the BLM. Optical density measurements, therefore, may help keep track of the accumulation of biomass MICALE but cannot act as a direct measurement of cell growth. Instead, other methods in combination with each other should be used to monitor the presence of live and adapted cells in the lower layers. For example, growing samples on spread plates and broth cultures with differing concentrations of the stressor, live/dead stains with flow cytometry, fluorescence microscopy, diluting samples into fresh media with stressor and monitoring optical density on a 96-well plate, and more. Except for flow cytometry, we performed variations of these tests but did not do it consistently enough to have results that are presentable beyond what was described here.

Altogether, this section highlights how MICALE's 3D design makes it difficult to visually observe adaptation and colonization of the stressful media, compared to studies such as

the MEGA-plate[24] and microfluidic gradient chamber[50] that can view cell growth on a 2D surface. Instead of visually observing colonization, experiments with MICALE must rely on secondary tests and analyses to understand the evolution dynamics occurring within MICALE. However, MICALE is not meant to be a replacement for other ALE methods but rather an additional tool to expands the variations of ALE experiments. The style and conditions of the experiment greatly influences the outcome[2]. Performing ALE evolution with the same stress type but in different laboratory environments can lead to exciting new results. Additionally, MICALE's liquid environment allows the study of marine microorganisms in the laboratory.

Our tracking of optical density show that a culture of *E. coli* is maintained in the upper layer, even when the BLM contained high concentrations of the antibiotic (Graph 2). This is confirmation that a culture of the wild type survives in the upper region. To operate similar to a chemostat, we attempted to keep a constant flow of media during runs, but mechanical issues, mainly clogged filters, frequently slowed and stopped the flow. However, these mechanical issues allowed us to observe how the cell populations respond to the flow rate based on their location. During times when the flow of media had stopped, the OD_{600} of samples from the PL rose, indicating an accumulation of biomass and, potentially, an increase in growth rate (Graph 3). Once the flow was running again, the PL OD_{600} would drop as cells were removed from the system and growth could not exceed the rate of flow. This is seen especially clearly in the high salinity run when spikes in PL OD_{600} occur during no-flow periods (Graph 3a). During the antibiotic run, there are three spikes in PL OD_{600} between 100 and 200 hours that occur when the flow rate dips and even appear to match the relative magnitude that the flow rate decreases with the increase in OD_{600} (Graph 3b). This trend is only seen in the PL and not the other three layers.

In the high salinity OD_{600} measurements, the IL and SL both rise to a certain level then stay relatively constant beyond some rises and falls that don't follow any pattern (Graph 2a). The observed relationship between the flow rate and PL but not with the IL, SL, and BL occurs at some time points during the chaotropic runs but artificial spikes in OD_{600} caused by cell matter aggregates make these patterns less distinct and difficult to draw direct comparisons (Graphs 2d and 3c). These data show that the biomass in the upper, permissive region of MICALE is controlled by the flow rate.

The flow rate, however, does not control the actual growth rate of the cell populations in the upper region. We hoped that a constant flow of media and removal of waste would keep a continuous culture of cells at a reduced rate of growth. In doing so, the fitness of cells in the lower regions, where growth is not restricted, would increase adding more selective pressure for stress tolerance adaptation. Instead of limiting cellular growth like a chemostat does, the data show that our design acts more similar to a turbidostat in which only the overall biomass is controlled rather than the growth rate of the cells[20,51]. This is seen especially in Graph 3. When the flow rate drops, the PL OD_{600} continues to rise and spike. If the cell populations were growth-limited by the input of nutrients, then they would not be able to grow without new nutrients.

In chemostats, turbidostats, and MICALE, a constant flow rate aids in maintaining a constant environment. Maintaining a constant environment during ALE is important because it reduces variables such as low oxygen, spent nutrients, and low pH that could cause unintended stress[52]. External factors must be under control during ALE in order to ensure that observed phenotypic change is a result of the intended adaptive pressure. If external pressures are not

mediated and become stronger than the intended stressor, evolution will be driven towards undesired adaptations.

To understand how conditions in MICALE could be changing, we measured the pH during the antibiotic run. In the previous high salinity and chaotropic stress runs, the waste media smelled fermented, indicating that cells could be undergoing anaerobic fermentation, potentially because of a lack of oxygen present. Both low oxygen and low pH could add physiological stress to the cells, pressuring adaptation to factors rather than the indented stressor. Additionally, we suspected that low oxygen and low pH in MICALE could be an indication of cells that are actively replicating in the lower layer.

Over the first half of the antibiotic stress run, no drastic changes are seen in the pH measurements (Graph 4). During the second half of the run, the pH begins to fall, decreasing especially after 200 hours. During this same time, we observe an increase in the OD_{600} of the IL, SL, and BL layers that had previously been stable (Graph 2e). We believed the decrease in pH was a potential indication that *E. coli* was successfully colonizing the lower layer. However, whole genome resequencing of the samples showed that all sequenced samples were contaminated with *Bacillus* (Table 3). It is likely that colonization of MICALE by *Bacillus* resulted in the decrease in pH. This contamination prevents us from understanding if there are external forces in MICALE that add selective pressure onto cells, since answering that question requires genetic knowledge of the adaptations that occurred.

One conclusion from the pH measurements is that change in pH is possible in MICALE, especially in the lower regions. Changes in pH, as well as other conditions, can provide insight into the current growth conditions in MICALE. During this experimental run, a change in pH was a likely indication of contamination. If future runs are completed without contamination,

changes in pH could also hint at cellular activity in the lower layers and when resources, such as oxygen, may be depleted in the lower layer. If resources are depleted in the lower layer, the BLM can be replaced with fresh media to keep the run going. Along with the density, flow rate, OD_{600}, and cell phenotypes, pH should continue to be monitored during MICALE runs as it provides another insight into the dynamics occurring in the apparatus. Furthermore, one interpretation from the pH measurements is that the pH in the PL layer changes less than the other layers. This suggests that the conditions in the upper layer, due to the flow, are more constant than the lower, static layer, as expected.

Due to the contamination in the antibiotic chemostat, we cannot determine if low oxygen and low pH added stress to cells in MICALE. Nor could we know if unintended stressors were significant enough to influence adaptation to low oxygen or low pH tolerance. Future work can attempt to investigate the influence of external factors by performing the adaptation analysis in conditions other than the stressor. For example, adaptation analysis tests with varying levels of pH, in anaerobic conditions, with increasing amounts of external cell matter as a food source, and more. These tests could reveal other growth phenotypes present in the population that were previously unseen. Furthermore, novel mutations in MICALE-grown strains should be investigated not only for their role in the presence of the intended stressor but also for how the mutation influences growth in other conditions.

The antibiotic run was clearly contaminated, indicating that the MICALEE system is not fully controlled. All samples, regardless of the culturing method, were identified through sequencing as a strain of *Bacillus* (Table 6). We suspect that *Bacillus* contamination growth took off around one week into the run because that is when the pH starts to drop and the OD_{600} starts

to rise (Graphs 2d, 2e, and 4). It is possible that the starting level of ciprofloxacin in the BLM was too high for the *E. coli* to grow effectively, facilitating an easy take over from *Bacillus.* Interestingly, ciprofloxacin is an antibiotic commonly prescribed for infections with *Bacillus* and studies have shown that multiple strains are susceptible to ciprofloxacin[53]. A more recent study found that the ciprofloxacin MIC for multiple isolates of *Bacillus cereus* and *Bacillus subtilis* ranged from 0.5 to 32 µg/mL, roughly 10 to 530 times the MIC of *E. coli* determined in this study[54]; *Bacillus ssp.* may have more tolerance to ciprofloxacin than *E. coli*, but the starting concentration of ciprofloxacin in MICALE, 120 µg/mL (2000 times the MIC for *E. coli*), is far past the observed *Bacillus* MIC. The pH during the antibiotic run dropped the lowest in the IL region. In this region, the concentration of ciprofloxacin may have been above the MIC for *E. coli* but still within tolerable levels for *Bacillus.* During the adaptation analysis, growth was observed in 100 xMIC (6 µg/mL ciprofloxacin) which is in the range of the MIC for *Bacillus* (Figure 11). Some strains, presumably also *Bacillus*, could not grow in 100 xMIC and some showed limited growth all the way up to 1000 xMIC. This calls into question if *Bacillus* underwent evolution and adaptation to ciprofloxacin during its time in MICALE or if multiple species of *Bacillus* with different tolerances separated themselves along the gradient of antibiotic in MICALE.

It is unclear if the contamination found in over half of the sequenced high salinity samples occurred when cultures were grown and isolated for DNA extraction or if it traces all the way back to MICALE. Some samples were contaminated with *Bacillus*, some fully mapped to the *E. coli* reference, and the reads for one sample, the SL_{early}, had less than half the genome map to *E. coli* and the other portion was identified as *Bacillus* (Table 2). When incubated on high salinity agar plates and broth, the previously frozen stocks grew very slowly, requiring over four

days to produce colonies or show signs of growth in broth. This slow growth may have allowed contaminants to outcompete the *E. coli* in both a culture and in MICALE. Interestingly, none of the samples incubated on low salinity media were contaminated. The samples incubated on high salinity media all returned some level of contamination, except for the BL sample. The strong evidence of contamination during the antibiotic run from both the pH measurements and sequencing supports the likelihood that contamination occurred during the high salinity run. It is interesting, however, how there are samples that fully mapped to the *E. coli* reference genome, indicating the isolated sample was not contaminated. Most of the non-contaminated samples were in low salinity media, except for the BL sample cultured in 60 ppt NaCl (Table 2).

For the chaotropic stress samples, only two samples from the chaotropic stress run were contaminated (Table 4). Both samples were identified as *Pseudomonas* and originated from the same PL culture plate on which diverse morphologies were observed (Figure 8b). The diversity on the plate with the sequencing identity suggests that the contamination likely originated from within MICALE. Interestingly, the unique *Pseudomonas* colony morphology was not seen on $MgCl_2$ plates of the same sample (Figure 8a). Instead, colonies isolated from these plates were identified as *E. coli.* Perhaps the *E. coli* had better evolved tolerance to $MgCl_2$ by the time contamination occurred or *E. coli* are naturally more resistant to chaotropic stress than *Pseudomonas,* restricting the contaminant to only the permissive region of MICALE.

Exposure to contaminants likely occurs during experimental set up, sampling, or during replacement of a clogged filter. The MICALE apparatus used for this experiment cannot be autoclaved, adding difficulty to fully sterilizing it before use. Future version of MICALE should prioritize materials safe for autoclaving. During sampling from the valves, we pushed the leftover media in the pump back into MICALE, stopping before air would be pushed in.

Although the sampling pump remained in the hood and was sterilized with ethanol, this may have still allowed for contamination. For future experiments, media should never be pumped back into MICALE once it leaves the system. Lastly, researchers should consider having fresh media flow in from above, or in some other fashion, to prevent cells from swimming out of MICALE, into the tubing, and clogging the filter. This would reduce the need to replace the filter, keeping a sterile system.

ALE experiments must add selective pressure that is specific for the targeted phenotype, especially by increasing the relative fitness of the targeted phenotype. To what degree is the current MICALE system able to achieve that? Looking at the results and interpretations presented prior on the density stratification, flow rate, and measured conditions during a run, we will attempt to outline how MICALE adds selective pressure and how it can be improved for a more effective ALE experiment. However, an important consideration is that our ability to postulate on the effectiveness of MICALE to add selective pressure on cells to evolve is limited by the presence of contamination that obscures evidence of genetically evolved strains. Non-contaminated genetic evidence could clearly show if and how much evolution occurred, thereby showing if the MICALE system was effective. The few mutations that did arise from WGS, discussed later, do not provide enough information to suggest whether MICALE had too much or too little selective pressure for the ideal phenotype.

Our intentions were that the upper layer flow rate and diluted media would subject the cells to growth restriction and nutrient limitation, pressuring adaptation downwards into MICALE. While the amount of *E. coli* biomass responded to the rate of the media flow, we do not believe that diluting the media to 50% was enough to impact the growth rate of the cells[20].

Instead, the upper region of MICALE operated like a traditional turbidostat. During run when the flow rate stopped, the cell population in the upper layer increased in density, indicating that the concentration of media in the upper layer supplied plentiful nutrients to do so. For example, at around 40 hours during the high salinity run, the OD_{600} measurement of the PL region doubled during a period of no flow (Graph 3a). Instead of limited growth, the cells were likely maintained at their maximal growth rate, defined by their intrinsic properties[20]. The population never reached a stationary phase because the flow rate provided fresh nutrients and restricted the overall cell density. Maintaining the cell population in exponential growth may be beneficial because fast-replicating cells increase the frequency of mutations[1]. However, cells with mutations that allow for stress resistance may not fix in the population if they are out competed by the fast-replicating wild type cells. As MICALE currently stands, the wild type cells in the upper regions appear to be happy and fast-growing. In short, there is little fitness advantage to gain by evolving stress resistance if cells in the upper region are well off.

Limiting the growth rate of cells in the upper layer may help add evolutionary pressure to evolve stress resistance. Gresham and Dunham (2014) discuss how growth inhibition in chemostats can be achieved by limiting a nutrient to a level so low the growth rate is equal to the rate of input of this nutrient[20]. Limiting a single nutrient in MICALE, rather than just diluting media, could "starve" the cells in the upper layer and push evolution downwards. However, starvation may result in evolved cells with undesired phenotypes, such as increased survival on waste products of deal cells[18]. Additionally, the amount of type of nutrient that is limited changes the level of persistence of the starved cells and leads to different adaptations[55]. For example, glucose starvation led to an increase in cAMP regulatory metabolites compared to other nutrient limitations[55]. To reduce the evolution of undesired phenotypes, the limited nutrient can be

provided in excess in the BLM. Instead of adapting to the limited nutrient, such as by altering one's metabolism, cells may instead focus on evolving to the stressor as they can sense an increase in the nutrient through chemotaxis[56]. For example, carbohydrates could be limited in the fresh media and glucose could be added to the BLM, in addition to sucrose[51].

Starving cells by limiting one nutrient in the TLM may also aid in the overall rate of adaptation by inducing the "general stress response" in *E. coli.* This response has been observed in response to nutritional stress, starvation, and environmental pressure such as osmotic pressure and low pH during which *E. coli* cells increase their rate of spontaneous mutation[18]. During stress-induced mutagenesis, known as adaptive mutation, nondividing and starving cells can mutate and evolve their genome[17]. Starving the cells, therefore, may serve as a "kick starter" to adaptation to the stressor.

An increasing gradient of stressor benefits the ALE experiment by facilitating adaptation to the stressor without imposing a time constraint on cells. The density measurement results confirm that there is an area permissive for wild type growth, an area with a high concentration of the stressor, and an area in between. Intermediate steps with lower concentrations of stress allows cells to gradually mutate to the stressor. The heterogeneous gradient also facilitates diversity in the cell population. Based on the experimental results, were these benefits, gradual adaptation and increased diversity, achieved in MICALE? Because of contamination in MICALE, it is difficult to know if the intermediate steps of the stressor adapted cells better than a homogeneous ALE experiment. However, the observed diversity in the cell cultures is an indication that diversity is present MICALE (Figures 8 and 10). Furthermore, samples isolated for the adaptation analysis and sequencing show diverse growth curve phenotypes and uncontaminated samples have diverse mutations. For example, the growth curves produced

during the high salinity adaptation analysis showed variation between samples on the rate of exponential growth, time of exponential growth, cellular biomass produced, and the shape of the curve between samples (Figure 7a). The sequencing results from the chaotropic stress run revealed three samples with unique mutations with no overlap (Table 8). Even the SL-200-W4 and BL-200-W4 samples that originated from adjacent regions in MICALE with high concentrations of $MgCl_2$ had different mutations. Even the contaminants in the antibiotic run showed diversity between layers, especially in the IL sample (Figure 10b). The genetic diversity found in MICALE is indicative of a heterogeneous environment, likely allowed by the density stratification of the media types.

As discussed, conditions in the chemostat must be under control to reduce the chance of unintended stressors driving the cells to evolve undesired adaptations. If experimental conditions are not controlled, then the observed novel phenotypes may not be related to the intended adaptive pressure. Due to the static nature of the BLM, the severity of unintended stressors, such as low oxygen, external cell matter, low nutrient levels, and decreased pH, may increase over time, especially if adapted cells have colonized the media. Additionally, the concentration of the chosen stressor decreases overtime due to diffusion into the upper regions and eventual removal by the waste pump, changing the conditions. The longer MICALE is run, the greater the impact unintended stressors may have while the chosen stressor's impact reduces. The conditions in MICALE need to be continuously monitored to notify if the unintended stressors have become too strong. Specifically, the amount of cellular biomass in the BLM pH in the lower region can indicate when too much cell matter has accumulated, and nutrients and oxygen have been depleted.

Looking at the MICALE run results, we propose that MICALE runs should be limited to two weeks, without alteration of the BLM. We chose this time frame because, in both the NaCl and $MgCl_2$ adaptation analyses, the samples taken at two weeks performed better in the stressor than samples from 25 hours and 4 weeks, respectively (Figures 7 and 9). Running MICALE for longer than two weeks may decrease the concentration of stressor and available resources in the system too much. Additionally, it has been shown that beneficial mutations rates decrease with longer evolutionary periods[3].

However, the run length of MICALE can be easily increased by adding fresh BLM to the system after two weeks. Fresh BLM can be added through the bottom valve, replenishing nutrients while maintaining the dentistry stratification. Researchers could take this even further by increasing the concentration of the stressor in the fresh BLM to push the bounds of the adapted phenotypes, given that there is evidence of living cell populations in the lower region.

A key prerequisite to post-run analyses with MICALE samples is the need for a culturing process that does not introduce a significant number of genetic changes (Figure 3). This is especially important since the 3D structure of MICALE prevents many direct observations of the cell growth dynamics and requires that phenotypic analysis happen outside of the apparatus. Samples were cultured in a concentration of the stressor that we believed was high enough to maintain evolutionary pressure but lower than the starting concentration in the BLM to avoid introducing more change. Unsure of what this exact concentration was, we cultured samples in multiple amounts of the stressor as well as blank LB, as seen in the agar plates in Figures 8 and 10. For the adaptation analysis, we selected colonies originating from the same sample but cultured in different amounts of stressor to see how our culturing process may impact the

observed growth phenotypes. We mainly did so with samples from the PL and Il regions since we expected more diversity but less adaptation to occur in the permissive media.

In the chaotropic stress adaptation analysis we cultured the Ancestor and a PL sample in blank LB and LB with 200 mM $MgCl_2$ (Figures 8 and 9). Culturing the Ancestor in media with stressor served as a control that allowed us to see the influence that the culturing method has on resistance. The Ancestor strain cultured in 200 mM $MgCl_2$ has a low exponential growth rate in $MgCl_2$ than its counterpart cultured in blank LB but a higher cell proliferation value (Figures 9b and 9c). The Ancestor sample grown in blank LB is the one of two samples that showed a sign of growth in 250 mM $MgCl_2$. This was partially expected because the ancestor strain was able to grow colonies on a 250 mM plate but odd because so few samples grew in 250 mM $MgCl_2$. The PL samples cultured on blank LB and in 200 mM $MgCl_2$ show difference between the shapes of their OD600 curves. Similar to the Ancestor strain, the PL sample cultured in blank LB had one well with growth in 250 mM $MgCl_2$ whereas the PL sample cultured in 200 mM $MgCl_2$ could not. Overall, the PL-200 sample appears to have better, more consistent growth in 200 mM $MgCl_2$ compared to the PL-000-Col1 in which the three triplicate wells have very different growth abilities. The differences in growth seen in the ancestor and PL sample between cultures grown in blank LB and 200 mM $MgCl_2$ may only be representative of the cellular response to magnesium chloride and not indicative of how the culturing methods effects the MICALE process. The cultures grown in blank LB survived in higher concentrations of $MgCl_2$ than the cultures grown in 200 mM $MgCl_2$.

For the antibiotic adaptation analysis, we again tested pairs of the same sample cultured in different media: the PL samples grown in blank LB and 10 xMIC (PL-00 and PL-0.6) and the IL samples grown in blank LB and 250 xMIC (Figure 10). These results are clearer than the

magnesium chloride results; the samples could only grow in a concentration of antibiotic as high as what they were cultured in (Figure 11). If samples did grow beyond the concentration that they were cultured in, the growth was remarkably poor and occurred usually in one of the triplicate wells. PL-0.6 only grew up to 10 xMIC (0.6 μg/mL ciprofloxacin), all three wells for the IL-15-Col1 and IL-15-Col2 (cultured in 250 xMIC) grew in 100 xMIC but only one well showed a sign of growth in 1000 xMIC, IL-00 in trial one had some but very limited growth in antibiotic, and PL-00 showed poor growth in 10 xMIC for only one well out of the six total.

Due to procedural error and limited resources, we cultured the BL sample first on an agar plate with 10 xMIC then transferred a colony to broth with 250 xMIC before the adaptation analysis. Transferring the cells into higher concentrations of antibiotic may have supported adaptation, similar to ALE experiments with serial batch transfer. It is possible this could have introduced adaptation, especially since mutations in bacterial populations occur naturally within a short time span[1].

On the other hand, while the culturing process may allow for cells to continue evolving, the cell populations go through significantly more generations in MICALE than the few days they are cultured. The more likely reason for the observed differences in antibiotic resistance between colonies from one sample cultured in different media types is that the culturing process sorts cells with the resistance phenotype. The relatively large size and heterogeneous structure of MICALE supports great diversity in the community which we clearly see on LB agar plates with no stressor (Figures 8 and 10). The colony selected could be similar or completely different from the other colonies on the same plate. Adding stressor to the culture media reduces the diversity and allows us to select for the more adapted strains. Presumably, the SL and BL samples growing on media with a stressor are also the samples that are surviving in the lower region of

MICALE and not unadapted cells that floated downwards. A future test to look at the diversity present in MICALE is to perform an adaptation analysis on multiple colonies from only one sample.

There are many limitations to the adaptation analysis, some of which we worked to alleviate. However, the lack of understanding on microbial growth curves makes it difficult to discern between unique growth phenotypes and inaccurate results. Different growth strategies cause different growth curves, many of which are in response to external stress. For example, it has been observed that bacteria with an extended lag phase in the presence of antibiotic have higher resistance, slowing their growth rate to allow time to develop tolerance[57]. Despite significant variation in growth strategies, however, there is little background information on what growth curve shapes different growth phenotypes cause. Furthermore, there are many variables that can affect OD_{600} measurements, such as cell inoculation number, evaporation, and biofilm formation, producing growth curves far from the established "S" shaped model[34]. We alleviated some of these variables by removing measurements inflated from biofilm formation, using a rolling regression to find the exponential growth rate to account for curve shape variability, performing visual checks for the location of the exponential growth rate, and taking note of the wells most effected by evaporation (Figure A2). However, insufficient evidence and understanding prevents us from removing all the variables we thought possible. For example, the apparent growth of the ancestor strain in 250 mM $MgCl_2$ could not be counted out even though measurements may have been due to machine noise and evaporation (Figure 9 and Figure A2). Samples in the high salinity adaptation analysis appear to increase their growth rate in higher salinities (Figure 7). Due to machine noise, OD_{600} measurements naturally jump up and down in

small increments. These jumps are so small that the noise is not seen in wells with growing cells but can be seen in wells with little to no growth. Thus, it may be true that the high salinity samples increased their growth rate, but machine noise may have caused a small but sharp increase in OD_{600}, resulting in a sharp first derivative and fast growth rate.

In wells with a high concentration of cells and biomass, the OD_{600} can be artificially inflated, decoupling the relationship between OD_{600} and cell count. OD_{600} is a measurement to indicate the cell count in a sample based on the Beer-Lambert Law[58]. However, once the concentration of cells reaches high density, the relationship between OD_{600} and cell count is decoupled. This is observed in the second half of the adaptation analysis growth curves when growth curves slowly rise, despite no longer being in exponential growth phase, such as the 5 ppt NaCl curves in Figure 7a and all chaotropic stress curves in Figure 9a. At this point, the rise in OD_{600} is not due to cell growth. In addition to the cell count affecting measurements, the cell size also significantly affects the measurements. The size of *E. coli* cells may shrink in response to nutritional stress, such as during late stationary phase, lengthen or induce filamentation in the presence of antibiotics, and shorten when shifting from mid log phase to early stationary phase[58]. Each of these conditions results causes different OD_{600} measurements with the same cell count. Given these insights from previous research, we believe that our observed OD_{600} curves are not directly linked with cell count at all timepoints, especially given that each cell performs differently in each stressor and at which concentration. However, there is still remarkable similarity between trial 1 and trial 2 of the antibiotic adaptation analyses that supports the observed results (Figure 11). While OD_{600} may not directly correspond with cell count, the observed OD_{600} measurements appear to be representative of each sample's overall growth dynamics.

Lastly, an important limitation to the adaptation analysis is that the observed samples may not be representative of the cell populations in MICALE. Colonies are isolated and grown up before the adaptation analysis and sequencing to ensure similar cell counts and that each sample comes from the same parental colony. Doing so, however, reduces the density present in the sample. The adaptation analysis, therefore, offers only a limited look at the growth phenotypes in the community. For a better look at the community, we attempted to sequence a culture of cells grown directly from MICALE, without selecting a colony. These samples, however, were from the antibiotic run that was contaminated with *Bacillus* so we were unable to obtain these data. The diversity in MICALE is both a challenge and an advantage. It is challenging to process and understand so much diversity. On the other hand, the diversity presents more opportunities for unique adaptations to occur and, while adding some degree of complication, may be a better representation of evolution dynamics occurring outside of the laboratory.

The adaptation analysis and downstream dose-response curve calculations were developed to obtain qualitative and quantitative data from the growth phenotypes of isolated samples. We hoped to use these data as evidence for or against stress tolerance adaptations in MICALE. Looking at the OD_{600} curves from each adaptation analysis, each treatment (concentration of the stressor) results in a different shaped curve. Far from the standard S-shaped curve, the unique shapes suggest different responses and growth mechanisms employed by cell populations, between different types of stressors and between samples of the same stressor. While some variation in OD_{600} curves could be due to differing cell inoculation numbers and evaporation, diverse growth strategies are clearly observed in the different curve

shapes as well as the appearance of growth on agar plates and broth. For example, a jump in OD_{600} measurements, seen in the IL-15-Col2 and BL-15 antibiotic samples, was often caused by formation of cellular aggregates, presumably biofilms or EPS (Figure 11). These aggregates were clearly visible on the 96-well plate after the run, forming clumps in the wells compared to the ancestor strain that produced a turbid culture instead. The variation in OD_{600} curve shape caused by different growth phenotypes, however, makes comparing and interpreting the OD_{600} curves inherently subjective but it also highlights the diversity present in MICALE samples. These observed phenotypes highlight how ALE completed in a heterogeneous environment supports diverse cell populations.

The greatest takeaway from the high salinity run is that MICALE-grown samples grew in a level of salinity higher than the ancestor strain could grow (Figure 7). In 90 ppt NaCl, the ancestor had an average cell proliferation amount less than 5%, designating no growth, compared to values above 15% for the three MICALE samples from the end of the run. These three samples, the PL, SL_{final}, and BL, have similar values for cell proliferation but their exponential growth rates show lots of variation from 60 to 90 ppt NaCl (Figures 7b and 7c). There is not enough information on what the shape of an OD_{600} curve could mean in terms of resistance but the diversity in shapes does suggest that different strategies are occurring.

For the chaotropic stress adaptation analysis, it is interesting that there was no sign of growth in 250 mM $MgCl_2$, except from an ancestor and PL-000-Col1 sample (Figure 9). The starting $MgCl_2$ concentration in the BLM of MICALE was 300 mM. Based on the OD_{600} growth curves, it appears that little to no adaptation occurred. However, growth from the ancestor in 250 mM $MgCl_2$ calls into question the methods. Most of the samples tested were collected from MICALE at the end of four weeks. It is possible that the experiment had gone on for too long

and samples had back mutated, loosing resistance to $MgCl_2$ in favor of resistance towards other stressors in MICALE. The growth rate ED50 values between samples are similar. The maximum OD600 measurements reached were by the PL-000-Col1 and SL-W2 sample growing in $MgCl_2$. While resistance to high salinity appears to be shrinking cell size and growth rate, observed in the adaptation analysis, resistance to magnesium chloride may involve larger cell size or the formation of aggregates. However, there is limited understanding of bacterial response to chaotropic stress.

Although all the antibiotic samples were contaminated with *Bacillus,* the adaptation analysis offers insight on the type of information that can be obtained using the adaptation analysis procedure (Figures 11, 12, and 13). The two trials show very similar results in terms of a sample's resistance to ciprofloxacin. While the strength of response (exponential growth rate and cell proliferation) differs between the two trials, the presence or absence of growth remains similar. Interestingly, the *Bacillus* strains tested show increased ciprofloxacin tolerance in the lower regions of MICALE. As discussed prior, an important consideration with ALE is that the strength of selection must be strong enough to sort out strains with increased tolerance. Previous research shows that *Bacillus* tolerance to ciprofloxacin varies on a large scale. So, while the contaminants may not have evolved increased resistance, it appears that strains of *Bacillus* sorted themselves in MICALE based on resistance, as we had hoped. Despite similar results between he trials, the small differences in response between the trials can result in vastly different ED50 values due to the wide range of concentrations tested. Future adaptation analyses should first do a growth plate test over a wide range of stressor concentrations. Then, based on the results, choose a narrow concentration range to test again. This will produce more accurate ED50 values.

Whole-genome resequencing (WGS) and analysis with *breseq* provides evidence that genetic changes occurred in MICALE but cannot yet state if these changes resulted in high-tolerance phenotypes. Four samples returned mutations unique from the ancestor, three of which had a mutation involving an Insertion Sequence (IS) mobile element (Table 8). IS mobile elements have been observed to influence local gene expression as well overall genetic evolution[6,59]. IS elements can inactivate genes when inserted into the coding region, alter gene expression when inserted into noncoding regions, such as by providing a promoter, enhance a promoter, deactivate a repressor, or enhance expression of a repressor[59]. On a genome-wide scale, these individual mobile events may initiate larger recombination events, such as chromosomal inversions or deletions, overall contributing significantly to bacterial mutagenesis and maintaining diversity in a population[6]. In adaptive laboratory studies, mobile genetic elements were shown to be involved in adaptation to a variety of stressors, including in high osmolarity conditions[60,61].

The high salinity sample IL-05 removed the *insH21* gene, belonging within the IS*5* mobile element, from its original placement upstream of the promoter for the oppABCDF operon. Schnetz and Rak (1992) showed that the IS*5* mobile element can act as an activator when inserted upstream or downstream of a promoter[59]. Because of its role as a high affinity oligopeptide transporter, oppABCDF plays an important role in cell nutrition[62]. Notably, the transporter reuptakes previously released cell wall peptides. These peptides can then be reincorporated into the cell wall, an essential function for growth in media that is poor of peptidoglycan precursors[63]. IS*5* mobility as also appeared in many experiments related to starvation[61]. The insertion of *insH21* suggests that IL-05 may be up or downregulating this

operon but we cannot be sure if that change is linked to the high salinity conditions within MICALE.

The chaotropic stress SL-W2 sample inserted the mobile element IS*186* in reverse into the *crr* gene, after the 484th nucleotide of the gene's total 510. It has been shown experimentally that the protein sequences at the start and in the middle of Enzyme IIA^{Glc}, the enzyme encoded for by *crr,* are responsible for its important functions of interacting with its counterpart, enzyme IIB^{Glc}, and as the enzymes active site[64,65]. The IS*186* insertion is not near either of these regions and therefore likely does not have an effect. However, Enzyme IIA^{Glc} is very specific for its function with glucose so the mutation may still have an effect[66]. Enzyme IIA^{Glc} is notably a central regulatory protein, involved with many processes related to carbohydrate metabolism and energy conservation[67]. Processes including but not limited to the phosphotransferase system involved in the transport of carbohydrates, negative regulation of glycerol kinase (*glpK*), an enzyme involved in glycerol catabolism, and activation of adenylate cyclase, a key player in gene expression regulation[68,69]. These regulatory actions can be triggered by a change in the carbohydrate nutrient source[66]. This mutation, therefore, could be in response to changes in nutrient sources for SL-W2. Perhaps a decreasing availability of preferred carbohydrates caused cells to switch to secondary sources, such as amino acids, surrounding cell matter, or the sucrose present in the BLM.

The chaotropic stress BL-W4 sample inserted IS*1* in an intergenic region downstream of *yahM* and the promoter for *yahM.* We have not determined if this insertion causes a significant frameshift. Furthermore, the YahM protein is uncharacterized so inferences on the function of this protein cannot be made.

The presence of *IS* elements is an indication of evolutionary processes occurring in MICALE. In other adaptive laboratory studies, mobile genetic elements were shown to be involved in adaptation to a variety of stressors, including in high osmolarity conditions, low pH, and starvation[60,61]. While it is unclear which type of stress the observed *IS* changes are a result of, the presence of *IS* elements linked to stress suggests that adaptative evolution is occurring, rather than genetic drift. The phenotypic effect of these mutations requires further research.

The high salinity sample, IL-05, has two other mutations, one a SNP that results in a missense codon change and the other a SNP that occurs in cAMP-CRP inhibitor for the *azuC* gene. The AzuC protein is uncharacterized, so it is unclear what function it serves. The IL-05 was not included in the adaptation analysis so we cannot make estimates about its phenotype. However, none of the samples used for the high salinity adaptation analysis originated from the same colonies as those grown up for DNA extraction and sequencing. Therefore, the BL-60 sample that performed well in the adaptation analysis did not return any mutations, but it is possible that an unevolved colony was selected for growth (Figure 7).

On the other hand, the chaotropic stress samples that returned mutations, SL-W2 and SL-W4 do come from the same colony as the adaptation analysis thus allowing for better comparison. SL-W2 achieved the highest OD_{600} measurements of the adaptation analysis in 200 mM $MgCl_2$, outperforming its own growth in media without magnesium chloride (Figure 9). In 200 mM $MgCl_2$, SL-W2 increased its cell proliferation value by 41% relative to its response in blank media. SL-W4, on the other hand, still performed well in 200 mM $MgCl_2$ but only increased its cell proliferation by 2% relative to its response in blank media. Looking at exponential growth rate, SL-W4 performs better in 200 mM $MgCl_2$ than SL-W2, achieving a growth rate 42% of that in blank media compared to 22%.

The SL-W4 sample has a single SNP in the gene *sspA,* switching an aspartic amino acid for tyrosine in the stringent starvation protein (SspA). The RCSDB Protein Data Bank, shows the effected amino acid is in a helix facing the outside of the protein and not within any of the areas discussed by Hansen *et al* (2005) as potential important areas for function[70–72]. While the SNP may not be in the sspA active site, Scheiner *et al* (2002) discuss that the amino acid Tyrosine is often on the outer edges of proteins because its unique ability to form hydrogen bonds while remaining overall neutral aids in an enzyme's stability with the surrounding solvent[73]. There is evidence suggesting that chaotropic solutes inhibit cellular systems by disrupting hydrogen bonding and may also partition into hydrophobic areas of macromolecules[10,27,74]. Perhaps this amino acid change allows for greater stability of SspA in the presence of magnesium chloride. SspA is an RNA polymerase-associated protein which aids in a bacteria's ability to respond to environmental stresses and nutrient-limited conditions[70,75]. *sspA* mutants survived worse during periods of starvation or extended stationary phase and showed decrease expression of multiple genes involved in acid resistance[76]. SspA inhibits H-NS, a repressor for many genes that are involved in stress response to multiple conditions such as osmotic, oxidative, and acid stress[70]. Notably, H-NS-deficient strains had increased resistance in high osmolarity and low pH conditions[77]. The previous research that shows how H-NS and SspA are linked with response to environmental stresses suggests that this mutation is a result of the stress endured in the lower region of MICALE. However, is in unclear if inhibition of H-NS has any relation to cellular response to chaotropic stress, highlighting the lack of understanding for adaptation to chaotropic stress and opening a new subject for future research. SL-W4 had the second highest ED50 growth rate value in magnesium chloride and maintained its relative cell proliferation from blank media to media with $MgCl_2$. So, while it does not perform as exceptionally in $MgCl_2$ as SL-W2,

it does not perform poorly. Altogether, it is possible that the *sspA* mutation in SL-W4 evolved as a response to other stressors, such as low pH, occurring in MICALE that were likely causing significant pressure since the BLM was a month old. Comparatively, the mutation in SL-W2 appears to be related to nutritional resources and energy metabolism. Perhaps a decrease in nutritional resources from two weeks to four weeks in the run shifted cells in the SL regions to focus more on stress-related adaptations.

The chaotropic stress BL-W4, in addition to its IS1 mobile element mutation, has a SNP mutation upstream of the *shiA* gene and a SNP in the *ratA* gene. ShiA has been shown to be involved in transport of shikimate, an intermediate compound in biosynthesis of aromatic amino acids[48,49]. It is unclear how an upstream SNP may impact expression of the *shiA* gene but a mutation involving amino acid metabolism fits with the challenges we excepted BL-W4 to have endured in the lower region of MICALE. LB broth contains a low concentration of sugars so microbes will switch to using amino acids as a carbon source once the sugars are depelated[51]. The media at the bottom of MICALE, where BL-W4 was sampled from, had been there for a month without fresh input of media. If cells were active in the lower region, we would expect the media to be low in preferred carbon sources and perhaps even amino acids. When starved for amino acids, cells will down regulate protein synthesis and up-regulate protein turnover[18].

The SNP mutation in the *ratA* gene also offers insight to the conditions faced by *E. coli* cells in the lower region of MICALE. The *ratA* gene is responsible for RatA, a toxin involved in a toxin-antitoxin system. Toxin-antitoxin systems are upregulated in stressed cells and may help with biofilm formation and persistence[78]. The lower region of MICALE likely has the highest concentration of $MgCl_2$, shown by density measurements, and was likely very low in nutrients by the end of the month. In an experimental study involving a different strain of *E. coli*, deletion of

ratA decreased persistence in antibiotics[78]. The *ratA* gene, therefore, may be important for BL-W4 survival in the lower region of MICALE. Additionally, the RatA toxin binds to 50S ribosomal subunits, inhibiting translation and growth[79]. Perhaps the mutation in BL-W4 allows the strain to slow growth and persist at the bottom of MICALE or the mutation reduces RatA toxicity, allowing for unchallenged growth. Like many of the mutations studied thus, the *ratA* gene is linked to a broad range of stressors, making it difficult to determine if a genetic change is in response to the intended stressor or in response to low nutrient, oxidative, nitrosative, or other stress that could occur in MICALE.

Whole-genome resequencing and analysis with *breseq* on samples from high salinity and chaotropic stress runs shows evidence that genetic changes occurred in MICALE but cannot yet state if these changes resulted in high-tolerance phenotypes. At the foundation, these mutations do highlight the diversity present in MICALE. Samples from the SL and BL regions have different mutations, despite being sampled the same time. The difference in mutations between the SL-W2 and SL-W4 sample highlight how multiple strains may be present in a region at the same time or how the dynamic the genetic diversity is, changing drastically within a two-week period. WGS analysis allowed for comparison of one full genome to another. However, this requires a reduction of the bacterial community down to just one colony isolate. Therefore, it is unclear how much diversity is present and how well our isolated samples represent the community. In addition to WGS, future studies could perform metagenomic sampling of MICALE communities to look for trends in the mutational diversity such as a higher frequency of mutations in one area of the genome.

Many of the mutations occur within or near genes showed to be involved in stress responses. However, many of the responses are activated by numerous stressors such as nutrient

limitation, osmotic stress, and low pH. Thus, it is unclear if the mutation is in response to the intended stressor, osmotic and chaotropic stress, or in response to other factors in MICALE such as nutrient limitation, low oxygen, low pH, and the presence of sucrose. Future research should test the ability of the strains to grow in media with these potential other stressors. Such an analysis may reveal growth phenotypes and resistance to other stressors that were hidden during the adaptation analysis. Furthermore, the wealth of research on genetic and transcriptional responses to chaotropic stress is lacking compared to that on osmotic stress. The mutations found in the chaotropic samples highlight regions of interest for future studies on chaotropic stress resistance.

CONCLUSION

Overall, the work provided thus demonstrates how the Multilayered Instrument for Continuous Adaptive Laboratory Evolution (MICALE) functions as intended and the developed methods provide a foundation for future ALE experiments. Contamination, however, prevents us from determining MICALE's effectiveness at producing adapted strains. Our data suggests that the density separation, and therefore a difference in the level of stress, is maintained throughout MICALE runs (Graph 1). The media in the upper region has low levels of stress thereby allowing growth of the wild type. Meanwhile, the density measurements of the SL and BL samples show that the lower regions have a concentration of stressor too high for wild type survival. This density separation is critical for creating a structured, heterogeneous environment with a region permissive for the wild type and a region with a level of stress that only adapted strains can survive in. The adaptation analysis provides phenotypic evidence that cells in the lower regions have higher levels of resistance than the ancestor. The flow rate controls the amount of biomass in the upper region but not the lower areas, maintaining a continuous culture of cells in the permissive upper region only (Graph 3). Altogether, MICALE allows for wild type survival in the upper region and selects for strains with increased resistance in the lower region, two of the three requirements for ALE presented in this paper. It is difficult to discern if the third requirement for ALE, coupling the favored phenotype with increased fitness, was achieved with the outlined protocols. Regardless, our careful measurements and analyses revealed specific areas for future improvements. These improvements will increase the selective pressure on cells to evolve the desired phenotype for a more effective ALE experiment. For example, implementing stronger nutrient limitation in the upper region will increase the relative fitness of stress-tolerant cells as they can access the excess nutrients in the stressful region. While we

cannot link the mutations found in MICALE-grown strains to increased tolerance to the added stressor, the mutations confirm that genetic change does occur in MICALE and that diverse cell populations are present. The observed genetic diversity is likely a product of MICALE's density gradient that creates a heterogeneous environment with multiple niches for diversification. Previous experiments have achieved a heterogeneous structure only on solid surfaces[24] or in liquid micro-scale environments[23]. MICALE is the first apparatus of its kind that utilizes a liquid, heterogeneous environment with accessible materials. Its customizable nature provides limitless applications for ALE. By using different stressors, media types, and microorganisms, MICALE can expand our understanding of bacterial evolution, develop new microbial strains, and draw better comparisons between laboratory and natural evolution.

APPENDIX

Figure A1: Photo of Samples from the Chaotropic Stress Run
The sample tube on the left contained a goopy aggregate that was suspected to be EPS. This aggregate artificially inflated the OD_{600} measurements by increasing the turbidity without increasing the cell count. The vial on the right is a normal sample of the media without any aggregates.

a)

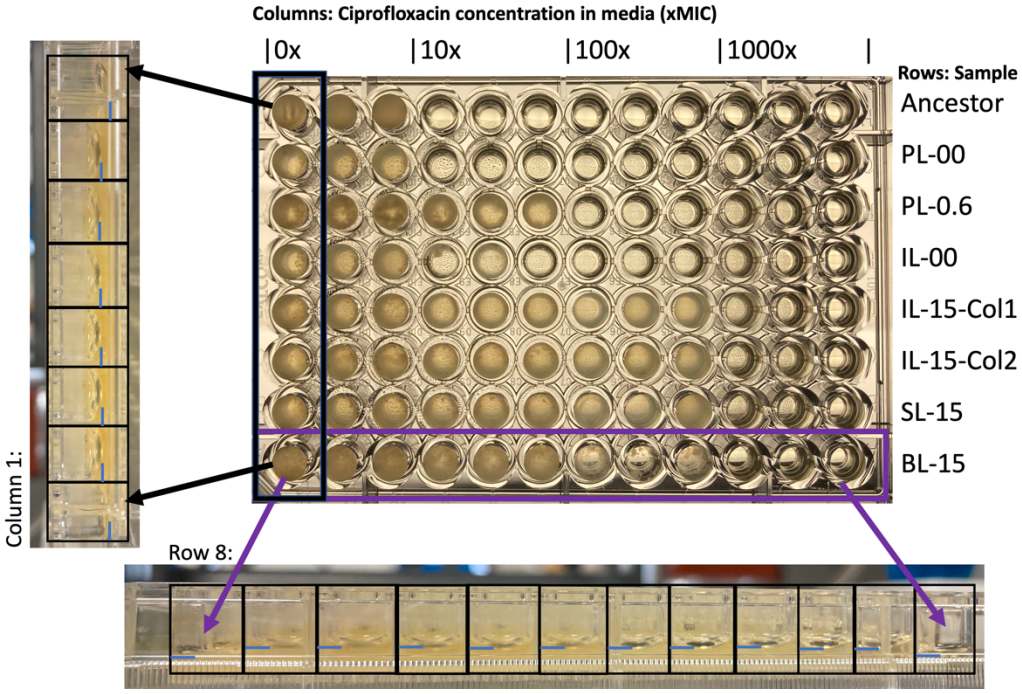

b)

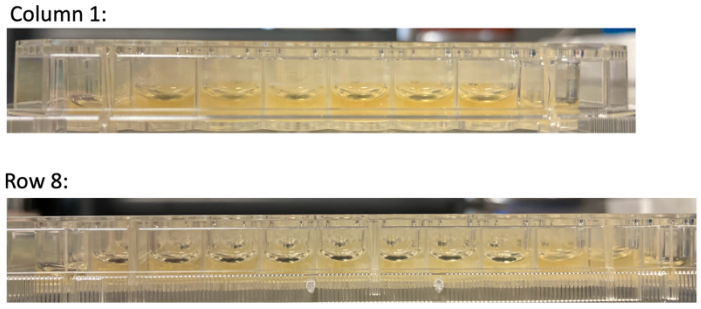

Figure A2: Evaporation on 96-Well Plate After Adaptation Analysis
a) The full 96-well plate after the four-day adaptation analysis for the antibiotic run, the results of which are seen in Figure 11. Columns are separated by the amount of ciprofloxacin in the media (xMIC) and rows are separated by the sample isolate added to the well. A description of the sample names can be found in Table 4. The boxed column and row point with arrows to photos taken of the side of the plate. The outer-most wells of the plate are the most effected by evaporation. On the side profiles, black boxes separate each well and blue lines represent the estimated level of the media's meniscus. The media level shows how the corner wells are the most effected by evaporation and have the lowest media level. Thus, the Ancestor and BL-15 measurements are the most effected by evaporation, being the outside rows of the plate, and their one well in 0x and 1000x MIC media is the most effected. **b)** The same side-profiles of column 1 and row 8 without added lines.

WORKS CITED

1. Dragosits, M. & Mattanovich, D. Adaptive laboratory evolution – principles and applications for biotechnology. *Microb Cell Fact* 12, 64–64 (2013).

2. Sandberg, T. E., Salazar, M. J., Weng, L. L., Palsson, B. O. & Feist, A. M. The emergence of adaptive laboratory evolution as an efficient tool for biological discovery and industrial biotechnology. *Metab Eng* 56, 1–16 (2019).

3. Lee, S. & Kim, P. Current Status and Applications of Adaptive Laboratory Evolution in Industrial Microorganisms. *J Microbiol Biotechn* 30, 793–803 (2020).

4. Sanghavi, G., Gupta, P., Rajput, M., Oza, T., Trivedi, U. & Singh, N. K. Engineering of Microbial Biosynthetic Pathways. 11–32 (2020). doi:10.1007/978-981-15-2604-6_2

5. Choe, D., Lee, J. H., Yoo, M., Hwang, S., Sung, B. H., Cho, S., Palsson, B., Kim, S. C. & Cho, B.-K. Adaptive laboratory evolution of a genome-reduced Escherichia coli. *Nat Commun* 10, 935 (2019).

6. Schneider, D. & Lenski, R. E. Dynamics of insertion sequence elements during experimental evolution of bacteria. *Res Microbiol* 155, 319–327 (2004).

7. Jansen, G., Barbosa, C. & Schulenburg, H. Experimental evolution as an efficient tool to dissect adaptive paths to antibiotic resistance. *Drug Resist Update* 16, 96–107 (2013).

8. Zhou, L., Alcalde, R. E., Deng, J., Zuniga, B., Sanford, R. A., Fouke, B. W. & Werth, C. J. Impact of antibiotic concentration gradients on nitrate reduction and antibiotic resistance in a microfluidic gradient chamber. *Sci Total Environ* 779, 146503 (2021).

9. Naylor, D. & Coleman-Derr, D. Drought Stress and Root-Associated Bacterial Communities. *Front Plant Sci* 08, 2223 (2018).

10. Hallsworth, J. E. Stress-free microbes lack vitality. *Fungal Biol-uk* 122, 379–385 (2018).

11. Simonsen, A. K. Environmental stress leads to genome streamlining in a widely distributed species of soil bacteria. *Isme J* 16, 423–434 (2022).

12. Yan, N., Marschner, P., Cao, W., Zuo, C. & Qin, W. Influence of salinity and water content on soil microorganisms. *Int Soil Water Conservation Res* 3, 316–323 (2015).

13. Horinouchi, T., Tamaoka, K., Furusawa, C., Ono, N., Suzuki, S., Hirasawa, T., Yomo, T. & Shimizu, H. Transcriptome analysis of parallel-evolved Escherichia coli strains under ethanol stress. *Bmc Genomics* 11, 579 (2010).

14. Du, B., Olson, C. A., Sastry, A. V., Fang, X., Phaneuf, P. V., Chen, K., Wu, M., Szubin, R., Xu, S., Gao, Y., Hefner, Y., Feist, A. M. & Palsson, B. O. Adaptive laboratory evolution of Escherichia coli under acid stress. *Microbiology+* 166, 141–148 (2020).

15. Harden, M. M., He, A., Creamer, K., Clark, M. W., Hamdallah, I., Martinez, K. A., Kresslein, R. L., Bush, S. P. & Slonczewski, J. L. Acid-Adapted Strains of Escherichia coli K-12 Obtained by Experimental Evolution. *Appl Environ Microb* 81, 1932–1941 (2015).

16. Baquero, F. Environmental stress and evolvability in microbial systems. *Clin Microbiol Infec* 15, 5–10 (2009).

17. Martinez, J. L. & Baquero, F. Mutation Frequencies and Antibiotic Resistance. *Antimicrob Agents Ch* 44, 1771–1777 (2000).

18. Foster, P. L. Stress-Induced Mutagenesis in Bacteria. *Crit Rev Biochem Mol* 42, 373–397 (2008).

19. Barrick, J. E. & Lenski, R. E. Genome dynamics during experimental evolution. *Nat Rev Genet* 14, 827–839 (2013).

20. Gresham, D. & Dunham, M. J. The enduring utility of continuous culturing in experimental evolution. *Genomics* 104, 399–405 (2014).

21. Biselli, E., Schink, S. J. & Gerland, U. Slower growth of Escherichia coli leads to longer survival in carbon starvation due to a decrease in the maintenance rate. *Mol Syst Biol* 16, e9478 (2020).

22. Wiser, M. J. & Lenski, R. E. A Comparison of Methods to Measure Fitness in Escherichia coli. *Plos One* 10, e0126210 (2015).

23. Zhang, Q., Lambert, G., Liao, D., Kim, H., Robin, K., Tung, C., Pourmand, N. & Austin, R. H. Acceleration of Emergence of Bacterial Antibiotic Resistance in Connected Microenvironments. *Science* 333, 1764–1767 (2011).

24. Baym, M., Lieberman, T. D., Kelsic, E. D., Chait, R., Gross, R., Yelin, I. & Kishony, R. Spatiotemporal microbial evolution on antibiotic landscapes. *Science* 353, 1147–1151 (2016).

25. Rainey, P. B. & Travisano, M. Adaptive radiation in a heterogeneous environment. *Nature* 394, 69–72 (1998).

26. Harding, T., Roger, A. J. & Simpson, A. G. B. Adaptations to High Salt in a Halophilic Protist: Differential Expression and Gene Acquisitions through Duplications and Gene Transfers. *Front Microbiol* 8, 944 (2017).

27. Klempay, B., Arandia-Gorostidi, N., Dekas, A. E., Bartlett, D. H., Carr, C. E., Doran, P. T., Dutta, A., Erazo, N., Fisher, L. A., Glass, J. B., Pontefract, A., Som, S. M., Wilson, J. M.,

Schmidt, B. E. & Bowman, J. S. Microbial diversity and activity in Southern California salterns and bitterns: analogues for remnant ocean worlds. *Environ Microbiol* 23, 3825–3839 (2021).

28. Fisher, L. A., Pontefract, A., Som, S., Carr, C. E., Klempay, B., Schmidt, B., Bowman, J. & Bartlett, D. H. Current state of athalassohaline deep-sea hypersaline anoxic basin research—recommendations for future work and relevance to astrobiology. *Environ Microbiol* 23, 3360–3369 (2021).

29. Röderova, M., Halova, D., Papousek, I., Dolejska, M., Masarikova, M., Hanulik, V., Pudova, V., Broz, P., Htoutou-Sedlakova, M., Sauer, P., Bardon, J., Cizek, A., Kolar, M. & Literak, I. Characteristics of Quinolone Resistance in Escherichia coli Isolates from Humans, Animals, and the Environment in the Czech Republic. *Front Microbiol* 7, 2147 (2017).

30. McKenzie, G. J., Harris, R. S., Lee, P. L. & Rosenberg, S. M. The SOS response regulates adaptive mutation. *Proc National Acad Sci* 97, 6646–6651 (2000).

31. Galhardo, R. S., Hastings, P. J. & Rosenberg, S. M. Mutation as a Stress Response and the Regulation of Evolvability. *Crit Rev Biochem Mol* 42, 399–435 (2008).

32. Wiegand, I., Hilpert, K. & Hancock, R. E. W. Agar and broth dilution methods to determine the minimal inhibitory concentration (MIC) of antimicrobial substances. *Nat Protoc* 3, 163–175 (2008).

33. Blattner, F. R., III, G. P., Bloch, C. A., Perna, N. T., Burland, V., Riley, M., Collado-Vides, J., Glasner, J. D., Rode, C. K., Mayhew, G. F., Gregor, J., Davis, N. W., Kirkpatrick, H. A., Goeden, M. A., Rose, D. J., Mau, B. & Shao, Y. The Complete Genome Sequence of Escherichia coli K-12. *Science* 277, 1453–1462 (1997).

34. Padfield, D. Calculating microbial growth rates from OD measurements using rolling regression in the tidyverse. (2019). at <https://padpadpadpad.github.io/post/calculating-microbial-growth-rates-from-od-using-rolling-regression/>

35. Ritz, C. & Streibig, J. C. Bioassay Analysis Using R. *Journal of Statistical Software* 5, 1–22 (2005).

36. Ritz, C., Baty, F., Streibig, J. C. & Gerhard, D. Dose-Response Analysis Using R. *Plos One* 10, e0146021 (2015).

37. Seefeldt, S. S., Jensen, J. E. & Fuerst, E. P. Log-Logistic Analysis of Herbicide Dose-Response Relationships. *Weed Technol* 9, 218–227 (1995).

38. Team, Rs. *RStudio: Integrated Development for R*. (RStudio, 2020). at <http://www.rstudio.com/>

39. Team, R. C. *R: A language environment for statistical computing*. (R Foundation for Statistical Computing, 2022). at <https://www.R-project.org/>

40. Gilbert, J. A., Jansson, J. K. & Knight, R. The Earth Microbiome project: successes and aspirations. *Bmc Biol* 12, 69 (2014).

41. Thompson, L. R., Sanders, J. G., McDonald, D., Amir, A., Ladau, J., Locey, K. J., Prill, R. J., Tripathi, A., Gibbons, S. M., Ackermann, G., Navas-Molina, J. A., Janssen, S., Kopylova, E., Vázquez-Baeza, Y., González, A., Morton, J. T., Mirarab, S., Xu, Z. Z., Jiang, L., Haroon, M. F., Kanbar, J., Zhu, Q., Song, S. J., Kosciolek, T., Bokulich, N. A., Lefler, J., Brislawn, C. J., Humphrey, G., Owens, S. M., Hampton-Marcell, J., Berg-Lyons, D., McKenzie, V., Fierer, N., Fuhrman, J. A., Clauset, A., Stevens, R. L., Shade, A., Pollard, K. S., Goodwin, K. D., Jansson, J. K., Gilbert, J. A., Knight, R., Consortium, T. E. M. P., Rivera, J. L. A., Al-Moosawi, L., Alverdy, J., Amato, K. R., Andras, J., Angenent, L. T., Antonopoulos, D. A., Apprill, A., Armitage, D., Ballantine, K., Bárta, J., Baum, J. K., Berry, A., Bhatnagar, A., Bhatnagar, M., Biddle, J. F., Bittner, L., Boldgiv, B., Bottos, E., Boyer, D. M., Braun, J., Brazelton, W., Brearley, F. Q., Campbell, A. H., Caporaso, J. G., Cardona, C., Carroll, J., Cary, S. C., Casper, B. B., Charles, T. C., Chu, H., Claar, D. C., Clark, R. G., Clayton, J. B., Clemente, J. C., Cochran, A., Coleman, M. L., Collins, G., Colwell, R. R., Contreras, M., Crary, B. B., Creer, S., Cristol, D. A., Crump, B. C., Cui, D., Daly, S. E., Davalos, L., Dawson, R. D., Defazio, J., Delsuc, F., Dionisi, H. M., Dominguez-Bello, M. G., Dowell, R., Dubinsky, E. A., Dunn, P. O., Ercolini, D., Espinoza, R. E., Ezenwa, V., Fenner, N., Findlay, H. S., Fleming, I. D., Fogliano, V., Forsman, A., Freeman, C., Friedman, E. S., Galindo, G., Garcia, L., Garcia-Amado, M. A., Garshelis, D., Gasser, R. B., Gerdts, G., Gibson, M. K., Gifford, I., Gill, R. T., Giray, T., Gittel, A., Golyshin, P., Gong, D., Grossart, H.-P., Guyton, K., Haig, S.-J., Hale, V., Hall, R. S., Hallam, S. J., Handley, K. M., Hasan, N. A., Haydon, S. R., Hickman, J. E., Hidalgo, G., Hofmockel, K. S., Hooker, J., Hulth, S., Hultman, J., Hyde, E., Ibáñez-Álamo, J. D., Jastrow, J. D., Jex, A. R., Johnson, L. S., Johnston, E. R., Joseph, S., Jurburg, S. D., Jurelevicius, D., Karlsson, A., Karlsson, R., Kauppinen, S., Kellogg, C. T. E., Kennedy, S. J., Kerkhof, L. J., King, G. M., Kling, G. W., Koehler, A. V., Krezalek, M., Kueneman, J., Lamendella, R., Landon, E. M., Lane-deGraaf, K., LaRoche, J., Larsen, P., Laverock, B., Lax, S., Lentino, M., Levin, I. I., Liancourt, P., Liang, W., Linz, A. M., Lipson, D. A., Liu, Y., Lladser, M. E., Lozada, M., Spirito, C. M., MacCormack, W. P., MacRae-Crerar, A., Magris, M., Martín-Platero, A. M., Martín-Vivaldi, M., Martínez, L. M., Martínez-Bueno, M., Marzinelli, E. M., Mason, O. U., Mayer, G. D., McDevitt-Irwin, J. M., McDonald, J. E., McGuire, K. L., McMahon, K. D., McMinds, R., Medina, M., Mendelson, J. R., Metcalf, J. L., Meyer, F., Michelangeli, F., Miller, K., Mills, D. A., Minich, J., Mocali, S., Moitinho-Silva, L., Moore, A., Morgan-Kiss, R. M., Munroe, P., Myrold, D., Neufeld, J. D., Ni, Y., Nicol, G. W., Nielsen, S., Nissimov, J. I., Niu, K., Nolan, M. J., Noyce, K., O'Brien, S. L., Okamoto, N., Orlando, L., Castellano, Y. O., Osuolale, O., Oswald, W., Parnell, J., Peralta-Sánchez, J. M., Petraitis, P., Pfister, C., Pilon-Smits, E., Piombino, P., Pointing, S. B., Pollock, F. J., Potter, C., Prithiviraj, B., Quince, C., Rani, A., Ranjan, R., Rao, S., Rees, A. P., Richardson, M., Riebesell, U., Robinson, C., Rockne, K. J., Rodriguezl, S. M., Rohwer, F., Roundstone, W., Safran, R. J., Sangwan, N., Sanz, V., Schrenk, M., Schrenzel, M. D., Scott, N. M., Seger, R. L., Seguin-Orlando, A., Seldin, L., Seyler, L. M., Shakhsheer, B., Sheets, G. M., Shen, C., Shi, Y., Shin, H., Shogan, B. D., Shutler, D., Siegel, J., Simmons, S., Sjöling, S., Smith, D. P., Soler, J. J., Sperling, M., Steinberg, P. D., Stephens, B., Stevens, M. A., Taghavi, S., Tai, V., Tait, K., Tan, C. L., Tas¸, N., Taylor, D. L., Thomas, T., Timling, I., Turner, B. L., Urich, T., Ursell, L. K., Lelie, D. van der, Treuren, W. V., Zwieten, L. van, Vargas-Robles, D., Thurber, R. V., Vitaglione, P., Walker, D. A., Walters, W.

A., Wang, S., Wang, T., Weaver, T., Webster, N. S., Wehrle, B., Weisenhorn, P., Weiss, S., Werner, J. J., West, K., Whitehead, A., Whitehead, S. R., Whittingham, L. A., Willerslev, E., Williams, A. E., Wood, S. A., Woodhams, D. C., Yang, Y., Zaneveld, J., Zarraonaindia, I., Zhang, Q. & Zhao, H. A communal catalogue reveals Earth's multiscale microbial diversity. *Nature* 551, 457–463 (2017).

42. Deatherage, D. E. & Barrick, J. E. Engineering and Analyzing Multicellular Systems, Methods and Protocols. *Methods Mol Biology* 1151, 165–188 (2014).

43. Chen, S., Zhou, Y., Chen, Y. & Gu, J. fastp: an ultra-fast all-in-one FASTQ preprocessor. *Bioinformatics* 34, i884–i890 (2018).

44. Andrews. *FastQC: A Quality Control Tool for High Throughput Sequence Data*. (2010). at <http://www.bioinformatics.babraham.ac.uk/projects/fastqc/>

45. Camacho, C., Coulouris, G., Avagyan, V., Ma, N., Papadopoulos, J., Bealer, K. & Madden, T. L. BLAST+: architecture and applications. *Bmc Bioinformatics* 10, 421 (2009).

46. Altschul, S. F., Gish, W., Miller, W., Myers, E. W. & Lipman, D. J. Basic local alignment search tool. *J Mol Biol* 215, 403–410 (1990).

47. Keseler, I. M., Collado-Vides, J., Santos-Zavaleta, A., Peralta-Gil, M., Gama-Castro, S., Muñiz-Rascado, L., Bonavides-Martinez, C., Paley, S., Krummenacker, M., Altman, T., Kaipa, P., Spaulding, A., Pacheco, J., Latendresse, M., Fulcher, C., Sarker, M., Shearer, A. G., Mackie, A., Paulsen, I., Gunsalus, R. P. & Karp, P. D. EcoCyc: a comprehensive database of Escherichia coli biology. *Nucleic Acids Res* 39, D583–D590 (2011).

48. Whipp, M. J., Camakaris, H. & Pittard, A. J. Cloning and analysis of the shiA gene, which encodes the shikimate transport system of Escherichia coli K-12. *Gene* 209, 185–192 (1998).

49. Brown, K. D. & Doy, C. H. Transport and utilizing of the biosynthetic intermediate shikimic acid in Escherichia coli. *Biochimica Et Biophysica Acta Bba - Gen Subj* 428, 550–562 (1976).

50. Zhang, Q., Lambert, G., Liao, D., Kim, H., Robin, K., Tung, C., Pourmand, N. & Austin, R. H. Acceleration of Emergence of Bacterial Antibiotic Resistance in Connected Microenvironments. *Science* 333, 1764–1767 (2011).

51. Sezonov, G., Joseleau-Petit, D. & D'Ari, R. Escherichia coli Physiology in Luria-Bertani Broth. *J Bacteriol* 189, 8746–8749 (2007).

52. Westphal, L. L., Lau, J., Negro, Z., Moreno, I. J., Mohammed, W. I., Lee, H., Tang, H., Finkel, S. E. & Kram, K. E. Adaptation of Escherichia coli to long-term batch culture in various rich media. *Res Microbiol* 169, 145–156 (2018).

53. Luna, V. A., King, D. S., Gulledge, J., Cannons, A. C., Amuso, P. T. & Cattani, J. Susceptibility of Bacillus anthracis, Bacillus cereus, Bacillus mycoides, Bacillus

pseudomycoides and Bacillus thuringiensis to 24 antimicrobials using Sensititre® automated microbroth dilution and Etest® agar gradient diffusion methods. *J Antimicrob Chemoth* 60, 555–567 (2007).

54. Fahim, N. A. E., Ismail, G. A. E.-W., AbdelAleem, M. B., Elanany, M., Saber, S. M. & EL-Ashry, M. A. E.-R. Identification, characterization and antibiotic susceptibility testing for Bacillus species. *Iranian J Microbiol* (2022). doi:10.18502/ijm.v14i4.10234

55. Lemma, A. S., Soto-Echevarria, N. & Brynildsen, M. P. Fluoroquinolone Persistence in Escherichia coli Requires DNA Repair despite Differing between Starving Populations. *Microorg* 10, 286 (2022).

56. Colin, R., Ni, B., Laganenka, L. & Sourjik, V. Multiple functions of flagellar motility and chemotaxis in bacterial physiology. *Fems Microbiol Rev* 45, fuab038- (2021).

57. Li, B., Qiu, Y., Shi, H. & Yin, H. The importance of lag time extension in determining bacterial resistance to antibiotics. *Analyst* 141, 3059–3067 (2016).

58. Stevenson, K., McVey, A. F., Clark, I. B. N., Swain, P. S. & Pilizota, T. General calibration of microbial growth in microplate readers. *Sci Rep-uk* 6, 38828 (2016).

59. Schnetz, K. & Rak, B. IS5: a mobile enhancer of transcription in Escherichia coli. *Proc National Acad Sci* 89, 1244–1248 (1992).

60. Stoebel, D. M. & Dorman, C. J. The Effect of Mobile Element IS10 on Experimental Regulatory Evolution in Escherichia coli. *Mol Biol Evol* 27, 2105–2112 (2010).

61. Gaffé, J., McKenzie, C., Maharjan, R. P., Coursange, E., Ferenci, T. & Schneider, D. Insertion Sequence-Driven Evolution of Escherichia coli in Chemostats. *J Mol Evol* 72, 398–412 (2011).

62. Hiles, I. D., Gallagher, M. P., Jamieson, D. J. & Higgins, C. F. Molecular characterization of the oligopeptide permease of Salmonella typhimurium. *J Mol Biol* 195, 125–142 (1987).

63. Goodell, E. W. & Higgins, C. F. Uptake of cell wall peptides by Salmonella typhimurium and Escherichia coli. *J Bacteriol* 169, 3861–3865 (1987).

64. Meadow, N. D. & Roseman, S. Sugar transport by the bacterial phosphotransferase system. Isolation and characterization of a glucose-specific phosphocarrier protein (IIIGlc) from Salmonella typhimurium. *J Biol Chem* 257, 14526–14537 (1982).

65. Deutscher, J., Francke, C. & Postma, P. W. How Phosphotransferase System-Related Protein Phosphorylation Regulates Carbohydrate Metabolism in Bacteria. *Microbiol Mol Biol R* 70, 939–1031 (2006).

66. Deutscher, J., Francke, C. & Postma, P. W. How Phosphotransferase System-Related Protein Phosphorylation Regulates Carbohydrate Metabolism in Bacteria. *Microbiol Mol Biol R* 70, 939–1031 (2006).

67. McCloskey, D., Xu, S., Sandberg, T. E., Brunk, E., Hefner, Y., Szubin, R., Feist, A. M. & Palsson, B. O. Evolution of gene knockout strains of E. coli reveal regulatory architectures governed by metabolism. *Nat Commun* 9, 3796 (2018).

68. Herring, C. D., Raghunathan, A., Honisch, C., Patel, T., Applebee, M. K., Joyce, A. R., Albert, T. J., Blattner, F. R., Boom, D. van den, Cantor, C. R. & Palsson, B. Ø. Comparative genome sequencing of Escherichia coli allows observation of bacterial evolution on a laboratory timescale. *Nat Genet* 38, 1406–1412 (2006).

69. Postma, P. W., Lengeler, J. W. & Jacobson, G. R. Phosphoenolpyruvate:carbohydrate phosphotransferase systems of bacteria. *Microbiol Rev* 57, 543–594 (1993).

70. Hansen, A., Qiu, Y., Yeh, N., Blattner, F. R., Durfee, T. & Jin, D. J. SspA is required for acid resistance in stationary phase by downregulation of H-NS in Escherichia coli. *Mol Microbiol* 56, 719–734 (2005).

71. Berman, H. M., Westbrook, J., Feng, Z., Gilliland, G., Bhat, T. N., Weissig, H., Shindyalov, I. N. & Bourne, P. E. The Protein Data Bank. *Nucleic Acids Res* 28, 235–242 (2000).

72. Liu, L., Jiang, S., Xing, M., Chen, C., Lai, C., Li, N., Liu, G., Wu, D., Gao, H., Hong, L., Tan, P., Chen, S., Deng, Z., Wu, G. & Wang, L. Structural Analysis of an l-Cysteine Desulfurase from an Ssp DNA Phosphorothioation System. *Mbio* 11, e00488-20 (2020).

73. Scheiner, S., Kar, T. & Pattanayak, J. Comparison of Various Types of Hydrogen Bonds Involving Aromatic Amino Acids. *J Am Chem Soc* 124, 13257–13264 (2002).

74. Hallsworth, J. E., Yakimov, M. M., Golyshin, P. N., Gillion, J. L. M., D'Auria, G., Alves, F. D. L., Cono, V. L., Genovese, M., McKew, B. A., Hayes, S. L., Harris, G., Giuliano, L., Timmis, K. N. & McGenity, T. J. Limits of life in MgCl2-containing environments: chaotropicity defines the window. *Environ Microbiol* 9, 801–813 (2007).

75. Wu, X., Altman, R., Eiteman, M. A. & Altman, E. Adaptation of Escherichia coli to Elevated Sodium Concentrations Increases Cation Tolerance and Enables Greater Lactic Acid Production. *Appl Environ Microb* 80, 2880–2888 (2014).

76. Williams, M. D., Ouyang, T. X. & Flickinger, M. C. Starvation-induced expression of SspA and SspB: the effects of a null mutation in sspA on Escherichia coli protein synthesis and survival during growth and prolonged starvation. *Mol Microbiol* 11, 1029–1043 (1994).

77. Hommais, F., Krin, E., Laurent-Winter, C., Soutourina, O., Malpertuy, A., Caer, J. L., Danchin, A. & Bertin, P. Large-scale monitoring of pleiotropic regulation of gene expression by the prokaryotic nucleoid-associated protein, H-NS. *Mol Microbiol* 40, 20–36 (2001).

78. Norton, J. P. & Mulvey, M. A. Toxin-Antitoxin Systems Are Important for Niche-Specific Colonization and Stress Resistance of Uropathogenic Escherichia coli. *Plos Pathog* 8, e1002954 (2012).

79. Zhang, Y. & Inouye, M. RatA (YfjG), an Escherichia coli toxin, inhibits 70S ribosome association to block translation initiation. *Mol Microbiol* 79, 1418–1429 (2011).